

Evaluating nature-based solutions to storm wave impacts in the Virginia Coast Reserve

Amy Elaine Ferguson
Charlottesville, VA

B.S. Geology, The College of William and Mary, 2010

A Thesis presented to the Graduate Faculty
of the University of Virginia in Candidacy for the Degree of
Master of Science

Department of Environmental Sciences

University of Virginia
May, 2018

ABSTRACT

Sea level rise, increased storminess, and human population growth amplify coastal erosion problems, pressuring landowners to implement shoreline protection measures. Growing concern over the negative impacts of traditional shoreline protection methods has increased interest in nature-based solutions, called “living shorelines.” The goal of this study was to develop a better understanding of the characteristics that contribute to the vulnerability of salt marshes fringing Virginia’s coastal bays and to recommend appropriate shoreline stabilization techniques.

Using GIS and remote sensing data, a Marsh Vulnerability Index (MVI) was developed to relate and map disparate physical, biological, and climatological factors that contribute to salt marsh erosion and inundation. The MVI, which indicates the level of vulnerability for individual shoreline segments, was calculated for the marsh shorelines fringing the bays of the Virginia Coast Reserve (VCR). The majority of VCR shoreline (86%, 1,007 km) was designated as having very low to low vulnerability; 14% (165 km) was resolved as moderate to very high vulnerability. Vulnerability was generally higher along mainland marshes than marsh islands or backbarrier marshes. Moderate to high vulnerability was primarily associated with high wave exposure, low marsh buffer width, and proximity to boat ramps. At one comparison site with relatively high wave exposure, there was a significant positive relationship between MVI and historical shoreline change rates. This was not true at two other sites with less wave exposure, which indicate that other factors such as existing shoreline stabilization structures or low overall vulnerability can alter the relationship between the MVI and shoreline change rates.

A field study was carried out to investigate the effects of constructed oyster reefs and marsh vegetation – materials commonly used in living shoreline design – on dampening waves, the main driver of shoreline erosion. Constructed oyster reefs were effective at dampening waves up

to 46% when water levels were low to moderate (< mean water depth); and, marsh vegetation was found to dampen waves by an average of 78% over a 20-meter marsh transect when water depths were high enough to flood the marsh. These results suggest that combining constructed oyster reefs with marsh vegetation may offer effective and sustainable long-term reduction in marsh vulnerability.

A spatial model, The Living Shoreline Explorer Model (LSEM), was developed to identify shorelines where conditions were suitable for the use of living shoreline stabilization methods. The LSEM designated 85% (237 km) of mainland shoreline along Virginia's coastal bays as suitable for nature-based shoreline stabilization projects, with the remaining 15% recommended for more traditional hard stabilization. The LSEM can be used as a screening tool for coastal stakeholders in examining living shoreline stabilization options, with the understanding that successful living shoreline design and placement requires a site visit for a final determination.

The MVI and LSEM developed for this study offer coastal stakeholders context for understanding their shoreline and a guidepost for pursuing an appropriate shoreline stabilization plan. Data from both spatial models were incorporated into The Nature Conservancy's *Coastal Resilience* web mapping decision-support tool, where they can be analyzed with other spatial data to visualize vulnerability and identify nature-based solutions to coastal erosion problems. Future iterations of the MVI and LSEM will benefit from access to this comprehensive data repository for marsh shorelines in the VCR.

ACKNOWLEDGEMENTS

First, I would like to thank my advisor, Patricia Wiberg, for her indefatigable support and mentorship. The unique opportunities offered to me by Pat – from studying abroad in Venice to collaborating with The Nature Conservancy – shaped my development as a person and as a science professional. I am forever thankful.

I would also like to thank my committee members, Karen McGlathery and Matt Reidenbach, for their approachability and advice throughout this process. This work would not have been possible without the many lessons from John Porter; our countless conversations and impromptu troubleshooting sessions over geospatial challenges were always fun and much appreciated. Dave Carr also acted as an important sounding board and mentor for my statistical analysis.

I was incredibly fortunate to have the opportunity to work closely with collaborators from The Nature Conservancy. Chris Bruce provided mentorship through my geospatial endeavors; without which I would not have pursued my certification as a GIS Professional. Big thanks to Bo Lusk for generously helping with field logistics and sharing his vast knowledge of the Virginia Eastern Shore along the way. Thank you to Gwynn Crichton and Cristina Carollo for allowing me a window into the world of an environmental non-profit by including me in community outreach events, technical workshops, grant proposals, and quality assurance reports.

Thanks to the Coastal Lab Group for productive and collegial lab meetings and for providing constructive feedback. Much appreciation to Ross P. for sharing his mathematical genius and patience in helping me through the most difficult course of my academic career: Environmental Fluid Mechanics. A heartfelt thanks to my officemate, Amelie B., who helped me in the field and provided countless hours of support and laughter; she has been an amazing friend and colleague throughout this process. My research would not have been possible without the dedicated field

assistance of the staff at the Anheuser Busch Coastal Research Center, especially Donna Fauber and David Lee.

Special thanks to my parents, Kris and Jeff R., and sister, Katie E., for their enthusiasm for my chosen career path and for hosting me during each field deployment to help care for my dogs. Finally, I would like to thank my husband, Stuart, for his unwavering encouragement through it all.

Funding for this project was provided by the Hurricane Sandy Coastal Resilience Fund 2300.14.042551 and the Virginia Coast Reserve Long Term Ecological Research project funded through the National Science Foundation Grants Division of Environmental Biology (DEB) 123772.

TABLE OF CONTENTS

Abstract	2
Acknowledgements	4
Table of Contents	6
List of Figures	7
List of Tables	9
Chapter 1: Introduction	10
1.1: Background.....	10
1.2: Objectives	17
1.3: Study area	17
1.4: Significance	19
1.5: Data management	20
Chapter 2: Characterizing marsh vulnerability to erosion and inundation	28
2.1: Objective.....	28
2.2: Methods	28
2.3: Results and Discussion	43
Chapter 3: Wave-dampening effects of oyster reefs and marsh vegetation	81
3.1: Objective.....	81
3.2: Study sites	81
3.3: Methods	82
3.4: Results.....	85
3.5: Discussion.....	88
Chapter 4: Modeling site suitability for living shorelines	126
4.1: Objective.....	126
4.2: Methods	126
4.3: Results.....	134
4.4: Discussion.....	139
Conclusions	164
References	167
Appendix A	177

LIST OF FIGURES

Figure 1.1: Hardened shoreline and living shoreline images and diagrams	21
Figure 1.2: Conceptual diagram of waves and reef surface interaction.....	22
Figure 1.3: Diagram of hybrid living shoreline design	22
Figure 1.4: Map of the Virginia Coast Reserve	23
Figure 1.5: Geomorphic setting of major marsh groups	24
Figure 2.1: General methodology for MVI development	53
Figure 2.2: Map of Relative Wave Exposure	54
Figure 2.3: Map of elevation.....	55
Figure 2.4: Map of slope.....	56
Figure 2.5: Map of vegetation buffer width	57
Figure 2.6: Map of vegetation height.....	58
Figure 2.7: Map of distance to boat activity	59
Figure 2.8: Map of storm surge	60
Figure 2.9: Map of comparison sites	61
Figure 2.10: WAHV2 wind rose January 2010 - December 2015.....	62
Figure 2.11: Comparison between wave power and wave exposure	62
Figure 2.12: Comparison between WEMo, YV96, and SWAN wave models.....	63
Figure 2.13: Comparison between measured and predicted maximum wave height	63
Figure 2.14: Comparison between LiDAR-derived and RTK-GPS-measured elevation	64
Figure 2.15: Comparison between land cover and vegetation buffer width determination.....	65
Figure 2.16: Maps of hot spot analysis for individual vulnerability variables	66
Figure 2.17: Scree plot for principal components analysis.....	67
Figure 2.18: Summary of grouping analysis for principal components	67
Figure 2.19: Map of grouping analysis results	68
Figure 2.20: Map of MVI results	69
Figure 2.21: Percentage and length of shoreline in each MVI risk category.....	70
Figure 2.22: Map of hot spot analysis for MVI results.....	71
Figure 2.23: Comparison of hot spot analysis by marsh type.....	72
Figure 2.24: Comparison between DSAS and AMBUR shoreline change calculations	73
Figure 2.25: Maps of MVI output and historical erosion rates at three comparison sites	74
Figure 2.26: Linear regression between shoreline change and MVI results.....	75
Figure 2.27: Image of <i>Living Shoreline Explorer</i> app displaying MVI data	76
Figure 3.1: Map of field sites.....	91
Figure 3.2: Images of field sites.....	92
Figure 3.3: Schematic cross-section of generalized transect configuration.....	93
Figure 3.4: Wave gauge field set up	93
Figure 3.5: Map of Tom’s Cove study site and sampling stations	94
Figure 3.6: Map of Fowling Point study site and sampling stations	95
Figure 3.7: Map of Box Tree Idaho study site and sampling stations	96
Figure 3.8: Map of Man and Boy East study site and sampling stations.....	97
Figure 3.9: Map of Man and Boy South study site and sampling stations	98

Figure 3.10: Wachapreague station and wave gauge water level comparison	99
Figure 3.11: Wind speed and direction, water depth, wave height time series for TC1-16	100
Figure 3.12: Wind speed and direction, water depth, wave height time series for TC2-16	101
Figure 3.13: Wind speed and direction, water depth, wave height time series for TCV-16	102
Figure 3.14: Wind speed and direction, water depth, wave height time series for FP-16	103
Figure 3.15: Wind speed and direction, water depth, wave height time series for BTI-16	104
Figure 3.16: Wind speed and direction, water depth, wave height time series for BTI-17	105
Figure 3.17: Wind speed and direction, water depth, wave height time series for MBE-16	106
Figure 3.18: Wind speed and direction, water depth, wave height time series for MBE-17	107
Figure 3.19: Wind speed and direction, water depth, wave height time series for MBS-16	108
Figure 3.20: NWS Wallops Island wind rose July 2016 - June 2017	109
Figure 3.21: Stem height and width of <i>Spartina</i> and <i>Salicornia</i>	110
Figure 3.22: Vegetation characteristics at FP-16, BTI-16, and MBE-17	111
Figure 3.23: Regression analysis of waves at TC1-16	112
Figure 3.24: Regression analysis of waves at TC2-16	112
Figure 3.25: Regression analysis of waves at BTI-16	113
Figure 3.26: Regression analysis of waves at BTI-17	113
Figure 3.27: Regression analysis of waves at MBE-16	114
Figure 3.28: Regression analysis of waves at MBE-17	114
Figure 3.29: Regression analysis of waves at MBS-16	115
Figure 3.30: Reduction and growth of wave height across marsh at FP-16	116
Figure 3.31: Reduction of wave height across marsh at MBE-17	116
Figure 3.32: Reduction of wave height across marsh at BTI-16 and BTI-17	117
Figure 3.33: Regression analysis of waves at TCV-16	118
Figure 3.34: Interpolating reduction of wave height across marsh at MBE-17 and FP-16	119
Figure 3.35: Wave and vegetation characteristics at FP-16, BTI-16, and MBE-17	120
Figure 4.1: General methodology for LSEM development	144
Figure 4.2: Map of Relative Wave Exposure	145
Figure 4.3: Map of distance to boat activity	146
Figure 4.4: Map of elevation	147
Figure 4.5: Map of slope	148
Figure 4.6: Map of vegetation buffer width	149
Figure 4.7: Map of LSEM results	150
Figure 4.8: Percentage and length of shoreline in each LSEM design output	151
Figure 4.9: Map of comparison sites	152
Figure 4.10: Maps of LSEM and LSSM recommendations for three sites	153
Figure 4.11: Map of VMRC living shoreline projects	154
Figure 4.12: Comparison between LSEM and living shoreline project plans	155
Figure 4.13: Maps of hardened structures at Upshur Neck	156
Figure 4.14: Maps of hardened structures and bathymetry at Oyster	156
Figure 4.15: Image of <i>Living Shoreline Explorer</i> app displaying LSEM data	157

LIST OF TABLES

Table 1.1: Summary of previous coastal vulnerability assessments	25
Table 1.2: Summary of previous living shoreline suitability assessments	26
Table 1.3: Model variables used by VIMS suitability model	26
Table 1.4: Conditions suitable for soft stabilization	27
Table 1.5: Conditions suitable for hybrid stabilization.....	27
Table 2.1: Summary of variables used for MVI	77
Table 2.2: MVI reclassification matrix	78
Table 2.3: Comparison between LiDAR-derived and field measured vegetation height	78
Table 2.4: Percent of shoreline within each MVI risk class	79
Table 2.5: PCA rotated component matrix	79
Table 2.6: MVI range for sequential levels of vulnerability.....	80
Table 2.7: MVI summary statistics for three comparison sites.....	80
Table 3.1: Summary of constructed oyster reef and marsh characteristics.....	121
Table 3.2: Field deployment schedule	121
Table 3.3: Summary of hours flooded for marsh sampling sites	122
Table 3.4: Summary of water depth, wind speed, and wave height	122
Table 3.5: Comparison between inner and outer station water levels	123
Table 3.6: Summary of vegetation characteristics	123
Table 3.7: Studies reporting <i>Spartina</i> and <i>Salicornia</i> vegetation characteristics	124
Table 3.8: Comparison of waves across constructed oyster reefs.....	124
Table 3.9: Wave summary across marsh sites	125
Table 3.10: Marsh buffer width interpolation at FP-16 and MBE-17	125
Table 4.1: Summary of variables used for LSEM	158
Table 4.2: LSEM data inventory.....	159
Table 4.3: LSEM reclassification scheme.....	160
Table 4.4: Living shoreline design output	160
Table 4.5: Summary of possible variable combinations for design outputs	161
Table 4.6: LSEM summary statistics for three comparison sites.....	161
Table 4.7: LSEM and LSSM recommendations at three comparison sites	162
Table 4.8: LSEM recommendations, VIMS decision tree tool, and permit comparisons	163

CHAPTER 1

INTRODUCTION

1.1 Background

Salt marshes

Salt marshes are a dynamic interface between land and water. Humans derive more ecosystem services (i.e., quantifiable benefits) from salt marshes than any other coastal environment (Gedan et al. 2009). Coastal wetlands support nursery habitat for fishes (Minello et al. 2003; Costa et al. 1994) and birds (Gjerdrum et al. 2005; Benoit and Askins, 2002); improve water quality (Cui et al. 2009); sequester carbon (Mcleod et al. 2011); and mitigate the impacts of storms (Möller et al. 1999). Changes in the physical and climatological processes that support salt marshes (e.g., sediment supply, inundation, wave climate) can have profound ecologic, economic, and societal consequences for coastal communities (Costanza et al. 2014).

Increasingly, natural and anthropogenic processes are threatening salt marshes worldwide (Gedan et al. 2009). Storms (Schwimmer, 2001), sea level rise (Kirwan and Megonigal, 2013), and human impacts (Kirwan and Megonigal, 2013) are the primary drivers of coastal wetland loss. The frequency of storm events – known to cause salt marsh retreat in shallow coastal bays (Leonardi et al. 2016) – has increased along the Virginia coast over the last century (Hayden and Hayden, 2003). Ecogeomorphic feedbacks between sediment deposition, inundation, and vegetation growth enable salt marshes to accrete vertically and keep pace with conservative projections of sea level rise (Kirwan et al. 2010), but human activities (e.g., conversion for agriculture and aquaculture, hardened shoreline stabilization structures) disrupt these feedbacks, leading to salt marsh drowning and instability (Kirwan and Megonigal, 2013). The ability of a

salt marsh to migrate landward (i.e., transgress) is also an important survivorship factor in the face of sea level rise (Brinson et al. 1995). A developed upland slope prevents overland migration; and, combined with marsh edge erosion, leads to salt marsh loss (Brinson et al. 1995).

Wave energy – the dominant force behind erosional processes at marsh-bay boundaries (McLoughlin et al. 2015) – is positively correlated with wind speed and water depth (Mariotti et al. 2010). Consequently, increased storminess (i.e., higher wind speed) and sea level rise (i.e., deeper water) are expected to escalate wave energy; and, as a result, amplify coastal erosion problems (Mariotti et al. 2010; Hayden and Hayden, 2003). Given the destructive capacity of wave attack, landowners are pressured to install shoreline stabilization structures to protect valuable property (Culp, 2007; Burke et al. 2005), further exacerbating the loss of salt marshes (Kirwan and Megonigal, 2013).

Shoreline stabilization

Hard stabilization – often termed “shoreline armoring” – is common along Virginia’s coastline (Figure 1.1) (Moon, 2012; Duhring et al. 2006). Hardened structures are valued by coastal engineers because they are effective at reflecting waves away from the shoreline (Scyphers et al. 2011; Plant and Griggs, 1992). However, there is growing concern that these coastal modifications have physical and biological tradeoffs (Bilkovic and Mitchell, 2013; Duhring et al. 2006; Burke et al. 2005). Shore-parallel structures (e.g., seawalls, revetments, and bulkheads) can fragment or destroy intertidal habitats (Peterson et al. 2000; Douglass and Pickel, 1999; Plant and Griggs, 1992), alter vegetation and benthic community structure (Bilkovic and Mitchell, 2013), disrupt sediment budgets (Bozek and Burdick, 2005; Lee et al. 1999), and increase wave energy at adjacent properties (Moon, 2012; Scyphers et al. 2011). These adverse effects on coastal habitats and organisms are well-documented and have increased interest in

nature-based solutions that balance erosion control and ecological services (Bilkovic and Mitchell, 2013; Duhring et al. 2006; Burke et al. 2005).

A promising alternative to hard stabilization lies in management treatments called “living shorelines,” which utilize soft (i.e., non-structural) or hybrid (i.e., structural and non-structural) designs to stabilize the shoreline while maintaining ecosystem functions (Duhring et al. 2006; Burke et al. 2005). The living shoreline approach aims to preserve connectivity between terrestrial, intertidal, and marine habitats (Currin et al. 2010). Materials used for living shoreline treatments most often consist of natural vegetation, beach nourishment, fiber logs, rock sills (i.e., low, offset, shore-parallel wall), constructed oyster reefs, or a combination thereof (Figure 1.1) (Duhring, 2006). Quantitative studies offer encouraging findings that living shorelines address erosion control without severing natural processes and connections (Bilkovic and Mitchell, 2013; Toft et al. 2013; Duhring et al. 2006; Burke et al. 2005). Oyster reefs (natural or constructed) and marsh vegetation, in particular, can stabilize and protect the shoreline by modifying the local physical environment through wave attenuation and sediment trapping (Kirwan et al. 2016; Borsje et al. 2011; Murray et al. 2002).

Oyster reefs

Field studies have investigated the efficacy of constructed oyster reefs in attenuating waves in Virginia’s coastal bays (Wiberg et al. *in revision*; Kremer, 2016; Taube, 2013) and in the Gulf and Mid-Atlantic United States (Scyphers et al. 2011; Stricklin et al. 2010; Piazza et al. 2005; Meyer et al. 1997). Taube (2013) found that wave power was reduced by 49% averaged over three reef sites in Virginia coastal bays. Oyster reefs in low energy environments can significantly reduce wave energy at intermediate water depths above the reef crest, but are less effective at dissipating waves in deep water conditions (e.g., storm surge events) because wave

orbitals do not interact with the reef surface (Wiberg et al. *in revision*; Taube, 2013; Piazza et al. 2005) (Figure 1.2). These studies indicate that constructed oyster reefs can attenuate waves and reduce erosion, but their efficacy may be limited by specific hydrologic conditions. The use of constructed oyster reefs for shoreline stabilization is considered a hybrid stabilization technique because it combines soft (the existing marsh) and hardened (the reef structure) design elements.

Marsh vegetation

Planting marshes to attenuate waves and control erosion has proven a successful restoration technique in the Chesapeake Bay region under lower energy conditions (Hardaway and Byrne, 1999; Garbisch and Garbisch, 1994). Wave dissipation is most dependent on stem density and vegetation height (Möller, 2006). Field measurements in the United Kingdom indicate salt marshes can reduce wave energy up to 50% over the first 10-20 meters (Möller, 2006; Möller et al. 1999). The presence of marsh vegetation can cause significant attenuation even during storm surge conditions (Möller et al. 2014). For water depth of 2 meters and wave heights up to 0.9 meters, Möller et al. (2014) found 16.9% wave dissipation over a 40-meter marsh transect. Moreover, Gittman et al. (2014) observed that marshes with or without sills were more durable and effective than traditional bulkheads during Category 1 hurricane conditions. The use of natural marsh vegetation in living shoreline design is known as marsh enhancement and is considered a soft stabilization method.

Reef-marsh pairing

Combining constructed oyster reefs with vegetated treatments for erosion control is appealing because it provides hard coastal defense of the marsh edge while allowing restoration and expansion of wave attenuating wetlands, increasing the effectiveness of shoreline protection

services (Gedan et al. 2011) (Figure 1.3). Thus, reef-marsh pairings may offer a sustainable and cost-effective long-term coastal protection solution (Gedan et al. 2011; Borsje et al. 2011; Duhring et al. 2006). However, an established framework to decide which, when, and where living shorelines should be applied is lacking (Borsje et al. 2011; Duhring et al. 2006). For living shorelines to perform shoreline stabilization and ecosystem maintenance effectively, they must be properly designed and placed according to individual shoreline needs (Crichton, 2013); therefore, stakeholders and decision-makers need to understand the variables influencing coastal vulnerability.

Coastal vulnerability assessments

The objective assessment of coastal vulnerability to erosion and inundation is facilitated through the development of dimensionless indices that relate physical, biological, and climatological variables in a quantifiable manner. Several studies have mapped the vulnerability of coastal environments using a GIS-based Coastal Vulnerability Index (CVI) or Sensitivity Index (SI) (Table 1.1). These studies provide a vulnerability determination for shoreline segments by analyzing and overlaying spatial data for variables known to contribute to coastal erosion and inundation. However, most coastal vulnerability assessments are generated over a low spatial resolution, and none have been developed specifically for the fringing salt marshes of the wave-dominated, microtidal environment of Virginia's coastal bays.

In a microtidal zone, wind-waves are the driving force behind erosion (McLoughlin et al. 2015); therefore, a vulnerability assessment that emphasizes the wave climate and marsh stability is important. Most coastal vulnerability studies assess factors related to wave climate (e.g., coastal exposure, wave height, storm statistics), but not at a scale that can accurately resolve spatial variation along a salt marsh shoreline. The highest resolution vulnerability assessment

discovered through literature review (Tibbetts and van Proosdij, 2013) was generated at a spatial resolution of 250 meters; Phillips (1986) found that shoreline segments closer than 100 meters could differ in shoreline change (i.e., erosion or accretion) by more than a meter. While lower resolution coastal vulnerability indices provide insight into which variables are most influential and where shoreline change may occur, their generalized simplicity leaves room for improvement; and, as such, can be viewed as a base for developing a more refined and site-specific inventory of variables influencing coastal vulnerability. Capturing spatial variation along a shoreline is important to stakeholders; therefore, higher resolution is needed to effectively identify and prioritize vulnerable shorelines. A well mapped landscape – facilitated by a high-resolution coastal vulnerability assessment – serves as a foundation for the development of nature-based shoreline stabilization recommendations.

Living shoreline site suitability

Site suitability analysis for living shoreline installations is complex; and, only a few decision-support tools exist to guide coastal stakeholders toward recommended treatments based on shoreline characteristics (CCRM, 2015) (Table 1.2). Several of these studies (e.g., Zylberman, 2016; Boyd et al. 2014; Carey, 2013) conducted Geographic Information System (GIS)-based analyses to model site suitability of living shorelines based on adjustments made to the Living Shoreline Suitability Model (LSSM) developed by Berman and Rudnicky (2008) for the Center for Coastal Resources Management (CCRM) at the Virginia Institute of Marine Science (VIMS). The LSSM was designed for use in a GIS environment and used spatial information of coastal characteristics to determine where the use of living shorelines was appropriate (Berman and Rudnicky, 2008). The LSSM is a binary spatial model, meaning it provides a straightforward “yes” or “no” assessment of a site according to specified design output criterion. Variables used

to quantify suitability by the LSSM included fetch, bathymetry, marsh presence, beach presence, bank condition, and tree canopy presence (Berman and Rudnicky, 2008) (Table 1.3). The model provides a suitability determination for shoreline segments by analyzing and overlaying spatial data for suitability variables. Model output includes recommendations for soft or hybrid stabilization and identifies areas where living shorelines are not suitable. Table 1.4 and 1.5 summarize the conditions considered suitable for soft and hybrid stabilization by the LSSM.

The implementation of living shoreline suitability analysis is site-specific and data quality dependent. Model thresholds developed for other sites may not be appropriate for Virginia's coastal bays. For example, Carey (2013) considered shorelines within 3.2 kilometers of a boat access ramp to be unsuitable for living shorelines. This threshold distance is likely too great for Virginia's coastal bays, where most inlets and harbors extended no more than 800 meters inland and open into wide, shallow bays. For living shoreline suitability tools to recommend the most appropriate action, current, high-resolution shoreline data is essential. Data sources used by previous studies, especially those characterizing the wave environment, may not provide the necessary resolution for meaningful site evaluation. For example, Berman and Rudnicky (2008) used fetch as a measure of the wave climate for the LSSM. Fetch is the overwater distance wind can blow and generate waves (Fagherazzi and Wiberg, 2009). Fetch was determined by the CCRM Exposure Model as the longest fetch length regardless of dominant wind direction cast every 100 meters along a shoreline (Berman and Rudnicky, 2008). This method does not capture other factors that contribute to wave climate, like water depth and wind characteristics. Effective determination of living shoreline suitability for a study area requires the curation of site-specific, current, and high-resolution data layers.

1.2 Objectives

The purpose of this study was to develop a better understanding of the characteristics that contribute to the vulnerability of fringing salt marshes and to suggest appropriate shoreline stabilization techniques. The three objectives of this study were to:

- Develop a Marsh Vulnerability Index (MVI) to quantify and map physical, biological, and climatological variables that contribute to salt marsh erosion and inundation.
- Measure the wave-dampening effects of fringing constructed oyster reefs and marsh vegetation to drive empirically-based shoreline stabilization recommendations.
- Design a Living Shoreline Explorer Model (LSEM) to determine site suitability of nature-based shoreline stabilization methods given shoreline-specific characteristics.

1.3 Study area

The study area encompasses the salt marshes fringing shallow coastal bays found within the Virginia Coast Reserve (VCR), a 100-kilometer long barrier-lagoon-marsh system on the Atlantic side of the Delmarva Peninsula, USA (Figure 1.4). The VCR – the longest expanse of coastal wilderness on the eastern seaboard – is managed by The Nature Conservancy (TNC) and was designated a biosphere reserve by the US Man and the Biosphere (MAB) program in 1979 (Hayden et al. 1991). In 1987, the VCR became the first coastal site in the national Long-Term Ecological Research (LTER) network (www.vcrlter.virginia.edu).

Fourteen undeveloped barrier islands form a double shoreline with the mainland peninsula to enclose intertidal and subtidal basins characterized by shallow tidal flats (1 meter below MLLW) and deep channels (10 meters below MSL) (Oertel, 2001). Several relatively stable tidal inlets connect the shallow lagoons to the Atlantic Ocean (Safak et al. 2015). The tides are semidiurnal,

and the mean tidal range is 1.2 meters (microtidal). Mean higher high water (MHHW) is 0.68 meter while mean lower low water (MLLW) is -0.70 meter with respect to mean sea level (MSL) (Leonardi and Fagherazzi, 2014). Residence time is sensitive to location and ranges from 6 hours or less near tidal inlets to weeks near the mainland (Safak et al. 2015). The rate of relative sea level rise in the region is $3.8 - 4.0 \text{ mm}\cdot\text{yr}^{-1}$, slightly exceeding the global average (NOAA Tides and Currents, 2015; IPCC, 2013). Dominant wind directions in the study area are from the N-NE and SSE-SSW with the highest winds coming from the NW and NE (Fagherazzi and Wiberg, 2009).

Approximately 52% of the total land area of the VCR is composed of salt marshes (NOAA C-CAP, 2010). These salt marshes can be further described according to their geomorphic setting: mainland marsh, marsh island, and backbarrier marsh (Brinson et al. 1995; Oertel et al. 1992) (Figure 1.5). Salt marsh vegetation is dominated by *Spartina alterniflora* (Brinson et al. 1995). There are two growth forms of *Spartina alterniflora*: tall-form *Spartina alterniflora* is less dense (i.e., fewer plants per unit area) and can reach stem heights of 2-3 meters (Valiela et al. 1978) and short-form *Spartina alterniflora* grows densely and exists within a height range between 10 and 40 cm (Valiela et al. 1978). Near the transition from intertidal (low) marsh to high marsh, *Distichlis spicata*, *Spartina patens*, and *Salicornia europaea* are present (Brinson et al. 1995).

Although there are no major urbanized areas within the VCR, this relatively pristine network of shallow bays, salt marshes, mudflats, forest uplands, and barrier and marsh islands is increasingly threatened by incompatible development, agriculture, fishing, forestry, and recreation practices (nature.org). The major land use within the VCR is agriculture (38% of land cover), with poultry farming becoming an especially important industry (Safak et al. 2015;

Stanhope et al. 2009). Watershed catchments are small; freshwater and nutrient inputs to the shallow bays occur through groundwater and approximately 56 streams (Stanhope et al. 2009).

1.4 Significance

Incorporating high-resolution shoreline vulnerability data into publically accessible online mapping platforms enables planners, officials, managers, and citizens to visualize interpreted research data at a scale that enables informed shoreline management decisions. The results of this research were integrated into the TNC *Coastal Resilience* platform which provides a publicly accessible web mapping decision-support tool to support coastal hazard mitigation and climate adaptation planning (coastalresilience.org). Specifically, data from this study drives the Living Shoreline Explorer (LSE) app, which illustrates shoreline vulnerability information for Virginia's coastal bays and provides recommendations for nature-based shoreline stabilization solutions (coastalresilience.org). The LSE app will help planners and managers identify and prioritize vulnerable shorelines through the use of the Marsh Vulnerability Index (MVI). Restoration managers will benefit from a synthesized repository of shoreline data that can be used to pursue nature-based shoreline stabilization solutions recommended by the Living Shoreline Explorer Model (LSEM). Field measurements collected for this study provide empirical evidence that nature-based solutions – combining constructed oyster reefs with marsh vegetation – may present an effective and sustainable long-term shoreline stabilization technique.

1.5 Data management

All spatial and tabular data from this study is archived and publically available through the VCR Data Catalog (<http://www.vcrlter.virginia.edu/home1/?q=dataCatalog>) and the Long-Term Ecological Research (LTER) data portal (portal.lter.net). Metadata for all spatial data is

included within vector and raster files in accordance with Federal Geographic Data Committee standards. All data is viewable on the TNC *Coastal Resilience* web mapping tool (<http://maps.coastalresilience.org/virginia/>).

Figures



Figure 1.1. Hardened shoreline constructed of stone revetment in Oyster, VA (*upper left*) (author). Living shoreline treatment constructed with Oyster Castles® at Man and Boy marsh, VA (*upper right*) (Lusk, 2015). Schematic of a traditional bulkhead (*lower left*) and of a living shoreline (*lower right*) (TNC, 2017).

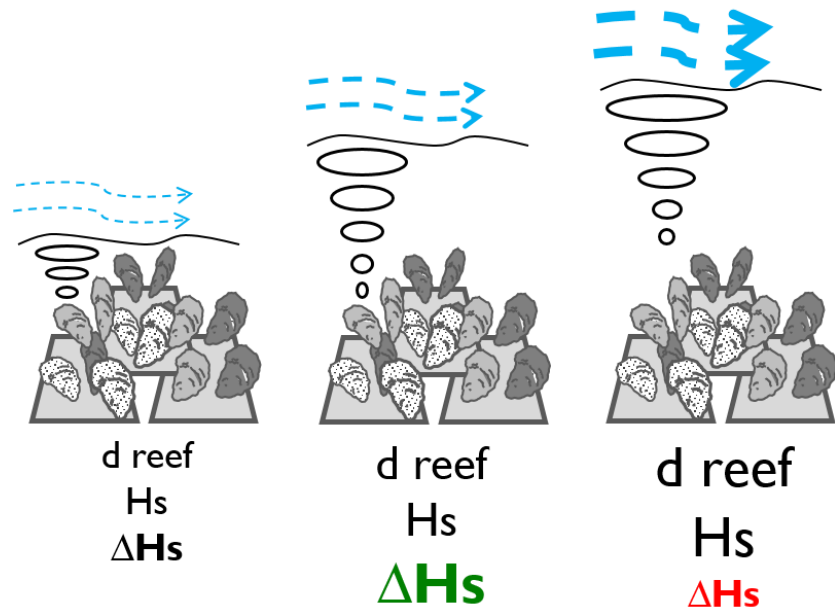


Figure 1.2. Diagram of wave dynamics over oyster reef under different water depth conditions. This diagram illustrates that as water depth increases to intermediate water depths above the reef crest, wave attenuation (ΔH_s) increases. However, wave attenuation is decreased in deeper water conditions (e.g., storm surge events) because wave orbitals do not interact with the reef surface. Figure modified from Taube (2013).

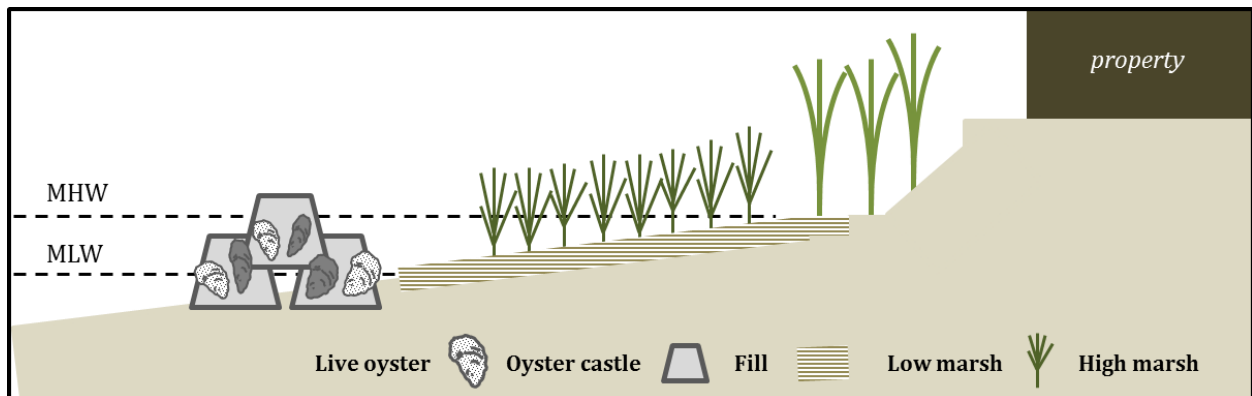


Figure 1.3. Schematic of hybrid living shoreline design with constructed oyster reef and existing marsh vegetation.

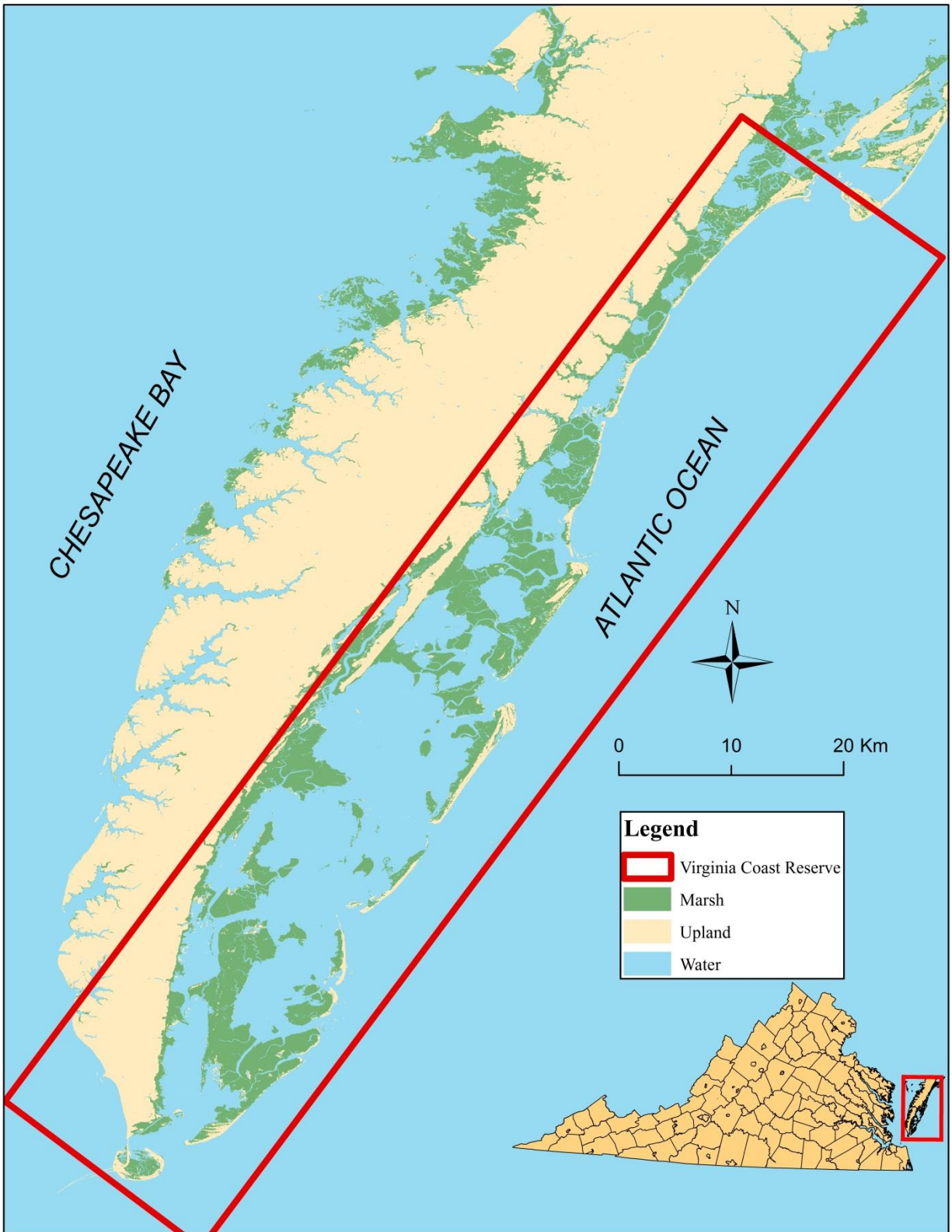


Figure 1.4. Map of the Virginia Coast Reserve. Land cover derived from NOAA’s Coastal Change Analysis Program Land Cover Data for 2010 (NOAA C-CAP, 2010).



Figure 1.5. Three major groups of salt marshes based on geomorphic setting in the Virginia Coast Reserve: mainland marshes, marsh islands, and backbarrier marshes. Figure modified from Brinson et al. (1995). Land cover derived from NOAA's Coastal Change Analysis Program Land Cover Data for 2010 (NOAA C-CAP, 2010).

Tables

Study	Location	Resolution	Equation	Variables
Tibbetts and Proosdij, 2013	Bay of Fundy, Canada	250 m	Weighted sum	Freeboard, coastline exposure, width of foreshore, presence of vegetation, coastal slope, observed erodibility, anthropogenic or natural protection, morphological resilience
Chandrasekar et al. 2013	Southern India	Not reported	Square root of geometric mean	Geomorphology, shoreline change rate, coastal slope, RSLR, mean wave height, mean tide range
Abuodha and Woodroffe, 2010	Southeast Australia	1.5 km	Square root of geometric mean	Rock types, coastal slope, geomorphology, barrier type, shoreline, shoreline change, RSLR, mean wave height, mean tide range
Kumar et al. 2010	Eastern India	1 km	Square root of geometric mean	Shoreline change rate, RSLR, coastal slope, significant wave height, tidal range, coastal regional elevation, coastal geomorphology, tsunami run-up
Pendleton et al. 2010	Gulf of Mexico, U.S.	~5.5 km	Square root of geometric mean	Geomorphology, historical shoreline change rate, regional coastal slope, RSLR, mean significant wave height, mean tidal range
Ozyurt and Ergin, 2010	Göksu Delta, Turkey	Not reported	Weighted sum / by sum of least vulnerable	RSLR, geomorphology, coastal slope, significant wave height, sediment budget, tidal range, proximity to coast, type of aquifer, hydraulic conductivity, depth to groundwater, river discharge, water depth, human parameters
Nageswara Rao et al. 2008	Andhra Pradesh, India	1.5 km	Weighted sum	Geomorphology, coastal slope, shoreline change, mean spring tide, significant wave height
Hegde and Reju, 2007	Mangalore, India	~110 km	Mean	Slope, geomorphology, population, erosion rate
Boruff et al. 2005	U.S. Coasts	Coastal counties	Square root of geometric mean	Social variables, mean tidal range, coastal slope, RLSR, shoreline erosion, mean wave height, geomorphology
Pendleton et al. 2004	Assateague Island, MD/V.A, U.S.	1.5 km	Square root of geometric mean	Geomorphology, historical shoreline change rate, regional coastal slope, RSLR, mean significant wave height, mean tidal range
Thieler and Hammar-Klose, 1999	U.S. Atlantic Coast	100 km	Square root of geometric mean	Geomorphology, RSLR, shoreline erosion, mean tide range, mean wave height
Shaw et al. 1998	Canadian coast	Not reported	Square root of geometric mean	Relief, rock type, landform, RSLR, shoreline displacement, tidal range, one year maximum wave height
Gornitz et al. 1994	U.S. Southeast	~375 m	Weighted sum	Elevation, geology, landform, RSLR, shoreline erosion, mean tide range, maximum wave height, annual tropical storms, annual hurricane prob., hurricane frequency, mean forward velocity, annual mean no. cyclones, mean hurricane surge
Gornitz et al. 1991	U.S. Coasts	~14 km	Square root of geometric mean	Relief, rock type, landform, RSLR, shoreline displacement, tidal range, wave height

Table 1.1. Summary of previous coastal vulnerability assessments.

Studies	Location	Variables
Dobbs et al. 2017	Florida	Bathymetry, land use, land value, population, sensitive shoreline, tree canopy, wave energy
Zylberman, 2016	Connecticut	Fetch, bathymetry, marsh presence, beach presence, erosion
Boyd et al. 2014	Alabama	Slope, shoreline condition, erosion, soil, fetch
Carey, 2013	North Carolina	Fetch, boat traffic, water depth, marsh presence, submerged aquatic vegetation presence
Berman and Rudnicky, 2008	Maryland	Fetch, bathymetry, marsh presence, beach presence, bank condition, and tree canopy presence

Table 1.2. Summary of previous living shoreline site suitability assessments.

Attribute	Values
Fetch	Low (0 – 1.0 mile) Moderate (1.0 – 5.0 miles) High (>5.0 mile)
Bathymetry	1m contour >10m from shoreline
Marsh presence	Present/Absent
Beach presence	Present/Absent
Bank condition	High: observed erosion Low: no observed erosion Undercut: bank toe erosion
Tree canopy	Present/Absent

Table 1.3. Model variables used by the LSSM. Table modified from Berman and Rudnicky (2008).

Attribute	Values
Fetch	Low (0 – 1.0 mile)
Bathymetry	Shallow (1m contour >10m from shoreline)
Marsh presence	Yes or no
Beach presence	Yes or no
Bank condition	High: observed erosion Low: no observed erosion
Tree canopy	No

Table 1.4. Conditions suitable for soft stabilization for the LSSM. Table modified from Berman and Rudnicky (2008).

Attribute	Values
Fetch	Low (0 – 1.0 mile) Moderate (1.0 – 5.0 miles)
Bathymetry	Shallow (1m contour >10m from shoreline)
Marsh presence	Present/Absent
Beach presence	Present/Absent
Bank condition	High: observed erosion Low: no observed erosion Undercut: bank toe erosion
Tree canopy	Present/Absent

Table 1.5. Conditions suitable for hybrid stabilization for the LSSM. Table modified from Berman and Rudnicky (2008).

CHAPTER 2

CHARACTERIZING MARSH VULNERABILITY TO EROSION AND INUNDATION

2.1 Objective

The first objective of this study was to quantify and map physical, biological, and climatological variables that contribute to salt marsh erosion and inundation within the Virginia Coast Reserve (VCR). Using remote sensing data and GIS, an index model called the Marsh Vulnerability Index (MVI) was developed. The MVI is a spatial modeling tool which assesses the vulnerability potential of salt marshes. MVI results reveal the spatial distribution of salt marsh vulnerability and provide insight into which vulnerability variables are most influential. Data from this study drives the Living Shoreline Explorer (LSE) app on the TNC *Coastal Resilience* web mapping decision-support platform which illustrates salt marsh vulnerability information for coastal stakeholders.

2.2 Methods

Selection of index variables

This study was conducted for fringing salt marshes within the VCR where wind-waves are the driving force of coastal processes (McLoughlin et al. 2015); therefore, factors that influence or attenuate wave climate were prioritized. Based on literature review, eight variables were identified (Table 2.1). Wave exposure, elevation, slope, relative sea level rise (RSLR) rate, and storm surge are common variables included in coastal vulnerability assessments. Vegetation height, vegetation buffer width, and distance to boat activity have either not been considered in previous coastal vulnerability assessments or were measured using a different metric. For example, Tibbetts and van Proosdij (2013) considered the presence of vegetation by type (e.g.,

shrub, forest), but not by physical characteristics (e.g., stem height, marsh buffer width). These additional variables were included due to their impact on wave attenuation over marshes and non-wind-wave action.

Model development

Vulnerability data includes quantitative and qualitative information at different resolutions and units; therefore, coastal vulnerability assessments commonly create a vulnerability matrix by ranking original data values by risk classes from 1 to 5 in order of increasing vulnerability (Gornitz et al. 1991). The resultant vulnerability matrix used for this study can be found in Table 2.2. A description of how range divisions were determined for each risk class is outlined in the following section.

Index values are generated for shoreline segments by combining risk classes, often by computing the square root of the product mean (Gornitz et al. 1991). This method accounts for omission and misclassification errors, expands the range of values, and compresses extremes (Gornitz et al. 1994). The MVI developed here was computed based on the following equation and vulnerability parameters: a = wave exposure, b = elevation, c = slope, d = RSLR rate, e = storm surge, f = vegetation height, g = vegetation buffer width, and h = distance to boat activity.

$$MVI = \sqrt{\left(\frac{a * b * c * d * e * f * g * h}{8}\right)}$$

All geospatial processing for the MVI was done within the Esri ArcGIS 10.5 platform. First, a system-wide shoreline was selected, the “Coastal Waters – Virginia and Vicinity” shoreline. This shoreline is an integrated feature class generated from the VIMS Comprehensive Coastal Inventory (CCIM) Mean High Water Shoreline Position (sourced from USGS 1:24,000 Digital

Line Graph Hydro Dataset) and 2011 National Agricultural Imagery Program (NAIP) aerial photography (Coastal Water, 2017). A coastal grid was developed along the shoreline with cell dimensions of 30 x 30 meters. Datasets varied in spatial resolution; therefore, all raster datasets were resampled to a 30-meter spatial resolution and extracted to the coastal grid. The “distance to boat activity” dataset, a point feature dataset, was converted to a raster dataset with 30-meter spatial resolution. Vulnerability variables were then reclassified from 1 (very low) to 5 (very high) based on range divisions defined in Table 2.2. An MVI value was calculated for each coastal grid cell by inputting the reclassified variables into Equation (1). The MVI output is a 30-meter resolution feature class dataset for VCR shorelines. Each coastal grid cell (900 m²) contains an index value that represents the vulnerability of the underlying shoreline segment to erosion and inundation. Higher index values translate to higher vulnerability. Figure 2.1 provides a general schematic of the methodology described above.

The MVI was designed to identify vulnerability potential along marsh-bay boundaries in shallow estuarine environments; therefore, it cannot reliably model tidal channels, the deeper estuarine environment of the Chesapeake Bay, or the ocean-facing shoreline of the barrier islands. Consequently, the Chesapeake Bay, Atlantic Ocean-facing shorelines, and tidal channels were excluded from the analysis. The MVI considered mainland marshes, marsh islands, and backbarrier marshes; the total length of shoreline assessed in the VCR was 1,172 kilometers.

Data collection and ranking

A description of how each of the eight vulnerability variables was quantified for use in the development of the MVI is outlined in the succeeding paragraphs. Figures 2.2 – 2.8 depict each variable in raw form extracted to the coastal grid; however, with the exception of wave exposure (which was calculated for discrete points along the shoreline), each dataset is also available for

the entire system. The accuracy of the MVI is limited to the quality and type of data used. When possible, data were compared to numerical models, field observations, and field samples that were calculated, measured, or collected for sites throughout the study area. Figure 2.9 shows the location of each site used in this validation process.

Wave exposure

Significance

Wind-wave exposure drives erosion at marsh boundaries (McLoughlin et al. 2015). Shorelines that are very exposed to wave action tend to experience a uniform erosion rate while sheltered sites experience more episodic and lower erosion rates (Leonardi and Fagherazzi, 2014). Wave energy is positively correlated with water depth, fetch, and wind characteristics (speed, direction, and duration) (Mariotti et al. 2010). Fetch is defined as the unobstructed distance over which wind can blow and is determined by wind direction and water level (Fagherazzi and Wiberg, 2009). Wind-waves are formed by an energy transfer from wind to the water surface; therefore, larger fetch (longer distance) facilitates the formation of higher energy waves (Rohweder et al. 2008). Water depth limits how large waves can grow for a given wind speed and fetch. Because Virginia's coastal bays are shallow, waves there tend to be small (heights on order of 10s of centimeters and periods of a few seconds).

Processing

The numerical Wave Exposure Model (WEMo) 4.0 developed by the NOAA National Centers for Coastal Ocean Science (NCCOS) was used to quantify the effect of wind-wave exposure. WEMo is a software tool that works in association with Esri ArcGIS. The model calculates wave height and wave energy by taking into account the effects of wind speed,

direction and frequency; local bathymetry; and, shoreline shape (Fonseca and Malhotra, 2010). WEMo's Representative Wave Energy (RWE) mode is based on linear wave theory and represents the combined effect of wave generation, propagation, and dissipation over weighted fetch to account for shoreline irregularities (Fonseca and Malhotra, 2010).

RWE (Figure 2.2) was generated for the study area using local bathymetry from the Integrated Topography and Bathymetry dataset for the Eastern Shore of Virginia (Richardson et al. 2014), shoreline data generated by VIMS CCIM, and wind data from the NOAA Station WAHV2 at Wachapreague, VA for the period of 1 January 2010 - 31 December 2015 (www.tidesandcurrents.noaa.gov). Winds were assumed uniform throughout the VCR (McLoughlin et al. 2015; Mariotti et al. 2010). Winds tended to most frequently blow from the southwest, with less frequent but occasionally strong winds from the northeast (Figure 2.10). The top 5% of wind speed events was used for analysis, which translates to wind events $>7.2 \text{ m}\cdot\text{s}^{-1}$ for the study period. Top 5% wind events primarily blew from $15^\circ - 225^\circ$ (northeast to southwest).

Validation

RWE values were compared to the Wind Wave Tidal Model (WWTM) results for the VCR. WWTM was developed by Mariotti et al. (2010) and is a finite-element model with a module for calculating wave power at marsh boundaries. Mariotti et al. (2010) found that wave energy at the marsh edge is sensitive to wind direction and identified a clear spatial pattern in the distribution of wave power and wind direction throughout the study area (Figure 2.11a). Visual analysis reveals a similar pattern in the spatial distribution of WEMo-calculated wave exposure and wind direction; generally, the highest values of wave exposure are found on the marsh boundaries facing northeast and south/southeast (the direction from which most of the top 5% wind speed

events occur) (Figure 2.11b). A discrepancy between the two models was noted along mainland marshes (e.g., BTI; Figure 2.9), where RWE results tended to be higher than WWTM results

McLoughlin et al. (2015) calculated and validated wave energy values for four sites in the study area – Matulakin Marsh (MM), Chimney Pole (CP), Hog Island (HI), and Fowling Point (FP) (Figure 2.9) – using the Young and Verhagen (1996) (YV96) parametric wave model and the Simulating Waves Nearshore (SWAN) spectral wave model. YV96 and SWAN model output indicates that MM received the highest wave energy while FP received the lowest wave energy relative to the other sites (McLoughlin et al. 2015) (Figure 2.12). Results from this study characterize MM, CP, and HI as eroding marshes, while FP as a stable marsh (McLoughlin et al. 2015). WEMo-calculated wave exposure indicates MM received the highest wave exposure of the four sites; however, FP received the second highest wave exposure (Figure 2.12). This seems counterintuitive given that FP is considered a stable marsh and high wave exposure would suggest higher lateral erosion rates (i.e., instability). The discrepancy between the relative ordering of the four sites by the three models is likely due to the use of top 5% wind events for analysis in WEMo. The MM marsh boundary faces south-southwest, and the FP marsh boundary faces southeast. As a result, both shorelines are subjected to a greater proportion of top 5% wind events. The CP marsh boundary is oriented west-southwest and receives some top 5% wind events. HI, however, is oriented northwest, and is therefore exposed to the least top 5% wind events.

RWE mode also generates values for maximum wave height (H_{max}). These values were compared to in situ wave data collected by wave sensors at a small marsh island located within the study area named Man and Boy (MB) (Figure 2.9). The time series of wave data was from May 9 - 31, 2017. Predicted H_{max} was averaged for consecutive 12-hour periods over five days to

expedite processing time and provide sufficient wind data for the model. Measured H_{max} was averaged over the same 12-hour periods. Figure 2.13 shows a scatterplot of predicted maximum wave heights and measured maximum waves heights. Maximum wave heights measured at MB were highly correlated with predicted wave heights ($R^2 = 0.92$).

Overall, WEMo-calculated wave exposure showed good agreement with other numerical models (WWTM, YV96, and SWAN) and excellent agreement with field measurements. Higher than expected wave exposure predictions may occur for some sites due to the wind statistics analysis method (i.e., using the top 5% wind events). Separation-distance between wind station and wave sensor sites (Malhotra and Fonseca, 2007) and errors in bathymetry data may introduce additional discrepancies. Further validation should include comparing WEMo-predicted maximum wave heights to more wave data measured in the field at a variety of sites with different shoreline orientations. Additionally, WEMo-calculated wave exposure using all available wind data should be explored.

Ranking

Shorelines with higher RWE values are considered to have a higher vulnerability (Tibbetts and van Proosdij, 2013). A study by Theuerkauf et al. (2016) found that natural oyster reefs did not persist at wave exposure values over $500 \text{ J}\cdot\text{m}^{-1}$, suggesting a threshold for high energy environments. This value was used to define the very high (5) risk class for the MVI matrix; and, because wave power and erosion exhibit a linear relationship (Leonardi et al. 2016; Marani et al. 2011), RWE values decreased linearly by subsequent risk class (Table 2.2).

Elevation

Significance

Marsh edge elevation affects flooding frequency and the likelihood of waves attacking the edge or propagating over the marsh platform (McLoughlin et al. 2015). This variable is considered a primary indicator of risk and is prioritized in many CVI calculations (Table 2.1).

Processing

A high-resolution (0.7-meter) Light Detection and Ranging (LiDAR)-based Digital Elevation Model (DEM) was used to derive elevation values (Figure 2.3). A United States Geologic Survey (USGS)-contracted LiDAR mission was flown during low tide conditions (± 2 hours of Mean Lower Low Water) from April 11 - 24, 2015 to maximize detection of low marsh conditions and adjacent tidal flat elevations.

Validation

The LiDAR-derived elevation values were compared to land survey measurements collected by McLoughlin (2010) in August 2010 using a Trimble R8 GNSS System, a Global Positioning System (GPS) enabled Real Time Kinematic (RTK) survey receiver (Trimble, Sunnyvale, CA). Survey points were collected almost every five meters along shore-normal transects (i.e., perpendicular to the edge) extending from the mud flat to the marsh interior (Figure 2.14). Comparisons between the LiDAR-derived elevation values and RTK-GPS land survey measurements for three transects at a mainland marsh site are shown in Figure 2.14. The agreement between the two data series is excellent ($R^2 = 0.87$).

Ranking

McLoughlin et al. (2015) found for marshes in the study area that the mean rate of shoreline change was greater for higher marsh elevations. Thus, elevation values measured for the McLoughlin et al. (2015) study at an eroding marsh (Matulakin Marsh; 0.39 ± 0.01 m) and a prograding/stable marsh (Fowling Point; 0.09 ± 0.03 m) were used to define the range of values from very high (5) to very low (1), respectively, for the MVI matrix (Table 2.2).

Slope

Significance

The ability of a marsh to transgress is an important factor in survivorship in the face of sea level rise (Brinson et al. 1995). A steep upland slope can stall overland migration; and, combined with marsh edge erosion, can lead to a net loss of marsh area (Brinson et al. 1995). In addition, marsh edges with a gradual slope tend to be more stable than those with steep or nearly vertical slopes, called scarps (McLoughlin et al. 2015).

Processing

Slope was derived from the 2015 LiDAR DEM (0.7-meter resolution) using the Esri ArcGIS “Slope” tool (Figure 2.4). This tool calculates for each pixel the maximum rate of change in value from one pixel to its neighboring pixels. The output slope raster is measured in degrees; the higher (lower) the value, the steeper (flatter) the terrain. Resampling this dataset to 30-meters to match the other datasets resulted in the loss of the ability to resolve the profile of the edge; and, so, the dataset should be interpreted as a measure of landscape-level slope, not local slope.

Ranking

The loss of marsh edge resolution caused by resampling was not discovered until after the MVI was fully developed; therefore, the range values were defined at a local-slope level. Future iterations of the MVI should incorporate landscape-level slope values for range divisions. McLoughlin et al. (2015) found for marshes in the study area that steep or vertical scarps were characteristic of eroding marsh edges. Average slope values were extracted from the LiDAR-derived slope dataset for an eroding marsh site (Matulakin Marsh; 24°) and a prograding/stable marsh site (Fowling Point; 12°) and used to define the range of values from very high (5) to very low (1), respectively, for the MVI matrix (Table 2.2).

Vegetation buffer width

Significance

The process of wave attenuation by aboveground vegetation is a function of hydrodynamic conditions (e.g., wave height, period, and direction; water depth; tides), meteorological (e.g., wind speed), geographic variables (e.g., fetch), and plant characteristics (e.g., structure, buoyancy, density, stiffness, canopy height, and spatial extent) (Anderson et al. 2011; Augustin et al. 2009; Möller, 2006). Wave dissipation and vegetation buffer width exhibit a nonlinear relationship; high attenuation across short distances suggest even narrow marsh buffers may offer substantial shoreline protection (Gedan et al. 2011).

Processing

A 1-meter resolution land cover dataset coordinated by the Virginia Geographic Information Network (VGIN) and its partners was used to establish the type and extent of coastal land cover. This dataset was processed to determine the marsh vegetation buffer width (up to 50-meters)

along the shoreline of the study area. To create this layer, the Land Cover dataset was first converted to a polygon feature dataset using the Esri ArcGIS “Raster to Polygon” tool. This new dataset was clipped to a 50-meter buffer along the shoreline. From this clipped layer, the land cover type “wetland” was extracted. A “Transect” toolbox developed by Ferreira (2012), was used to cast 50-meter transects landward from the shoreline. These transects were clipped to the extent of the “wetland” layer. This clipped transect layer was then converted to a raster using “Length” as its cell value. The “Length” raster was converted to points (Esri ArcGIS “Raster to Points” tool), and those points were used to interpolate a new raster surface using the inverse distance weighting (IDW) technique (Esri ArcGIS “IDW” tool). The final output was a raster dataset with coastal grid cells reflecting the marsh vegetation buffer width at that location (Figure 2.5).

Validation

The vegetation buffer width data were visually compared to high-resolution (1-meter) NAIP imagery acquired in 2016 of a developed mainland marsh site – Upshur Neck (UN) (Figure 2.9). Visual analysis indicates good agreement between the vegetation buffer width determination and the underlying imagery (Figure 2.15). Error is likely associated with the discrepancy between the VIMS CCIM shoreline position and the land cover data shoreline position due to different spatial resolution and collection methods of the two datasets; however, the data successfully identifies wide marsh buffers on either side of a narrow marsh buffer fronting the highly developed central shoreline segment of UN.

Ranking

Möller et al. (1999) found that most wave energy was attenuated over the first 10 - 50 meters of a salt marsh. This range of values was used to define the range of values for the MVI matrix; and, because wave attenuation is nonlinearly and negatively correlated with traverse distance (Gedan et al. 2011), buffer width values decreased nonlinearly by risk class (Table 2.2).

Vegetation height

Significance

Waves passing over emergent vegetation dissipate energy through drag induced by stems (Jadhav et al. 2013); and, vegetation stem height is a factor in controlling the amount of wave attenuation (Möller, 2006).

Processing

The 2015 LiDAR dataset was used to determine vegetation height for the study area. A Digital Surface Model (DSM) representing the maximum elevation (i.e., first laser returns) was created using the LiDAR point cloud data. The LiDAR DEM – which represents the ground elevation and is developed using the last laser returns – was subtracted from the DSM to create a new layer containing vegetation height values for the entire study area (Figure 2.6).

Validation

The LiDAR-derived vegetation height values were compared to vegetation samples collected within the study area. The LiDAR dataset was acquired in April 2015; therefore, a field dataset collected in May 2017 on a small marsh island, MB (Figure 2.9), was chosen to ensure temporal correspondence (i.e., both datasets reflect vegetation height during the spring growing

season). No significant difference was found between the LiDAR-derived and field-measured vegetation height (Table 2.3).

Ranking

Möller (2006) found that salt marsh canopy of 15 - 26 centimeters had a significant effect on wave attenuation, while a shorter canopy of 6 centimeters had no effect. This range of values was used to define the class divisions of very low (1) to very high (5), respectively, for the MVI matrix (Table 2.2).

Distance to boat activity

Significance

Salt marshes in VCR are minimally impacted by boat wake proximity due to low population density (McLoughlin et al. 2015). However, areas near public boat ramps may experience wake-induced erosion from a higher concentration of vessel traffic (Duhring et al. 2006).

Processing

Vector data for boating public access sites were collected from the VCR-LTER Data Catalog (<http://www1.vcr.lter.virginia.edu/>). The ArcGIS “Euclidean Distance” tool was used to determine the distance between coastal grid cells and boat ramp features (Figure 2.7).

Ranking

Carey (2013) suggested that marshes within 3200 meters of a boat ramp are vulnerable to wake-induced erosion. Boat wake proximity values greater than 3200 meters were used to define the very low (1) risk class for the MVI matrix; the very high (5) risk class included values less than 800 meters (Table 2.2).

Storm surge

Significance

Storms are the dominant driver of short-term disturbance in Virginia coastal bays (Hayden et al. 1995). Storm surge increases water depth, which increases wave height and wave power at the marsh-bay boundary (Mariotti et al. 2010). Moderate storms with a return period of approximately 2.5 months – rather than extreme storms and hurricanes – cause the most salt marsh retreat in shallow coastal bays (Leonardi et al. 2016).

Processing

Raster-based storm surge datasets that model coastal surge along the VCR were developed by Arcadis for the TNC *Coastal Resilience* platform. Data were generated using wind and pressure data from the Federal Emergency Management Agency's (FEMA) Flood Insurance Study (FIS) and the coupled ADvanced CIRCulation (ADCIRC) and Simulating WAVes Nearshore (SWAN) modeling system (Arcadis U.S. Inc., 2016). Multiple storm surge scenarios were computed for current and future conditions and varying levels of storm intensity. The raster dataset for storm surge depths under current conditions and moderate intensity storms was used for this analysis (Figure 2.8).

Ranking

Ranking storm surge risk classes was approached from the perspective of the capacity of a marsh to attenuate waves, and not in the context of inundation control. For a water depth of 2 meters and wave heights up to 0.9 meters, Möller et al. (2014) found 16.9% wave dissipation over a 40-meter transect. Storm surge values above 2.9 meters were defined as the very high (5)

risk class for the MVI matrix; storm surge values less than 2 meters were designated as the very low (1) risk class (Table 2.2).

Relative sea level rise

Significance

Marsh accretion rate must exceed sea level rise rate to prevent drowning (Kirwan et al. 2016). Also, sea level rise increases water depth which increases wave power; and, consequently, erosion at the marsh boundary (Mariotti et al. 2010).

Processing

The rate of sea level rise in the region is 3.8 - 4.0 mm·yr⁻¹, slightly exceeding the global average (www.tidesandcurrents.noaa.gov; IPCC, 2013). A constant raster was created using the Esri ArcGIS “Create Constant Raster” tool. Although this variable affects the shoreline equally across the study area, it was included because it can be modified for future climate scenarios.

Ranking

Kirwan et al. (2010) explain that salt marshes can keep pace with conservative projections of sea level rise (1.7 mm·yr⁻¹) through vertical accretion. However, numerical models indicate that most marshes will drown if more rapid projections of sea level rise (>10 mm·yr⁻¹) occur (Kirwan et al. 2010). *Spartina alterniflora* can increase its elevation by 5.5 mm·yr⁻¹ while *Spartina patens* and *Distichlis spicata* can increase elevation by 3.1 mm·yr⁻¹ (Blum et al. *in prep*). This range of values was used to define the class divisions of very high (5) to very low (1) risk class, respectively, for the MVI matrix (Table 2.2).

Statistical analysis

Statistical analyses were performed using the statistical software SPSS 24 (SPSS, Chicago, IL) and “R” 3.4.4. A Welch Two Sample T-test was used to compare LiDAR-derived and field-measured vegetation stem height. A principal components analysis (PCA) was conducted to investigate the relationship between the erosion and inundation variables used to generate the MVI and to determine how variables contributed to the variability in the dataset. MVI data were not normally distributed even after transformation; therefore, a nonparametric test, the Kruskal-Wallis H test, followed by a post-hoc comparisons test, the Dunn’s Test of Multiple Comparisons, was performed to investigate differences between MVI output, shoreline change rate, vulnerability variables, and hot spots at comparison sites.

Spatial statistics were performed using Esri ArcGIS 10.5. The Esri “Hot Spot Analysis” tool was used to calculate the Getis-Ord G_i^* statistic for the original vulnerability variable datasets (i.e., before reclassification), which revealed where features with high or low values clustered spatially. A hot spot was designated where a feature with a high value was surrounded by other features with high values; cold spots were designated likewise for low values. The Esri “Grouping Analysis” tool was used to group values based on principal component scores. Each group represented a subset of the data where all features within each group were as similar as possible, and all groups were as different as possible.

2.3 Results and discussion

Individual variables

Table 2.4 shows the percentage of shoreline in the study area that falls within each risk class as defined in Table 2.2. The preponderance of the shoreline was designated with low

vulnerability based on physical characteristics; 80% of the shoreline had an elevation of 0.19 meters or less, and 98% had a slope of 16° or less. For the climatological variables, 5% of the shoreline was subjected to wave exposure above 500 J m^{-1} ; more than three-fourths of the shoreline was exposed to episodic storm surge over 2.9 meters; and, RSLR rate introduced low vulnerability to shorelines equally throughout the study area. Among biological variables, the majority of the shoreline was characterized with low vulnerability; more than one-half of the shoreline had vegetation with stem height above 18 centimeters, and almost 95% had a marsh buffer of greater than 25 meters. About 15% of the shoreline was within a high vulnerability distance to boating activity.

Hot spot analysis revealed the spatial distribution of statistically significant clusters of high and low values for each original vulnerability variable dataset (i.e., before reclassification) (Figure 2.16). Relative sea level rise was not included because it represents a single, system-wide value (i.e., there was no variance throughout the system). Hot and cold spots for physical variables (elevation and slope) were variable throughout the study area with no clear spatial pattern. Climate-associated variables did exhibit distinct spatial patterns: wave exposure hot spots were clustered along northeast and south/southeast shorelines, and storm surge hot spots were concentrated along most mainland marshes. Biological variables revealed cold spots for vegetation buffer width along developed shorelines and shorelines where overwash deposits (i.e., sand transported by waves) were common along marsh islands and backbarrier marshes. Vegetation height hot spots were present along northernmost shorelines, while cold spots were more prevalent in the south; high variability between hot and cold spots was present throughout the middle of the study area. Distance to boat activity cold spots (i.e., shorter distances to boat activity) were concentrated along mainland marshes and near boating ramps.

Principal components analysis

Principal components analysis (PCA) was used to examine the underlying structure of the original datasets (i.e., pre-reclassification) used to generate the MVI. Seven of the eight vulnerability variables were considered. Relative sea level rise was not included because the dataset presented no variance throughout the system. Three principal components (PCs) accounted for 56.9% of the total variance (Figure 2.17). Initial eigenvalues indicated that the first three PCs explained 22%, 19%, and 16% of the variance, respectively. Correlations between variables were low; the highest correlation was found between elevation and slope ($R^2 = 0.242$). This suggests that, in general, each variable was accounting for its own factor and explains why each PC did not account for a huge amount of variation. Nevertheless, the three PCs together captured >50% of the overall variation and are helpful in determining which variables introduce the most variance in the system.

The rotated component matrix is presented in Table 2.5. This table estimates the correlation between variables and the principal components. The first principal component (PC1) had a strong positive correlation ($R^2 > 0.5$) with two of the original variables, storm surge and vegetation buffer width, and a strong negative correlation ($R^2 < -0.5$) with vegetation height (Table 2.5). For a shoreline segment with a high PC1 component score, vegetation buffer width was wider, storm surge values were higher, and vegetation height was lower. PC1 explained most of the total variance, meaning that vegetation characteristics and storm surge explained the greatest amount of variance throughout the system. The second principal component (PC2) had a strong positive correlation with elevation and slope. This component was interpreted as a measure of morphology; high PC2 component scores for a shoreline segment correspond to higher elevation and steeper slope. The third principal component (PC3) had a strong positive

correlation with distance to boat activity, a strong negative correlation with storm surge, and a moderate positive correlation ($R^2 > 0.4$) with wave exposure. For a shoreline segment with a high PC3 score, there was a greater distance to boating activity, lower storm surge, and more moderate wave exposure.

Grouping analysis of principal component scores illustrates how the most influential combinations of variables were distributed across the system. A parallel box plot graph summarizes the three groups and the variables within them (Figure 2.18). Group 1 (plotted in blue) reflects locations with the highest values of PC2; Group 2 (plotted in red), reflects locations with the highest values of PC1; and, Group 3 (plotted in green) reflects locations with the highest values of PC3. The grouping analysis map reflects a distinct spatial pattern between the three groups (Figure 2.19). Group 1 (PC2-dominant) is dispersed throughout the system and highlights shoreline segments that tend to correspond with developed areas and shorelines where overwash deposits were common along marsh islands and backbarrier marshes. Vulnerability along Group 1 shoreline segments are most influenced by morphologic characteristics (i.e., elevation and slope). Group 2 (PC1-dominant) is consolidated along most mainland marshes; vulnerability for these shorelines is most influenced by vegetation characteristics and storm surge. Group 3 (PC3-dominant) is predominantly concentrated along the NE facing slopes in the north and along marsh islands and backbarrier marshes located within the largest coastal bays near the center of the system. Vulnerability along Group 3 shoreline segments are most influenced by wave-climate variables (e.g., boat wake, storm surge, wave exposure).

Marsh Vulnerability Index

The results of the MVI analysis are shown in Figure 2.20. MVI values range from 0.5 (very low vulnerability) to 47.4 (very high vulnerability). The mean MVI value is 3.89, the median

value is 2.74, and the standard deviation is 3.36. The 25th and 75th percentiles are 1.94 and 5.00, respectively. MVI values were divided into risk categories by natural breaks to display the distribution of vulnerable areas as very low (< 3.00), low (3.00 – 6.32), moderate (6.32 – 11.18), high (11.18 – 20.12), and very high (>20.12) (Table 2.6). 51% (594 km) of shoreline was designated as very low vulnerability; 35% (413 km) as low vulnerability; 11% (127 km) as moderate vulnerability; 3% (33 km) as high vulnerability; and, 0.5% (5 km) was designated as very high vulnerability. Figure 2.21 shows the percentage and total length of shoreline in the study area for each risk category (very low to very high).

Visual analysis of hot spot mapping indicates the majority of high MVI values reside along mainland marshes (Figure 2.22). To support this visual assessment, MVI values were compared for three marsh sites selected based on their position within the study area: a mainland marsh – Fowling Point (FP), a marsh island – Man and Boy (MB), and a backbarrier marsh – Hog Island (HI) (Figure 2.9). Mean MVI values were significantly higher at the mainland marsh site (FP) than the marsh island (MB) or backbarrier marsh (HI) (Figure 2.23).

Model validation

To investigate the effectiveness of the MVI as a spatial modeling tool, MVI results were compared to shoreline change rates. Coastal segments that experience erosion should correspond to areas characterized as vulnerable by the MVI.

MVI and shoreline change rates

MVI values were compared to calculated shoreline change rates (i.e., erosion and accretion) at three comparison sites. Sites were selected based on differing marsh morphology and level of

human impact: a marsh island – Man and Boy (MB), a protected mainland marsh – BTI, and a developed mainland marsh – Upshur Neck (UN) (Figure 2.9).

Emery (2015) and Taube (2013) calculated shoreline change statistics for MB and UN, respectively, using the Digital Shoreline Analysis System (DSAS) 4.3 for Esri ArcGIS 10.3 (Thieler et al. 2012). BTI shorelines were manually digitized using Esri ArcGIS 10.5 and three National Agriculture Imagery Program (NAIP) aerial photographs spanning an eight-year period (2006, 2009, and 2014). These shorelines were analyzed by Analyzing Moving Boundaries Using R (AMBUR), an “R” package for calculating shoreline change (Jackson et al. 2011). Shoreline change rates calculated by DSAS and AMBUR show good agreement ($R^2 = 0.87$) (Figure 2.24).

A summary of MVI values, shoreline change, and vulnerability variables for the three comparison sites is provided in Table 2.7. There were significant differences between MVI, shoreline change, wave exposure, slope, vegetation height, and distance to boat activity at all three sites. Elevation and vegetation buffer width were significantly higher and lower, respectively, at UN compared to MB and BTI. Storm surge was significantly higher at BTI than MB and UN.

Areas of low (high) shoreline change were not always comparable with areas of low (high) vulnerability. Figure 2.25 depicts the spatial distribution of MVI values compared to shoreline change rates at each site. Overall, visual comparison suggests high variability in MVI values and shoreline change rates. Linear regression was calculated to predict shoreline change rates based on MVI values (Figure 2.26). Statistical results indicate a weak, but significant relationship between MVI values and shoreline change rates at MB and BTI. No significant relationship was found at UN. Significant differences existed between shoreline change rates grouped into risk

categories according to range divisions outlined in Table 2.2 for MB and BTI; no significant difference was found at UN (Figure 2.26).

MB was the only site to show a significant positive relationship between MVI values and shoreline change rates; a higher risk category tended to predict higher shoreline change rates. Linear regression results indicate a weak, negative relationship between MVI values and shoreline change rates at BTI; a higher risk category tended to predict lower shoreline change rates. Analysis of BTI shoreline change rates by risk category revealed a significant difference; BTI shoreline change rates within the “very low” risk category were significantly higher than those found in the “low” and “moderate” risk categories. Although UN is characterized by low erosion and accretion rates, MVI values were moderate to high across the site. Linear regression results and comparison between UN shoreline change rates by risk category showed no significant relationship between MVI values and shoreline change rates.

The discrepancy between MVI values and shoreline change rates suggests that the MVI does not predict shoreline change for a coastal segment, rather it predicts the potential for shoreline change. UN was characterized by the lowest mean shoreline change rate, yet reflected the highest mean MVI value (Table 2.7). UN is a highly developed shoreline featuring private residences, roads, docks, agriculture plots, and shoreline protection structures (bulkhead and riprap). These hardened structures are likely mitigating shoreline change rates; therefore, while UN is not actively eroding, the MVI still designates the overall vulnerability at the site as “moderate” because it is characterized by high elevation and slope, a narrow vegetation buffer, short vegetation height, moderate wave exposure, and very high storm surge. Considering these site-specific characteristics, UN was appropriately identified as a vulnerable area, a determination

that was further supported by the decision of landowners to install costly hardened structures to protect their valuable coastal property.

The contradictory relationship between MVI results and shoreline change rates found at MB and BTI is more difficult to explain. It is possible that, for a relatively sheltered shoreline like BTI, where wave exposure is very low, internal variables (e.g., sediment size, below ground biomass, and presence of invertebrates) may play a greater role in controlling shoreline change rates. This information is not captured in the current construct of the MVI. At MB, however, wind-waves are significantly higher and likely serve as the primary driver of erosion. In addition, errors in the vulnerability variable datasets or models (e.g., RWE, slope) outlined in the methods section of this study may be contributing to this discrepancy.

Recommendations for future work

Future work should consider the introduction of additional variables into the generation of the MVI, especially vegetation density, sediment size, land use, and presence of shoreline structures, to increase the robustness of the final vulnerability determination. However, the addition of variables may also introduce more sources of error and negate the importance of other response variables (Cooper and McLaughlin, 1998); further data reduction analysis may be necessary to determine which combination of variables is most influential.

Geoprocessing techniques and spatial resolution likely affected the accuracy of the MVI output. The decision to use top 5% wind events for the wave exposure model should be revisited and all wind conditions considered. The alongshore resolution of the datasets was very high (30 meters), but the cross-shore resolution was poor. This affected the ability to resolve the marsh

edge profile and instead provided information on the landscape-level slope. To accurately capture local slope, spatial processing must work to resolve this cross-shore variability.

A potential limitation of the MVI was the method used to rank vulnerability variables into risk classes for the vulnerability matrix. Range divisions for risk classes are site-specific and were determined through literature review and associated field observations; however, as Table 2.4 makes clear, range divisions resulted in a skewed distribution across the five risk classes. For example, thresholds assigned to the slope dataset led to the classification of 97% of the shoreline as very low vulnerability with respect to slope. Similarly, 77% of shorelines were classified as high vulnerability according to thresholds established for the storm surge dataset. As a result, the majority of each dataset lay outside the narrow band of values dictated by range divisions. An alternative approach is to calculate a relative vulnerability index which uses a standard classification method (e.g., natural breaks, quantile) to assign range divisions within the overall distribution of the datasets. While this approach does not produce absolute predictions, the advantage is that the full range of each dataset is considered and the objective of identifying shoreline segments that are more vulnerable relative to others is still accomplished.

Finally, this iteration of the MVI was generated based on the square root of the product mean of eight variables. There are alternative ways to calculate an index value, including the application of a weight to individual influential variables or groups of influential variables. Future iterations should consider a weighted approach to proportion appropriate influence on individual or grouped variables for the final determination of vulnerability. For example, the eight variables selected for this study could be separated into groups for physical and climatological conditions and weights could be determined and applied using a variety of methods (e.g., rank-sum approach).

Coastal management

To support coastal hazard mitigation and climate adaptation planning, vulnerable areas must be identified using the best available data. This study represents a straightforward approach to objectively assessing erosion and inundation vulnerability of fringing salt marshes in the wave-dominated, microtidal environment of the VCR. The results of this study offer a significant development for coastal management at the VCR: a comprehensive salt marsh vulnerability assessment database that is publically accessible through a robust web mapping decision-support tool for coastal stakeholders.

Salt marsh vulnerability data are available to the public via the Living Shoreline Explorer (LSE) app hosted on the TNC *Coastal Resilience* mapping platform (Figure 2.27). The LSE app enables planners, officials, managers, and citizens to visualize interpreted research data on coastal vulnerability in a local context.

Figures

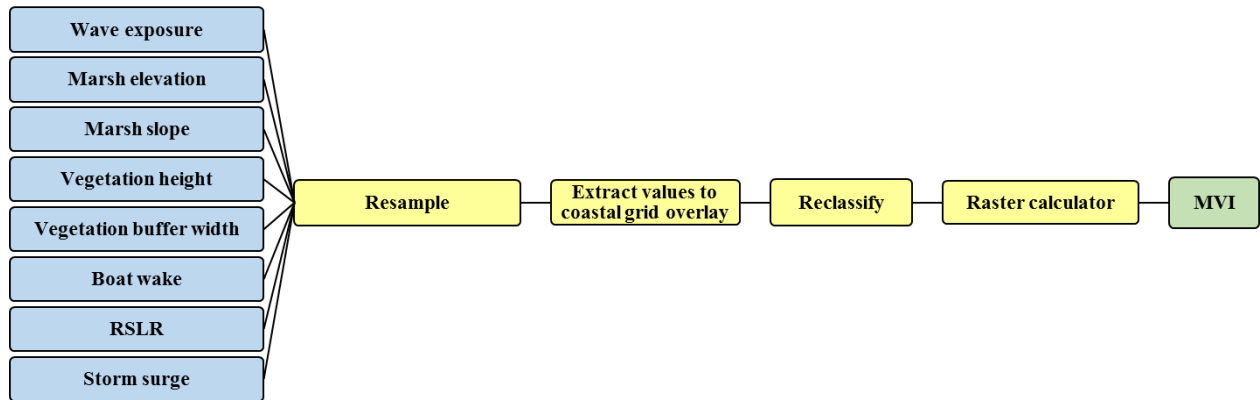


Figure 2.1. MVI general methodology. Blue = inputs, yellow = processing, green = output.

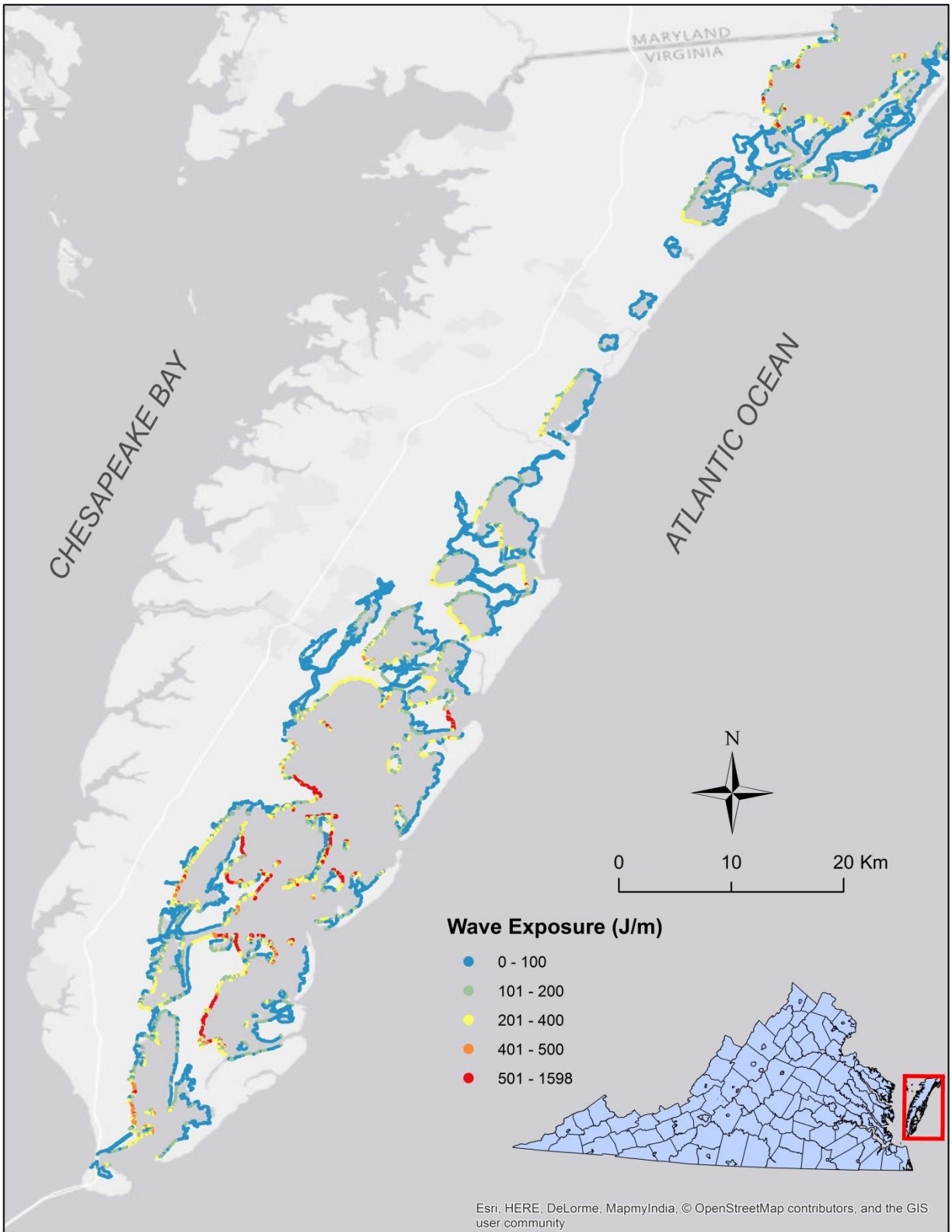


Figure 2.2. Relative Wave Exposure (RWE) in $\text{J}\cdot\text{m}^{-1}$ along the Virginia Coast Reserve.

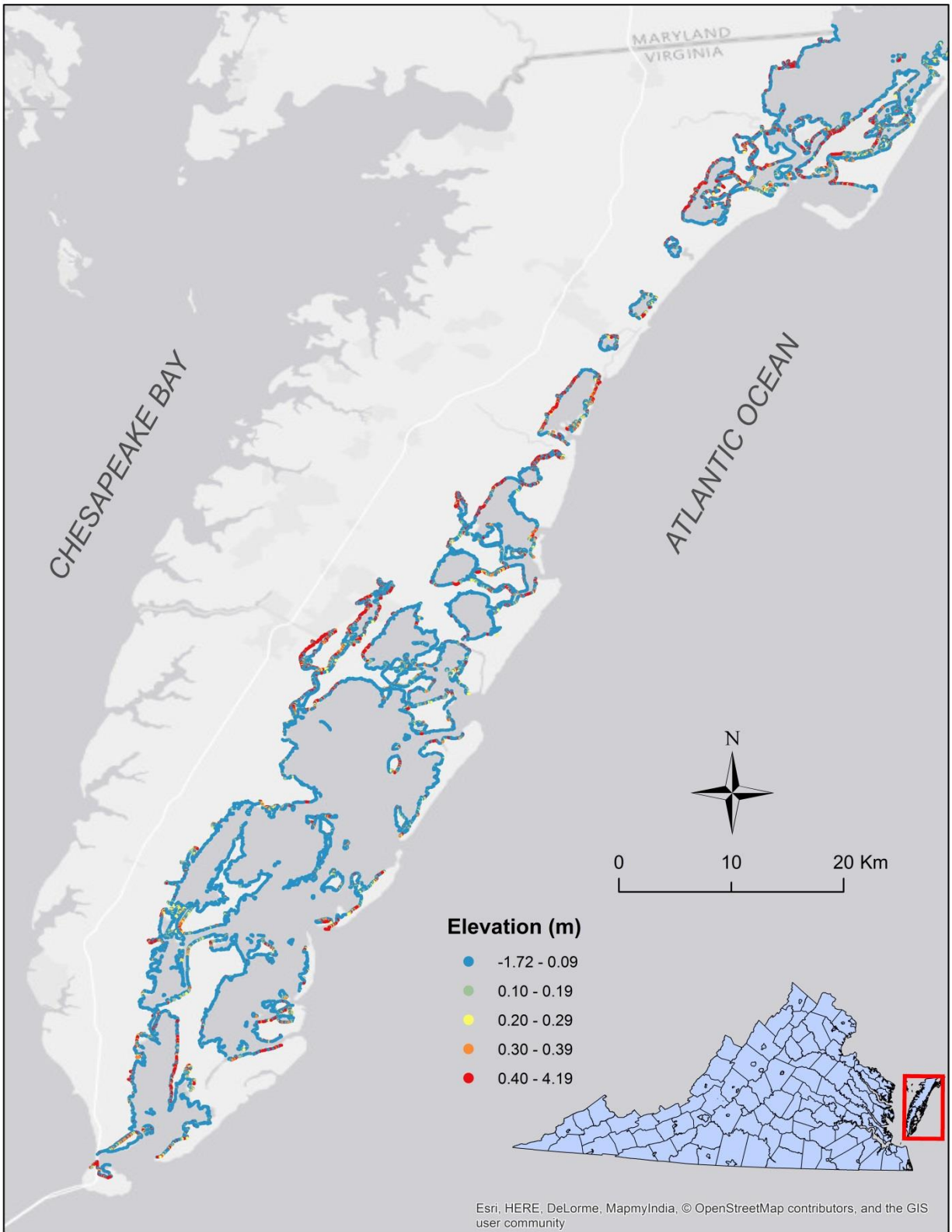


Figure 2.3. Marsh elevation in meters along the Virginia Coast Reserve.

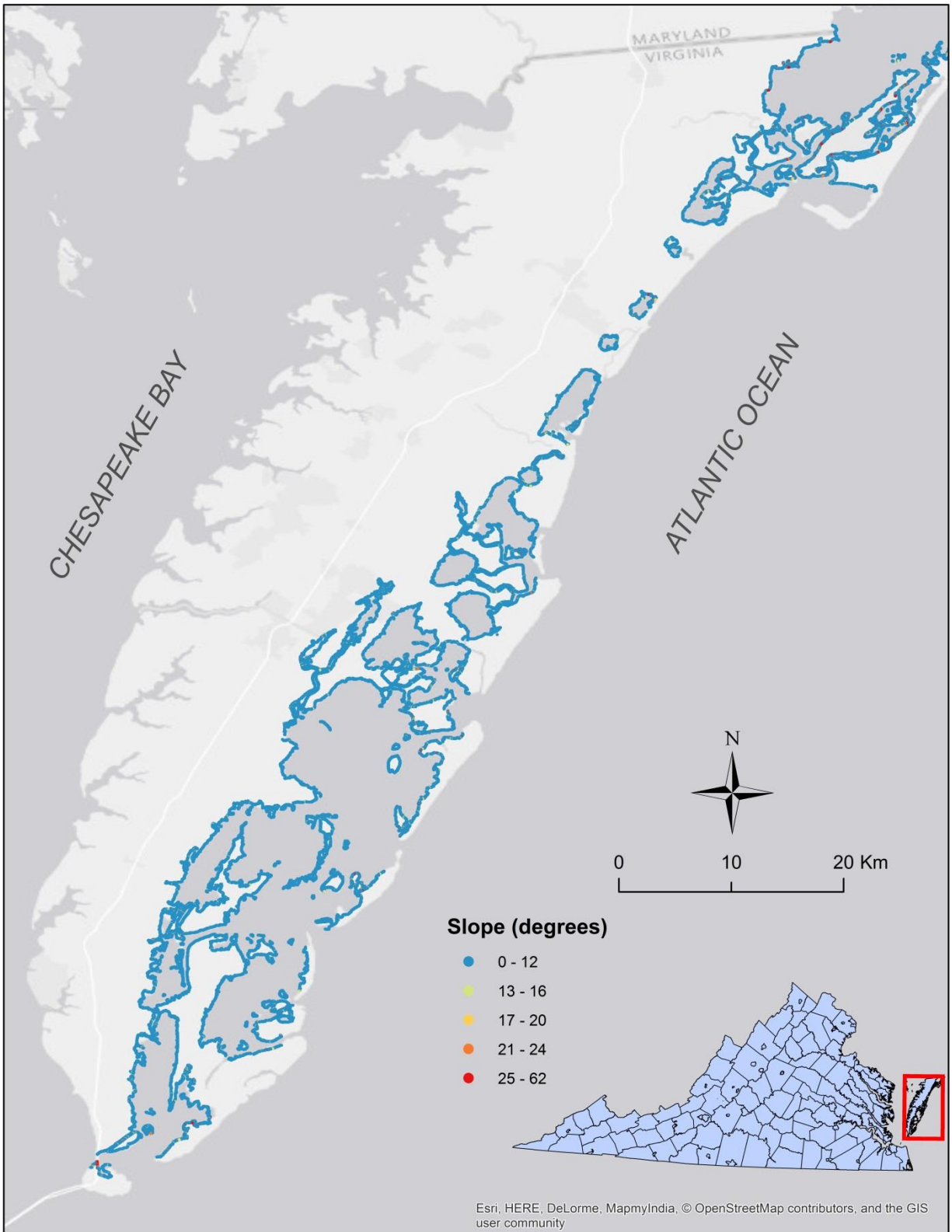


Figure 2.4. Marsh slope in degrees along the Virginia Coast Reserve.

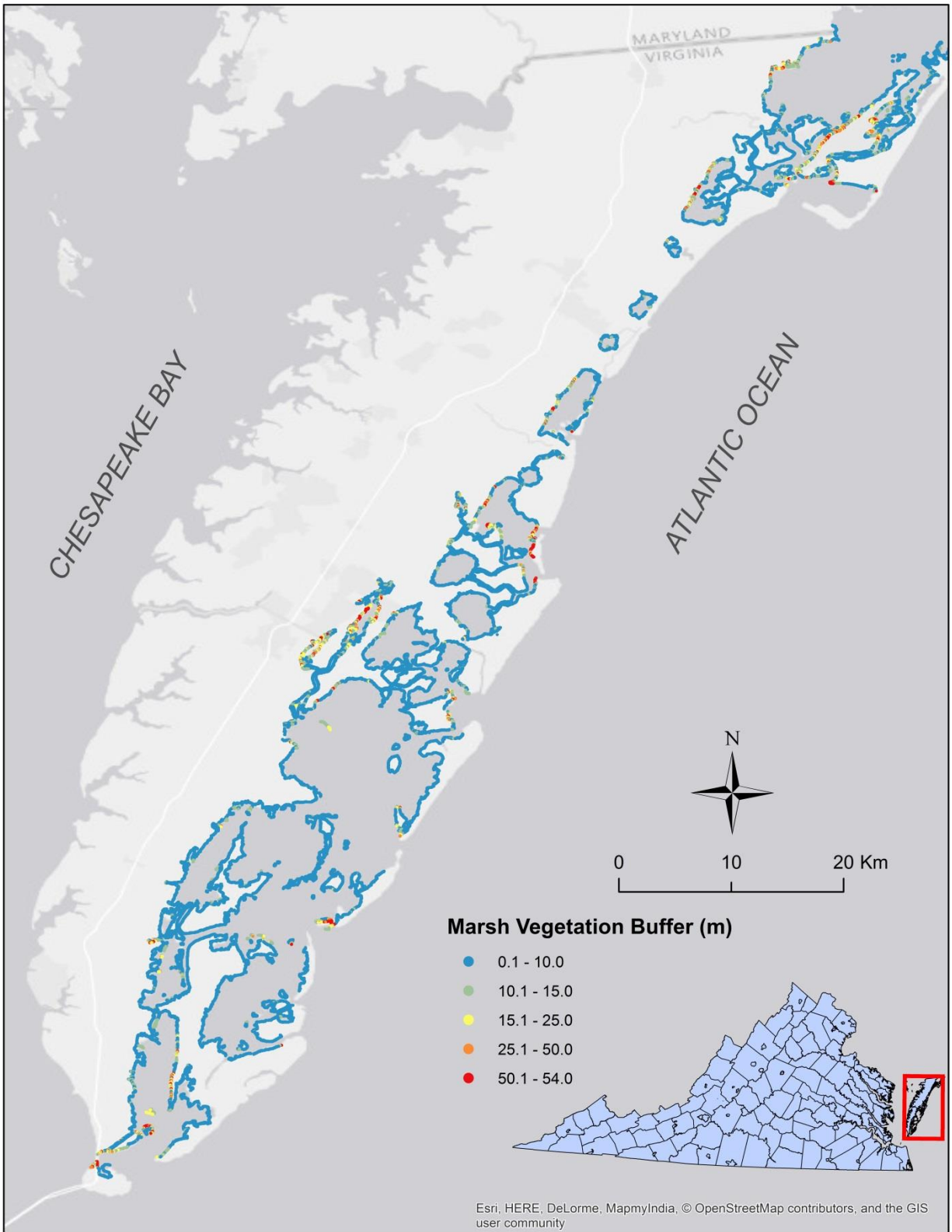


Figure 2.5. Marsh vegetation buffer width in meters along the Virginia Coast Reserve.

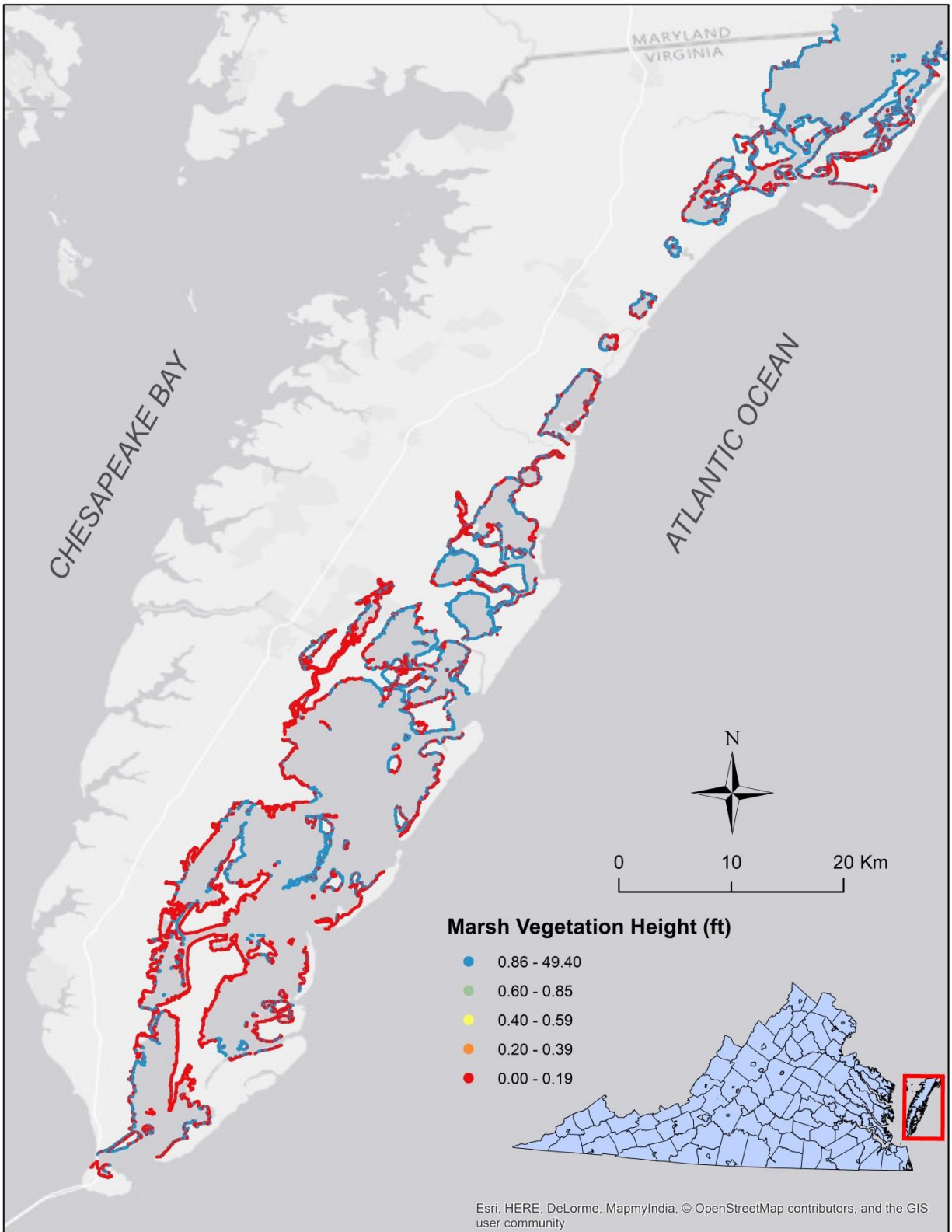


Figure 2.6. Marsh vegetation height in feet along the Virginia Coast Reserve.

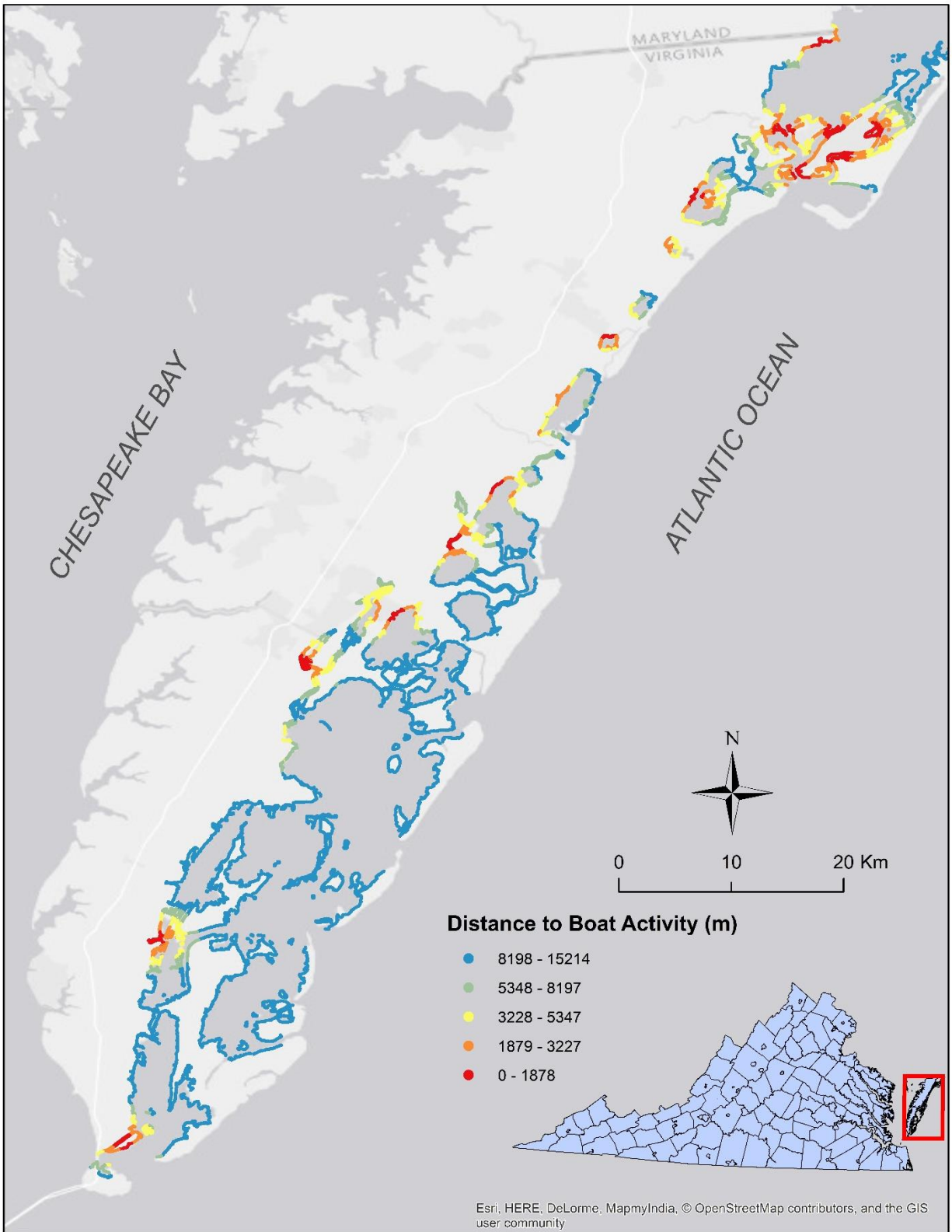


Figure 2.7. Distance to boat activity in meters along the Virginia Coast Reserve.

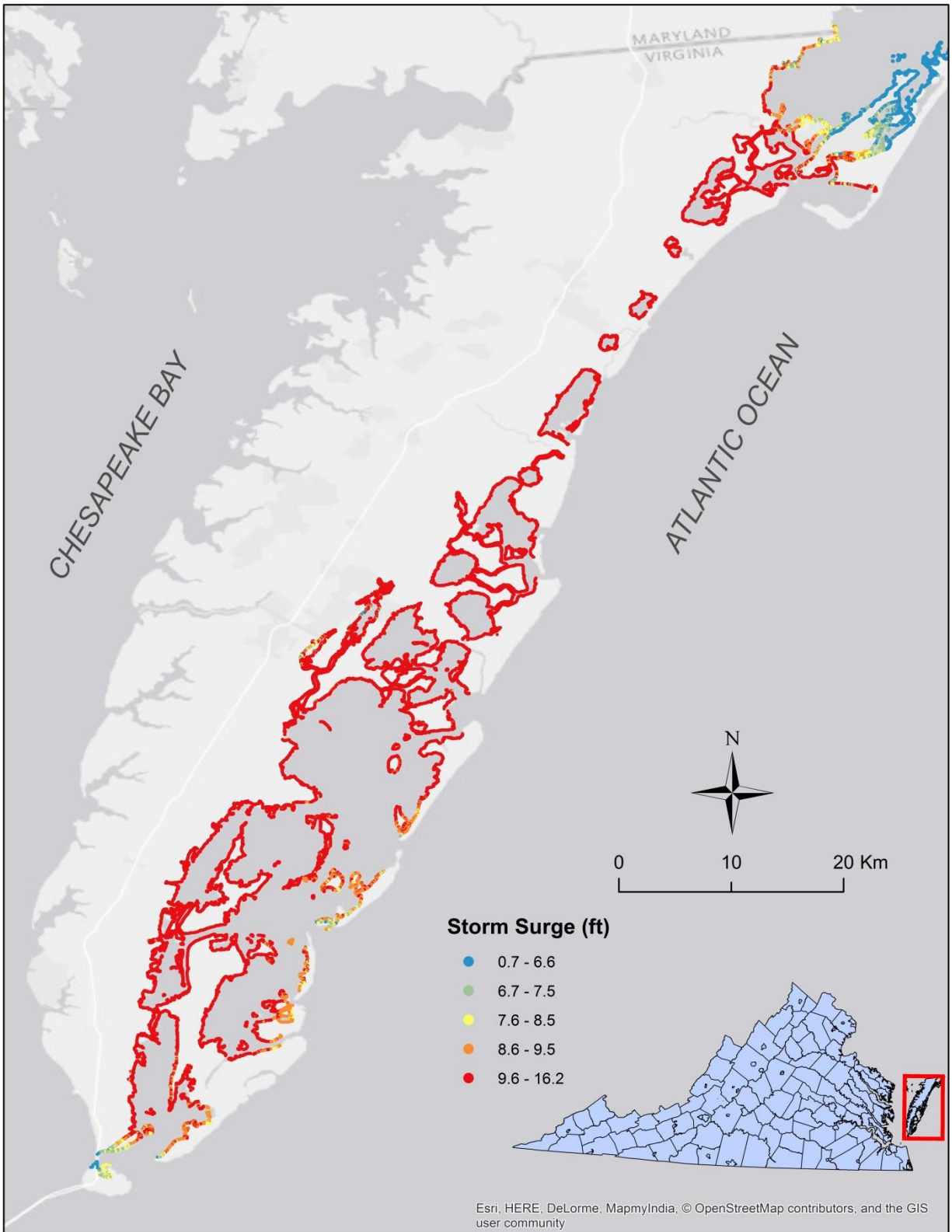


Figure 2.8. Storm surge in feet along the Virginia Coast Reserve.

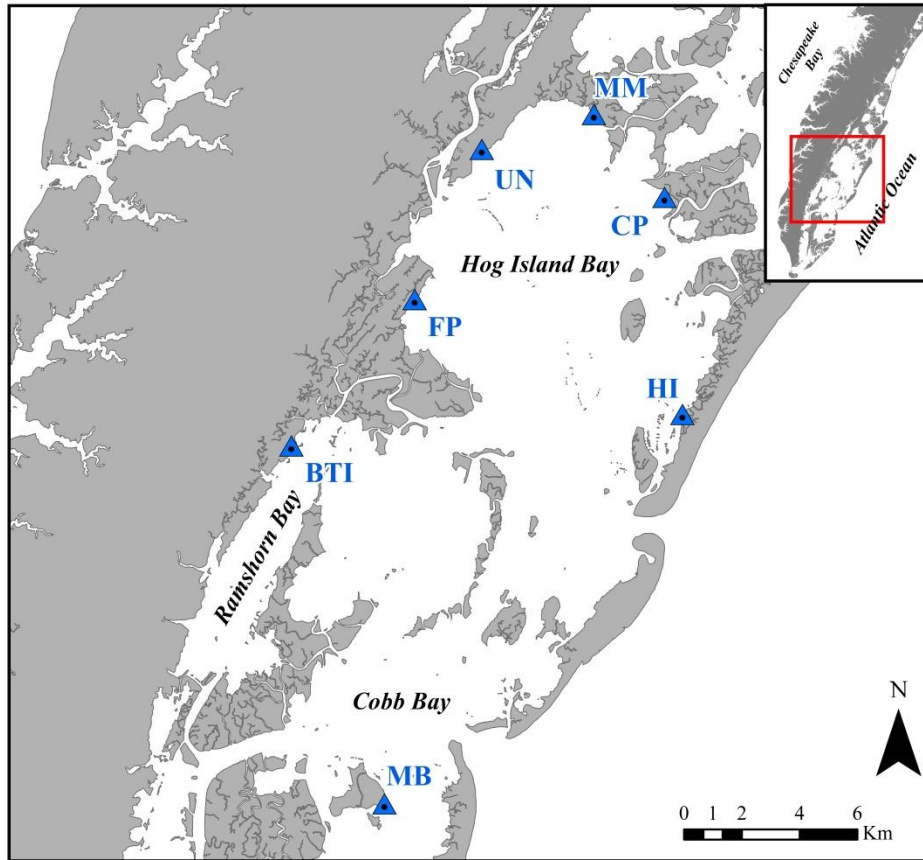


Figure 2.9. Sites used for validating MVI input data. Numerical modeling results for Matulakin Marsh (MM), Chimney Pole (CP), Hog Island (HI), and Fowling Point (FP) were compared to wave exposure data. In situ wave measurements from Man and Boy (MB) were compared to wave exposure data. Survey measurements from FP were compared to elevation data. Vegetation samples from MB were compared to vegetation height data. High-resolution imagery of Upshur Neck (UN) was compared to vegetation buffer width data. Erosion rates calculated for Box Tree Idaho (BTI), MB, and UN were compared to MVI results.

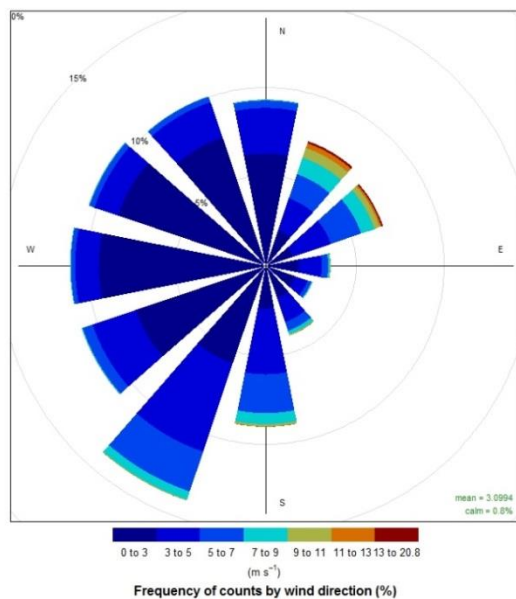


Figure 2.10. Wind rose of winds recorded at the NOAA Station WAHV2 during 1 January 2010 – 31 December 2015.

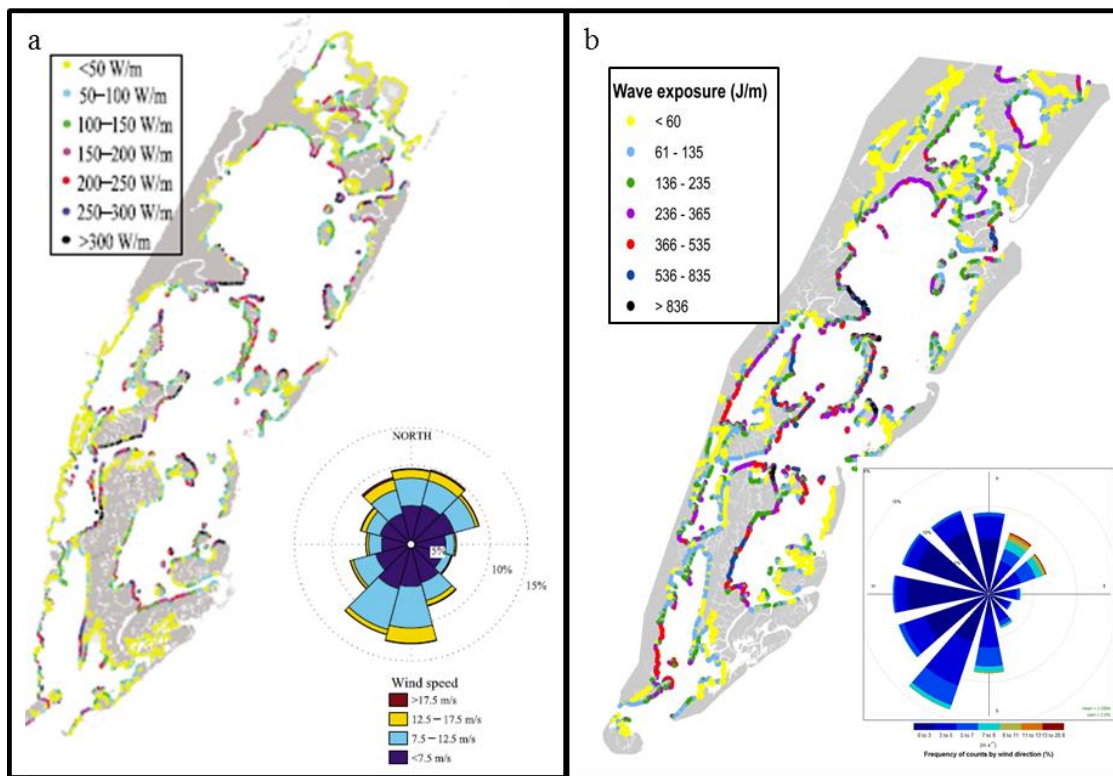


Figure 2.11. (a) Wave power at the marsh boundary and wind statistics from NOAA Station CHLV2 calculated by Mariotti et al. (2010). (b) Wave exposure at the marsh boundary and wind statistics from NOAA Station WAHV2.

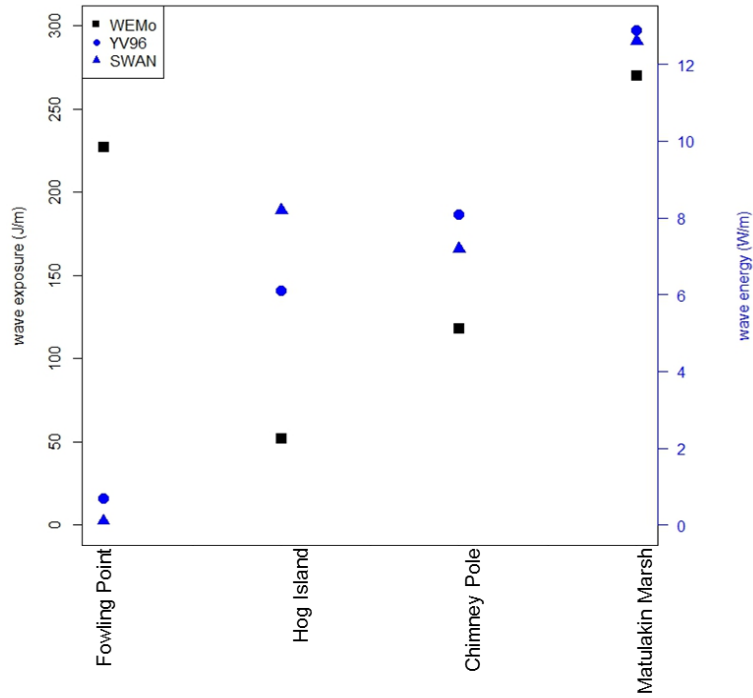


Figure 2.12. Comparison between WEMo-calculated wave exposure ($J \cdot m^{-1}$) and YV96 and SWAN-calculated wave energy ($W \cdot m^{-1}$) for four sites.

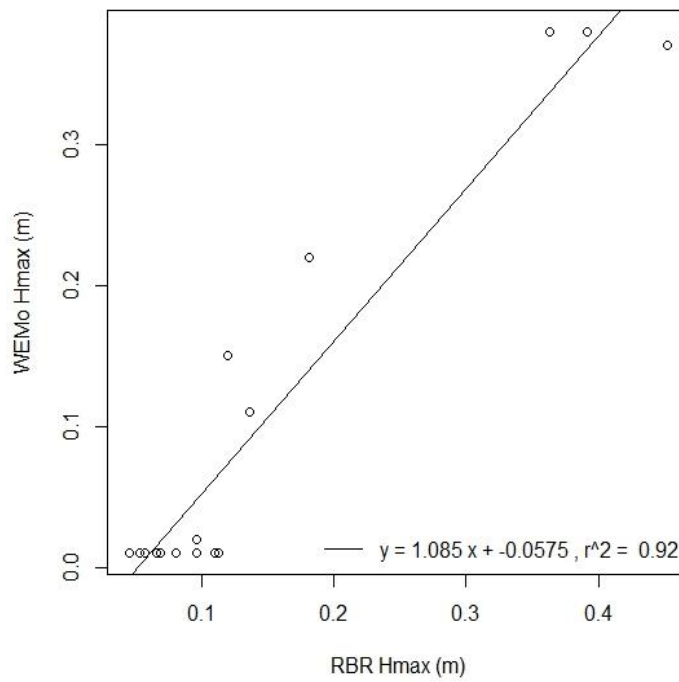


Figure 2.13. Comparison between measured (RBR H_{max}) and predicted (WEMo H_{max}) maximum wave height (m) at Man and Boy.

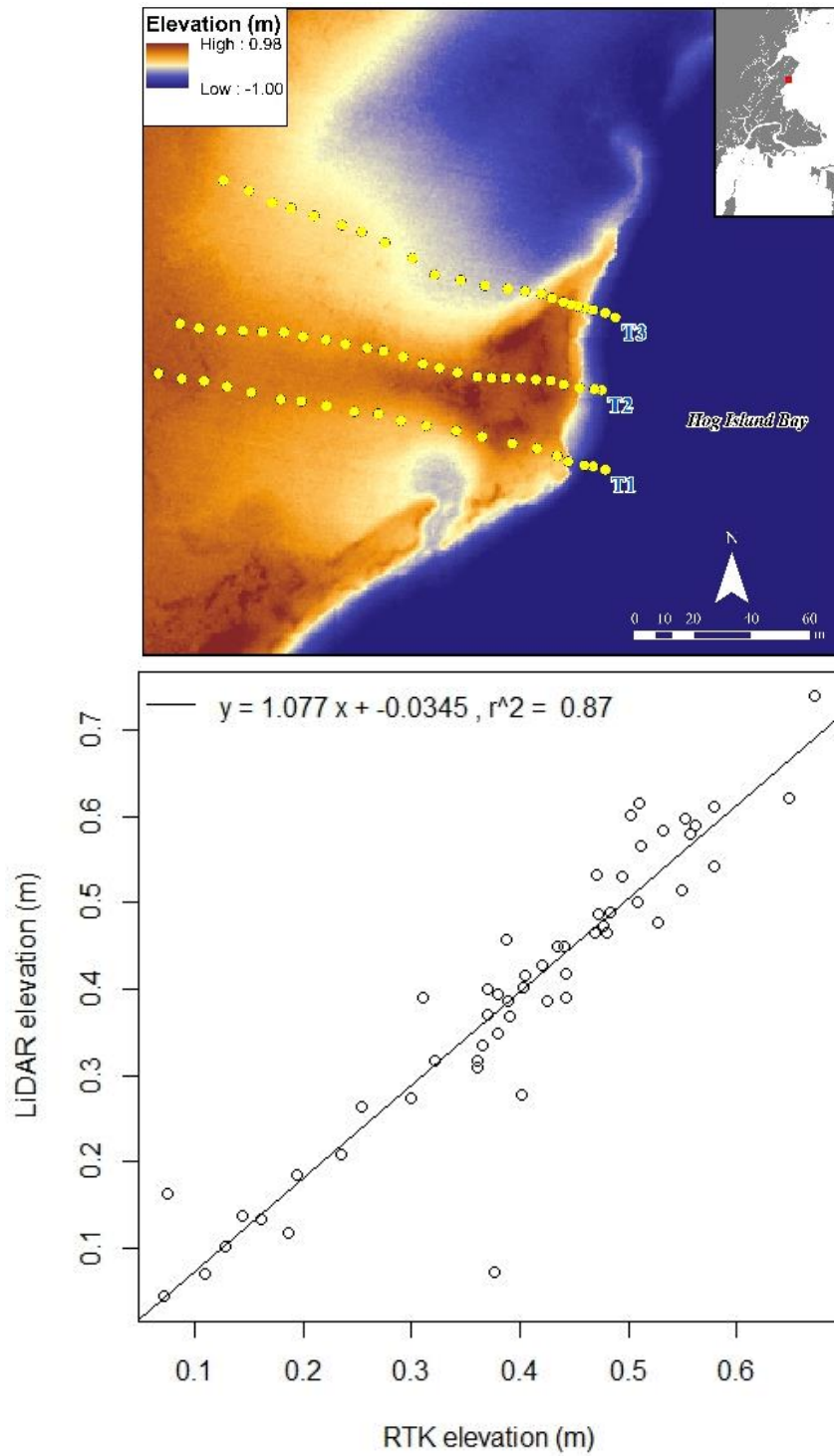


Figure 2.14. Map of Fowling Point with LiDAR digital elevation model and RTK-GPS land survey transects shown as yellow circles (*upper*) and comparison between LiDAR-derived elevation and RTK-GPS land survey elevation (*lower*).

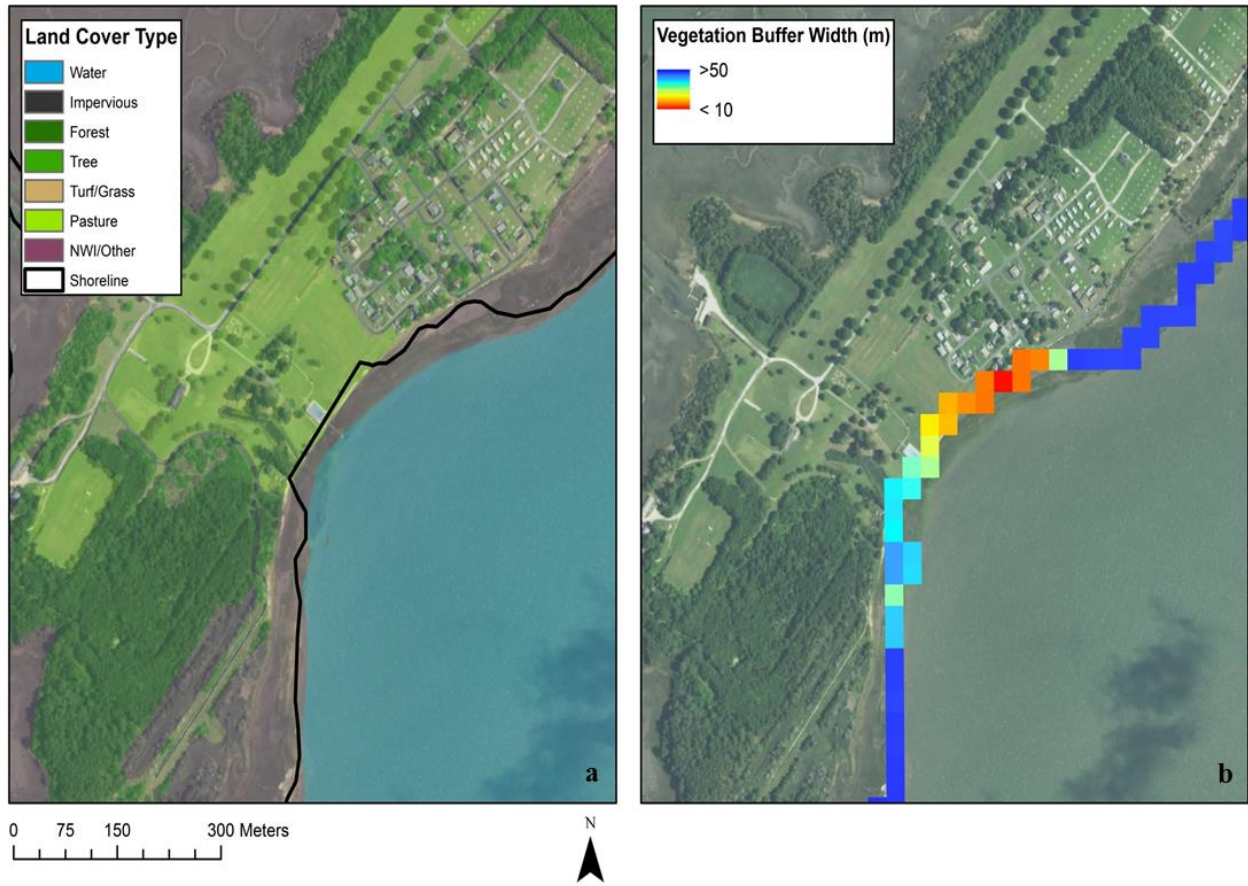


Figure 2.15. (a) Land cover dataset and shoreline overlaid on 2016 NAIP imagery. (b) vegetation buffer width determination overlaid on 2016 NAIP imagery.

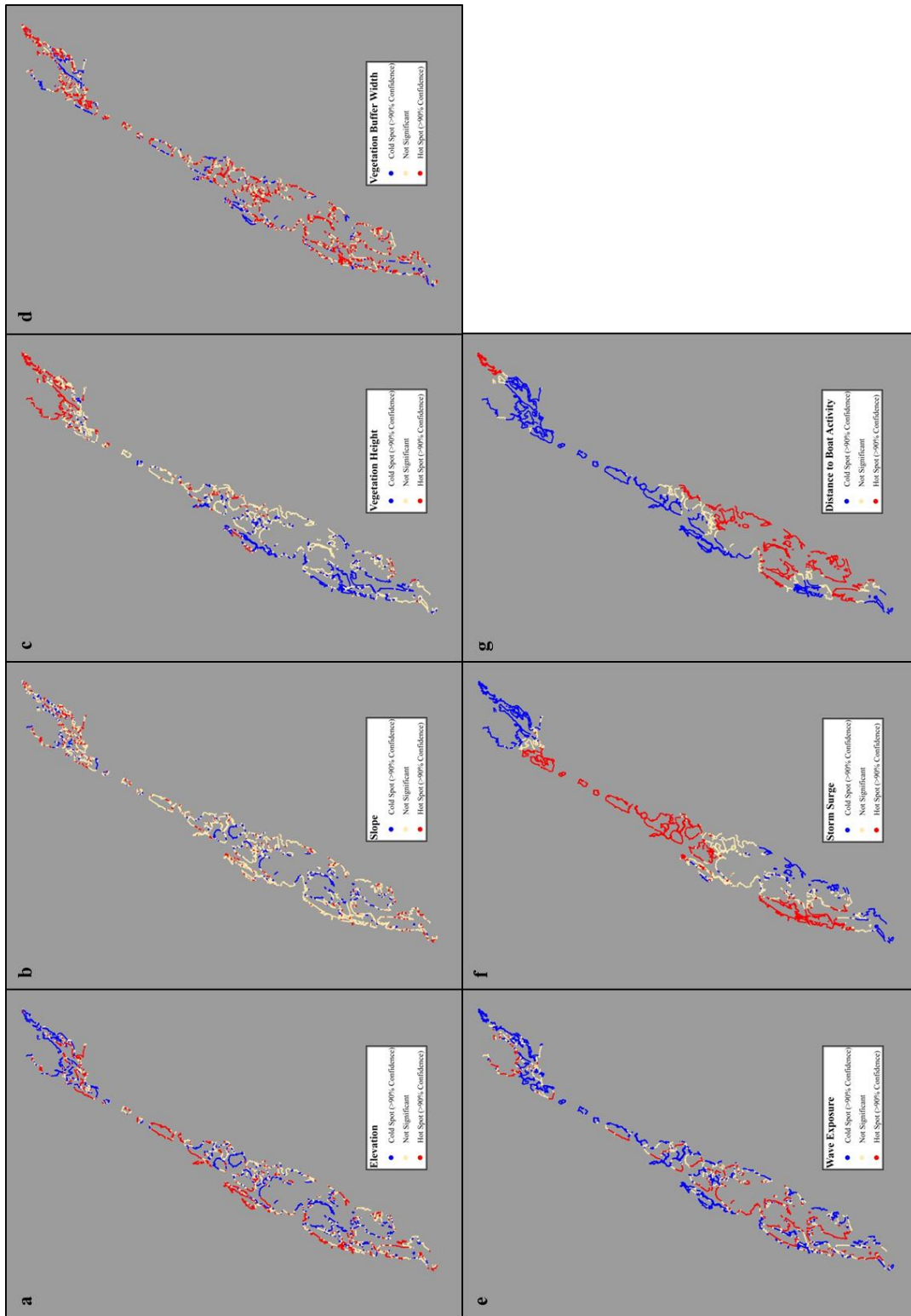


Figure 2.16. Hot spot analysis of original vulnerability variable datasets used to develop the MVI.

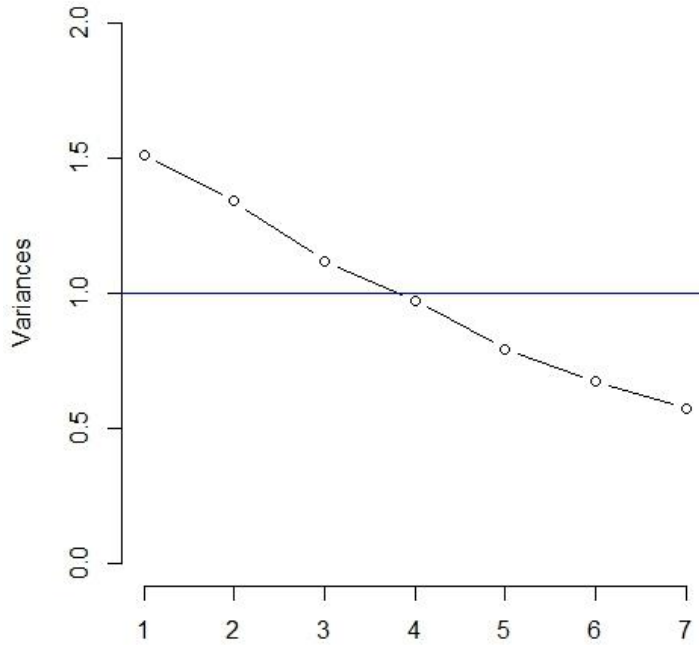


Figure 2.17. Scree plot depicting decreasing rate at which variation is explained by additional principal components. A threshold of variance ≥ 1.0 gives three principal components.

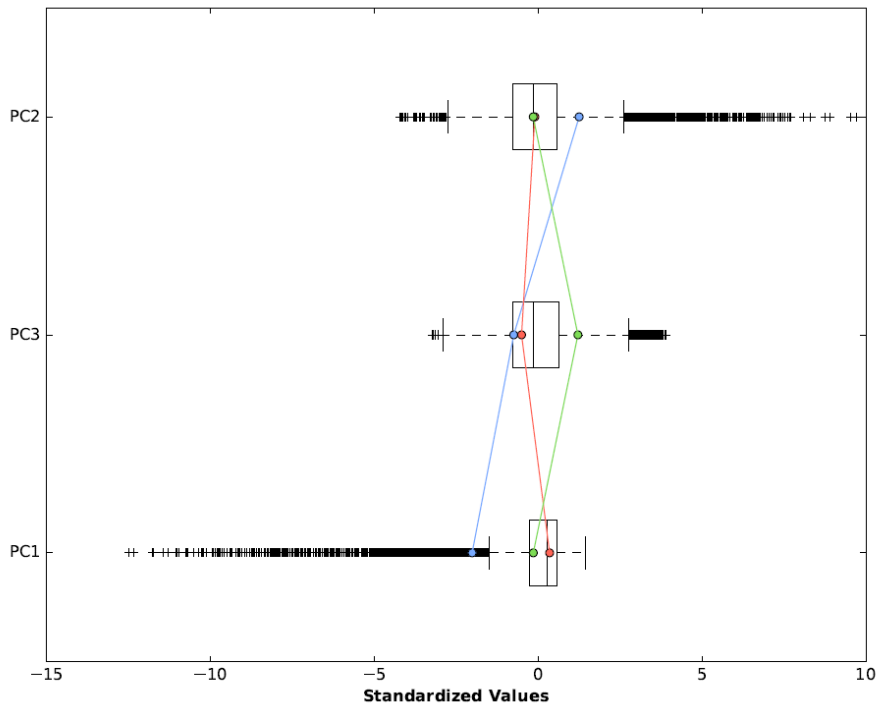


Figure 2.18. Parallel box plot summarizing groups and the principal component variables within them.

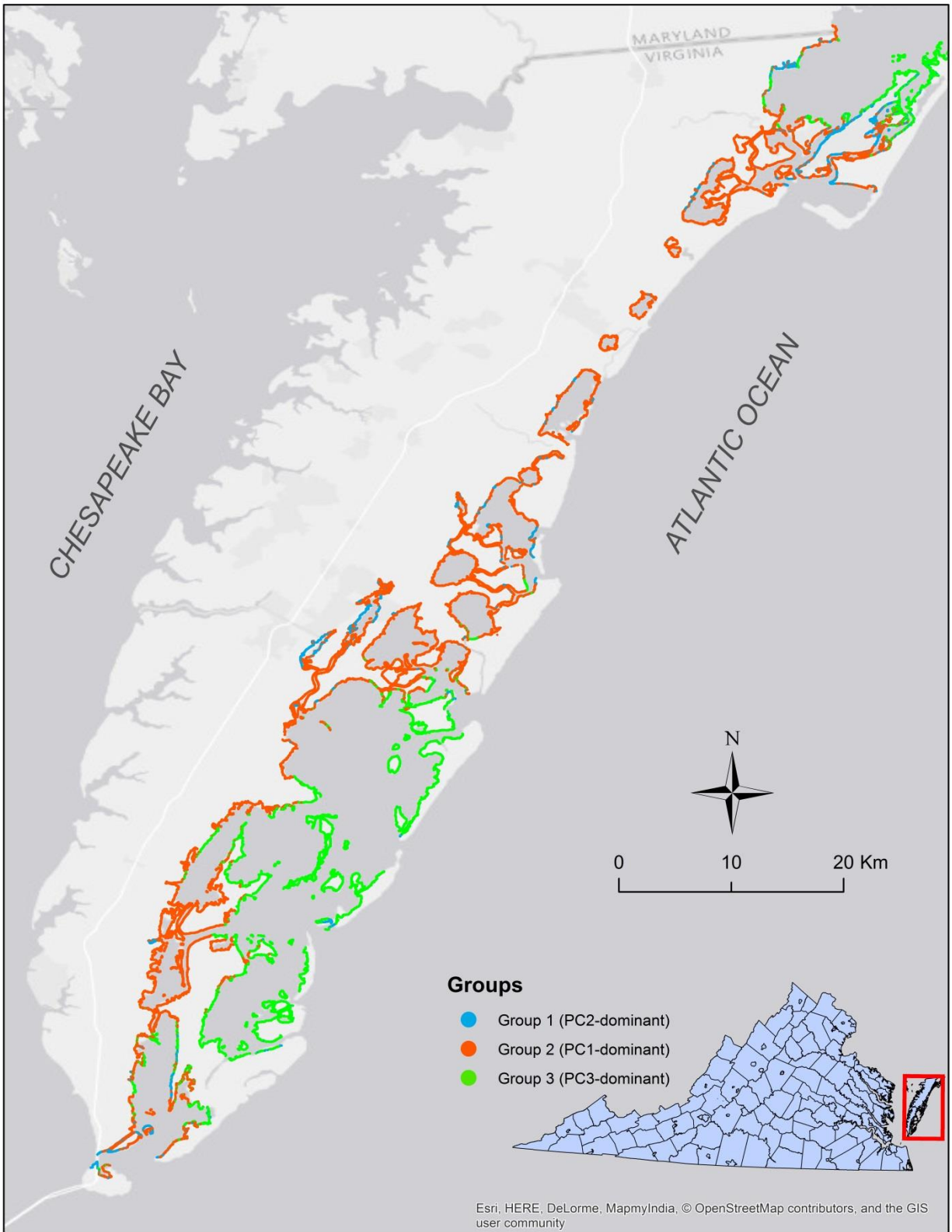


Figure 2.19. Grouping analysis results for principal component scores.

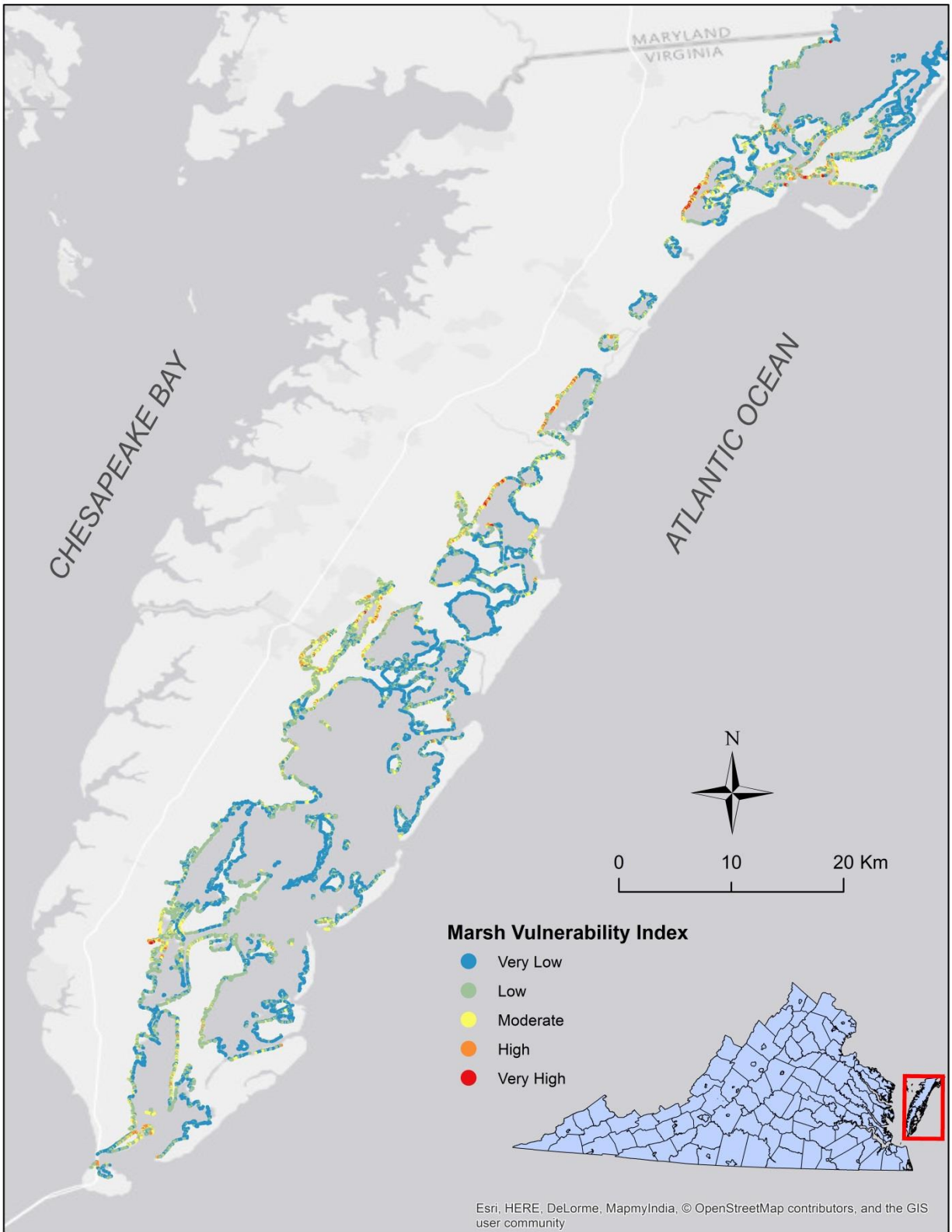


Figure 2.20. Marsh Vulnerability Index along the Virginia Eastern Shore.

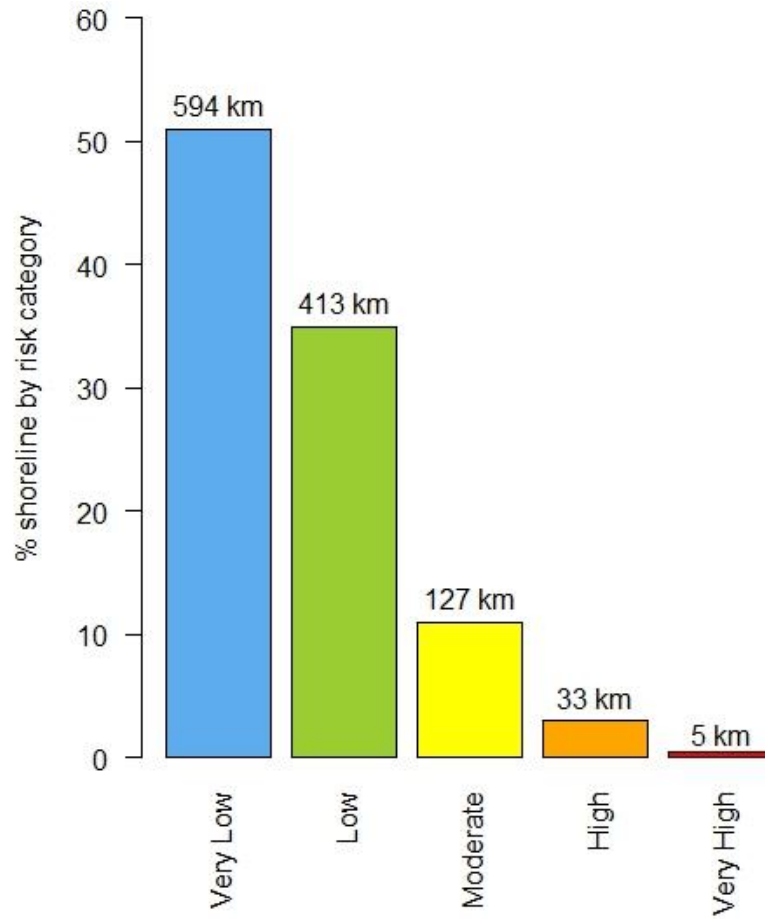


Figure 2.21. The percentage and length of shoreline for each MVI risk category. The total length of shoreline considered was 1,172 kilometers.

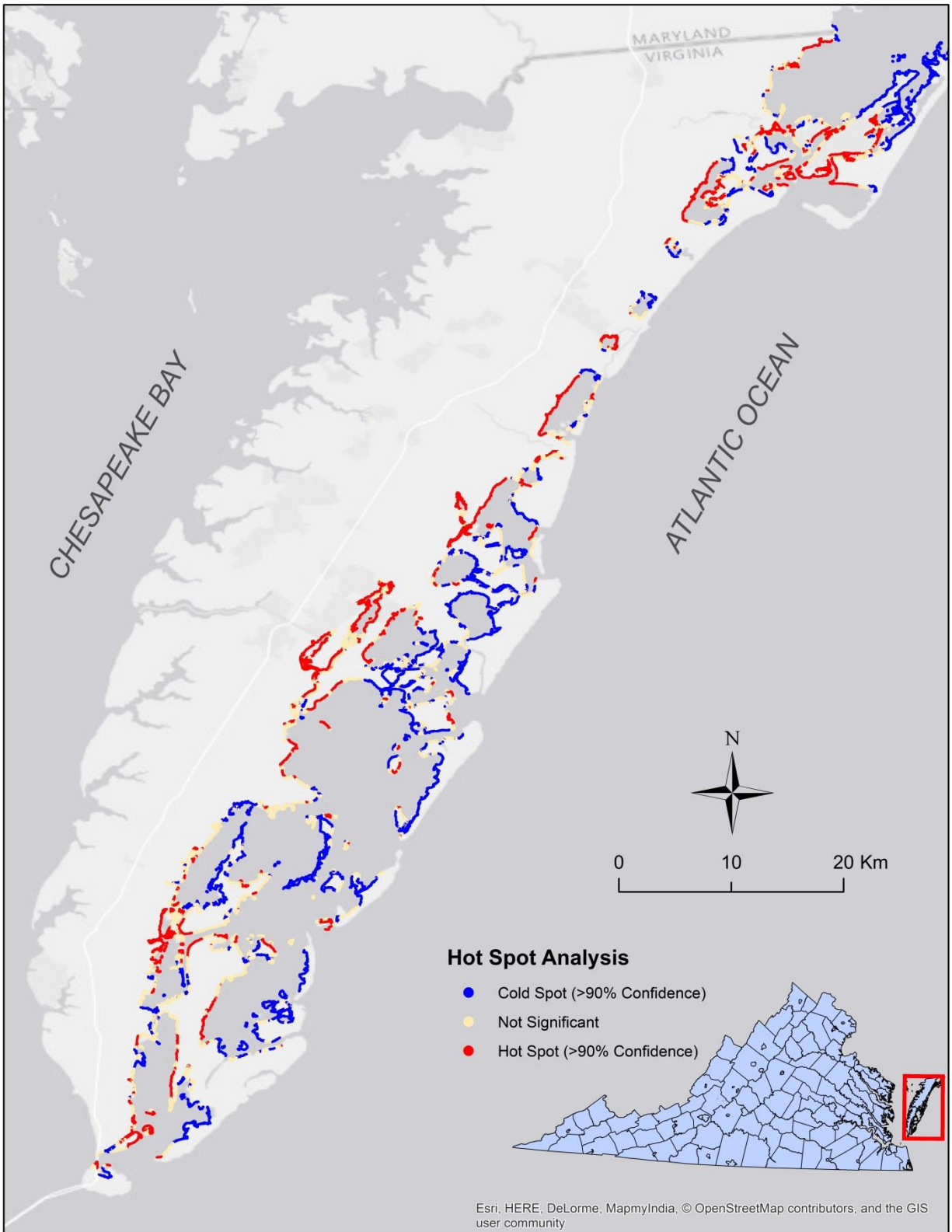


Figure 2.22. Hot spot analysis results for Marsh Vulnerability Index. Hot spots (high values) are generally concentrated along the mainland marshes.

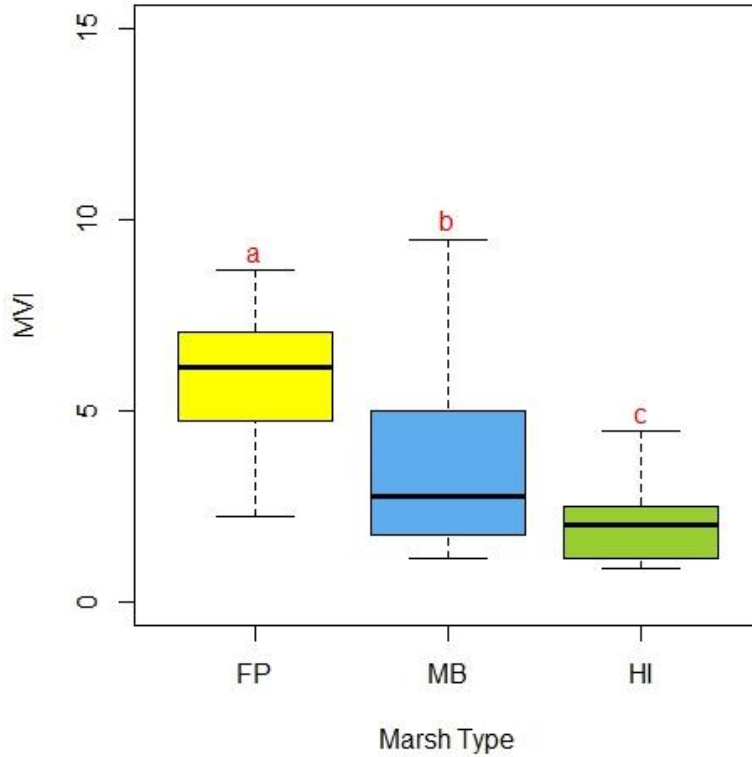


Figure 2.23. Analysis of hot spots indicates MVI values were higher along mainland marshes. Fowling Point (FP) is a mainland marsh, Man and Boy (MB) is a marsh island, and Hog Island (HI) is a backbarrier marsh. Letters indicate statistically significant differences between marshes ($p < 0.05$). Results from Kruskal-Wallis rank sum and Dunn's test can be found in Appendix A (1).

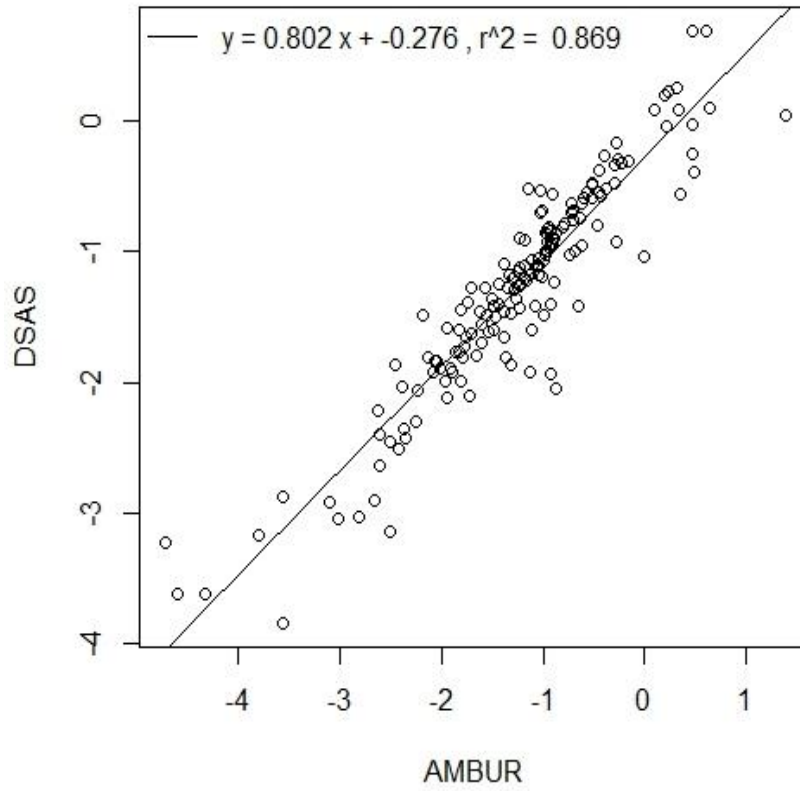


Figure 2.24. DSAS shoreline change calculations compared to AMBUR shoreline change calculations for a small marsh island, Man and Boy.

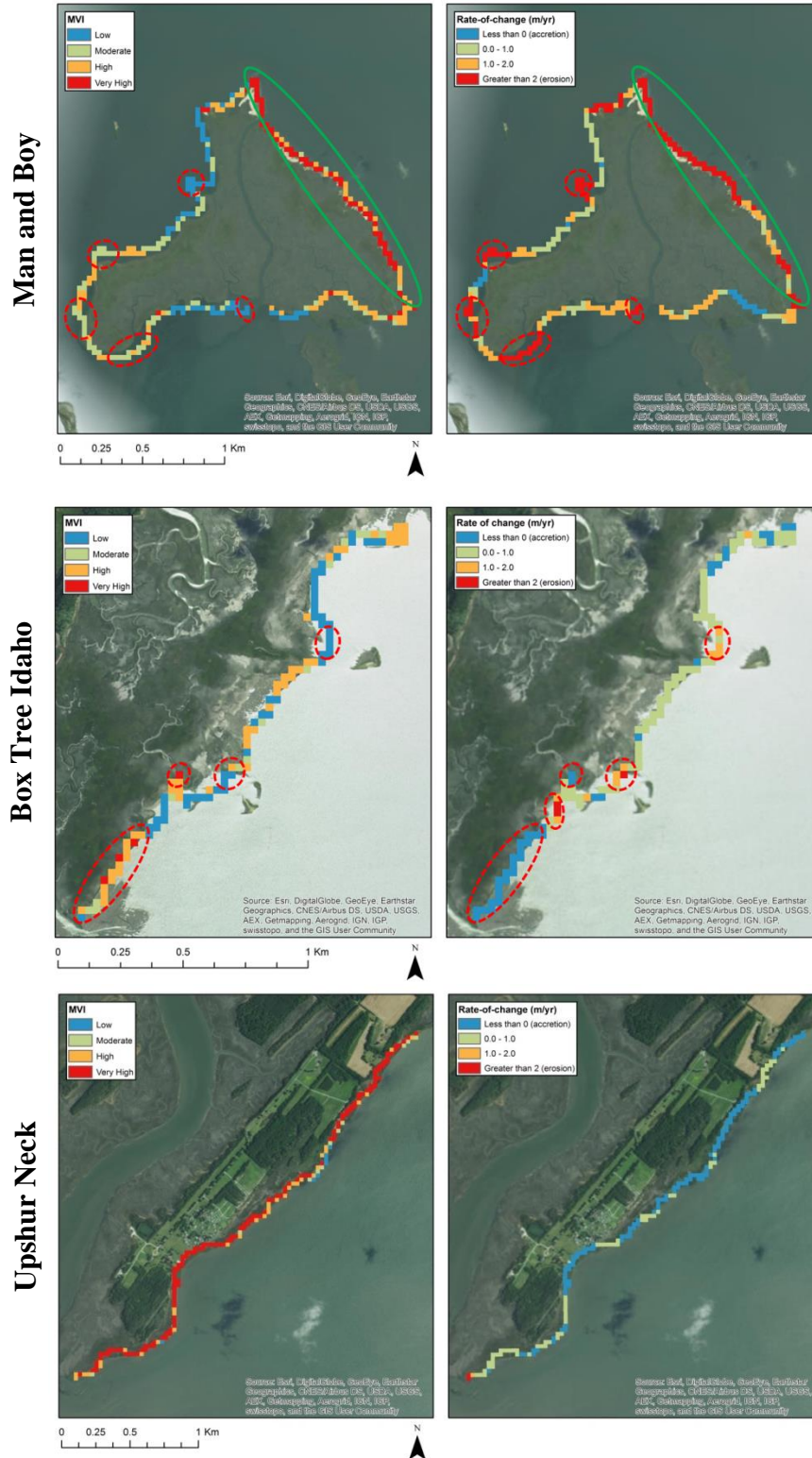


Figure 2.25. MVI output (*left*) and historical erosion rates (*right*) calculated for MB (*upper*), BTI (*middle*), and UN (*lower*). Green ovals represent areas where MVI values and erosion rates are generally aligned; red ovals indicate areas where there is discrepancy between MVI values and erosion rates.

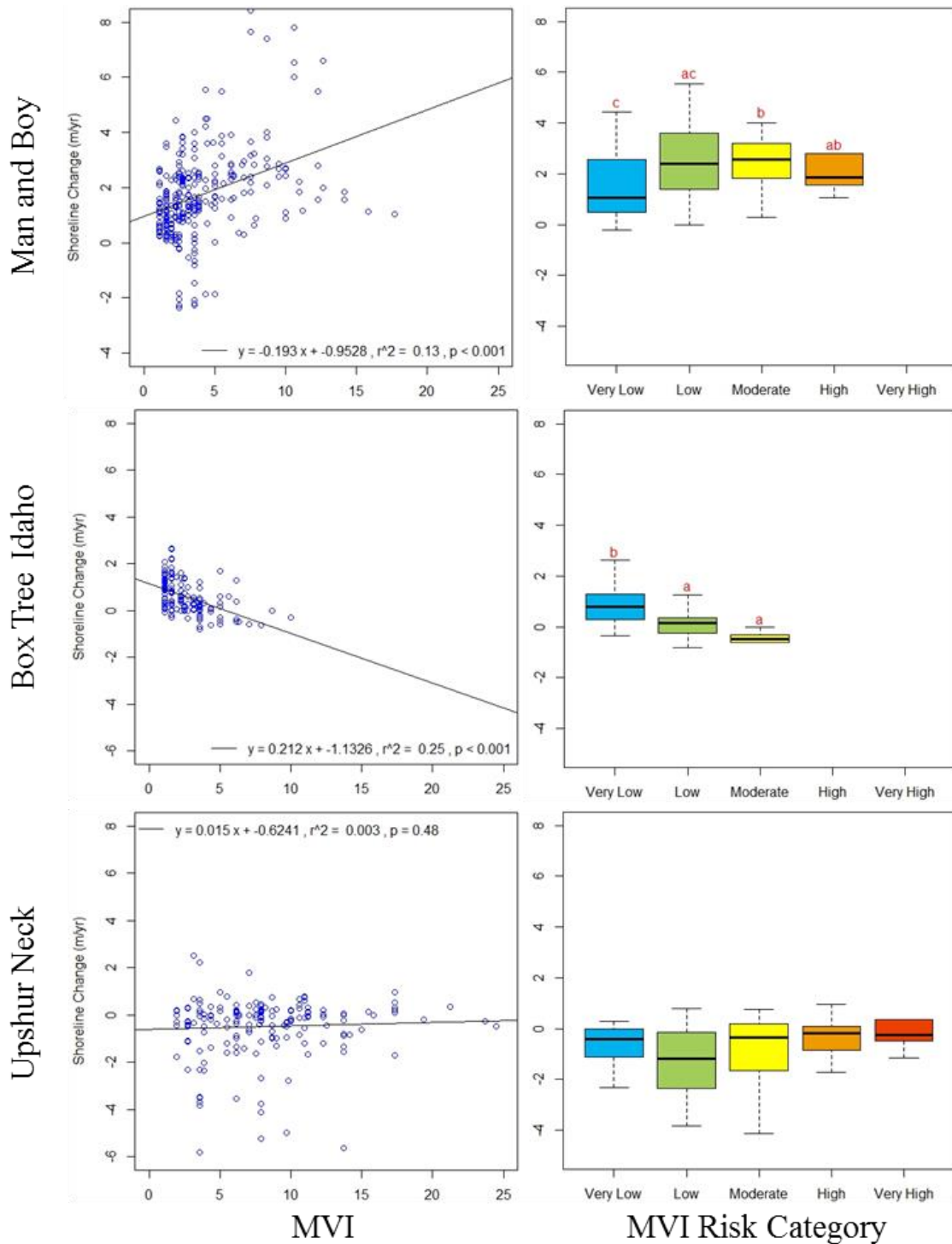


Figure 2.26. Linear regression results predicting shoreline change from MVI values at each site (*left column*). Results of comparison between MVI risk categories and shoreline change rates (*right column*). Positive (negative) values of shoreline change indicate erosion (accretion). Letters indicate statistically significant differences between risk categories ($p < 0.05$). Linear model, Kruskal-Wallis rank sum, and Dunn's test results can be found in Appendix A (2-5).

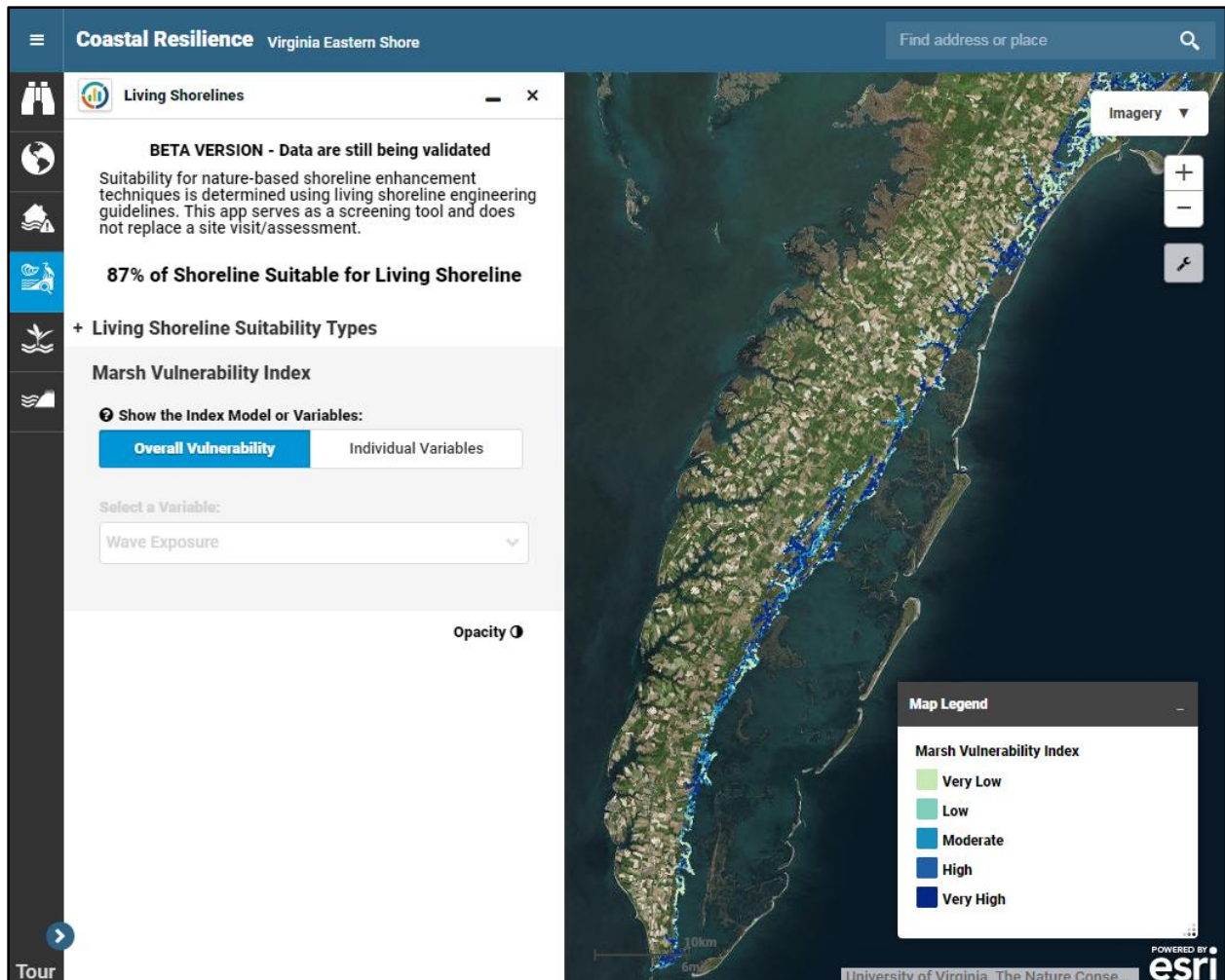


Figure 2.27. Screen capture of the Living Shoreline Explorer app on the TNC *Coastal Resilience* web mapping decision support platform. Marsh Vulnerability Index data are displayed in shades of blue according to vulnerability level.

Tables

Variable	Description	Coastal vulnerability studies
Wave exposure	Wave energy experienced at the shoreline; related to shoreline orientation, water depth, fetch length, and wind characteristics	Tibbetts and van Proosdij, 2013; Abuodha and Woodroffe, 2010; Ozyurt and Ergin, 2010; Kumar et al. 2010; Pendleton et al. 2004
Elevation	Influences susceptibility to erosion	Tibbetts and van Proosdij, 2013; Kumar et al. 2010; Nageswara Rao et al. 2008; Boruff et al. 2005; Pendleton et al. 2004; Thieler and Hammar-Klose, 1999; Cooper and McLaughlin, 1998; Shaw et al.1998; Gornitz et al. 1994, Gornitz et al. 1991
Slope	Reflects the ability of salt marshes to transgress; influences susceptibility to erosion	Chandrasekar et al. 2013; Tibbetts and van Proosdij, 2013; Abuodha and Woodroffe, 2010; Boruff et al. 2005, Gornitz et al. 1994, Kumar et al. 2010, Ozyurt and Ergin, 2010; Pendleton et al. 2010, Nageswara Rao et al. 2008; Thieler and Hammar-Klose, 1999
Relative sea level rise	Greater inundation risk under accelerated rates of sea level rise; deeper water increases wave energy	Chandrasekar et al. 2013; Pendleton et al. 2004; Shaw et al.1998; Thieler and Hammar-Klose, 1999; Gornitz et al. 1994; Gornitz et al. 1991
Storm surge	Exposes the shoreline to increased wave energy and inundation	Gornitz et al. 1994
Vegetation height	Vegetation stems dissipate waves	This study
Vegetation buffer width	Presence of wide fringing salt marshes dissipates waves	This study
Distance to boat activity	Boat wake subjects shorelines to short term wave attack	This study

Table 2.1. Summary of variables and associated definitions used to generate the MVI. Table modified from Tibbetts and Proosdij (2013).

Variable	Units	Very low (1)	Low (2)	Moderate (3)	High (4)	Very High (5)
Wave exposure	J m ⁻¹	<100	100 -200	200 – 400	400 – 500	>500
Elevation	m	<0.09	0.09 - 0.19	0.19-0.29	0.29 - 0.39	>0.39
Slope	deg	<12	12 – 16	16 – 20	20 – 24	>24
Relative sea level rise	mm yr ⁻¹	<3.1	3.1 - 3.8	3.8 - 4.3	4.3 - 5.5	>5.5
Storm surge	m	<2	2 - 2.3	2.3 - 2.6	2.6 - 2.9	>2.9
Vegetation height	cm	>26	26 – 18	18 – 12	12 – 6	<6
Vegetation buffer width	m	>50	50 – 25	25 – 15	15 – 10	<10
Distance to boat activity	m	>3200	3200 - 2400	2400 - 1600	1600 - 800	<800

Table 2.2. MVI matrix. Classification ranking (very low to very high) of variables used to generate the MVI.

Method	Mean stem height (cm)	Standard Deviation	Standard Error
LiDAR samples (n = 60)	12.75	4.82	0.43
Field samples (n = 163)	14.93	10.96	0.38

Table 2.3. Mean vegetation stem height for LiDAR and field measurements were not significantly different. Results from Mann-Whitney U test can be found in Appendix A (6).

Variable	Risk Class				
	Very Low	Low	Moderate	High	Very High
Wave exposure	63.8	18.6	12.6	2.1	2.9
Marsh elevation	76.3	4.1	4.5	4.1	11.0
Marsh slope	97.1	1.2	0.6	0.4	0.7
Relative sea level rise	0.0	100.0	0.0	0.0	0.0
Storm surge	9.1	2.8	3.4	7.2	77.4
Vegetation height	45.0	6.3	5.8	8.4	33.5
Vegetation buffer width	68.1	26.2	3.0	01.2	1.5
Distance to boat activity	60.4	12.2	11.7	9.7	5.9

Table 2.4. Percent of shoreline within each risk class as defined in Table 2.2.

	PC1	PC2	PC3
Vegetation height	-.778		
Storm surge	.642		-.509
Vegetation buffer width	.571		.310
Slope		.757	
Elevation		.743	
Distance to boat activity			.856
Wave exposure			.408

Table 2.5. PCA rotated component matrix.

Risk category	MVI range
Very Low	0.50 – 3.00
Low	3.00 – 6.32
Moderate	6.32 – 11.18
High	11.18 – 20.12
Very High	20.12 – 47.4

Table 2.6. MVI ranges for sequential levels of vulnerability.

Variable	Units	MB	BTI	UN
MVI	NA	3.9 ± 0.17 ^a	3.03 ± 0.14 ^b	8.1 ± 0.34 ^c
Shoreline change	m·yr ⁻¹	1.71 ± 0.09 ^a	0.30 ± 0.06 ^b	-0.51 ± .09 ^c
Wave exposure	J·m ⁻¹	164.0 ± 8.71 ^a	97.64 ± 2.33 ^b	230.6 ± 6.33 ^c
Elevation	m	-0.51 ± 0.03 ^a	-0.04 ± 0.04 ^a	0.35 ± 0.05 ^b
Slope	deg	1.45 ± 0.20 ^a	2.23 ± 0.25 ^b	3.16 ± 0.27 ^c
Veg. height	ft	0.43 ± 0.02 ^a	0.66 ± 0.05 ^b	0.85 ± 0.22 ^c
Veg. buffer width	m	49.13 ± 0.37 ^a	48.34 ± 0.5 ^a	41.93 ± 1.04 ^b
Distance to boat activity	km	7.71 ± 0.35 ^a	6.90 ± 0.48 ^b	3.54 ± 2.60 ^c
Storm surge	ft	10.45 ± 0.033 ^a	12.4 ± 0.03 ^b	10.27 ± 0.08 ^a

Table 2.7. Mean MVI, shoreline change, and vulnerability variables with ± 1 SE for MB, BTI, and UN. MB (n = 292), BTI (n = 145), and UN (n = 178). Positive (negative) values of shoreline change indicate erosion (accretion). Letters indicate significant differences between sites (p < 0.05). Results from Kruskal-Wallis rank sum and Dunn’s test can be found in Appendix A (7-15).

CHAPTER 3

WAVE-DAMPENING EFFECTS OF OYSTER REEFS AND MARSH VEGETATION

3.1 Objective

The second objective of this study was to measure the wave-dampening effects of constructed oyster reefs and marsh vegetation and under a variety of water level conditions in the Virginia Coast Reserve (VCR). Wave measurements were collected over four marsh sites, three of which were fronted by constructed oyster reefs. Changes in wave height across a constructed oyster reef or marsh transect were used as an indicator of wave attenuation. Vegetation samples were collected to characterize each site. Quantifying wave attenuation by constructed oyster reefs and marsh vegetation helped drive empirically-based shoreline stabilization recommendations.

3.2 Study sites

Four salt marsh sites within the VCR were selected for their varying morphology and the presence or absence of a constructed oyster reef (Figure 3.1). Marsh sites varied in latitude and wave exposure; oyster reefs varied in design and placement. This method provided variability among sites and facilitated comparison between sites (McLoughlin et al. 2011). Each of the constructed oyster reefs was composed of interlocking Oyster Castle® bio-concrete spat blocks and configured as an array of staggered rows or as a mostly continuous structure. The oysters that settled on these constructed reefs were American Eastern Oysters, *Crassostrea virginica*.

The northernmost site, Tom's Cove (TC) (Figure 3.2a) is a narrow fringing marsh fronting a road inside an embayment on Chincoteague Island. The marsh is fronted with a staggered array of constructed oyster reef rows constructed by The Nature Conservancy (TNC) in 2016. Fowling

Point (FP) (Figure 3.2b) is a stable, low-lying mainland marsh situated in Hog Island Bay, fronted by an extensive tidal flat. There is no oyster reef present at Fowling Point. The Box Tree Idaho site (BTI) (Figure 3.2c) is a mainland marsh located in Ramshorn Bay and hosts a large, mostly continuous constructed oyster reef system. The BTI oyster reef was constructed in 2014 by TNC over an old, dead, natural reef and is offset from the marsh edge by ~600 meters. This reef was constructed with oyster restoration as the primary purpose (i.e., not for shoreline protection). The Man and Boy site (MB) includes two shorelines, East (MBE) (Figure 3.2d) and South (MBS) (Figure 3.2e), along a small marsh island separating South Bay and Cobb Bay. Each MB shoreline is fronted by two staggered arrays of constructed oyster reef rows. The MB oyster reefs were installed by TNC in 2015 and repaired in 2017 after a bio-concrete mix failure caused the Oyster Castle® blocks to disintegrate. A summary of constructed oyster reef and marsh characteristics for each site is listed in Table 3.1. Site names are abbreviated using the naming convention, “site-sampling year” (e.g., Fowling Point sampled in 2016 = FP-16).

3.3 Methods

Field measurements

Measurements of water levels and wave conditions were collected at each site using Richard Branker Research (RBR) Submersible Tide and Wave Recorders (RBR Ltd., Ontario, Canada), commonly known as wave gauges. Deploying wave gauges simultaneously along a transect allows for the resolution of wave transformation from the bay to the inner marsh. Wave gauges were positioned at stations 10-20 meters from either side of the constructed oyster reef (if present) and up onto the marsh platform (Figure 3.3). Most transects consisted of a bay, tidal flat, outer edge, inner edge, outer marsh, and inner marsh sampling station. The wave gauges were attached to metal frames with zip ties and staked flush with the bed surface (Figure 3.4). Wave

gauges deployed at deeper stations were secured onto concrete blocks with zip ties, and this height difference was accounted for in water depth measurements. Wave gauges were deployed for a minimum of three weeks (full spring-neap cycle), measuring wave conditions every 30 minutes at a speed of 4Hz and a burst length (samples) of 1024. Tidal elevations are measured with a burst rate of 4Hz and averaged over 4 minutes every 30 minutes. Figures 3.5- 3.9 depict the transect configuration of each study site, organized from the northernmost to southernmost site; Table 3.2 provides the sampling schedule of deployments.

Field sampling

Stem height, width, and density were sampled at marsh-based stations for FP-16, BTI-16, and MBE-17. Three random replicates were taken at each marsh-based station. Using a 30 cm² quadrat to define the sample area, the stems inside the quadrat were clipped at the sediment surface. Samples were placed into plastic bags, returned to the lab, and transferred to paper bags to dry. At the lab, all stalks were counted to determine density and measured with a 1-meter ruler for stem height and calipers for stem width.

Data analysis

Meteorological observations (wind speed and direction, barometric pressure) and water levels recorded at the National Oceanic and Atmospheric Administration (NOAA) station (Station ID: 86310440) at Wachapreague, VA (www.tidesandcurrents.noaa.gov) were used to characterize meteorological conditions. Barometric pressure was used to correct pressure measured by the wave gauges to account for effects of atmospheric pressure. If data from the NOAA Wachapreague station were not available, records from the NOAA station (Station ID: 8632200) at Kiptopeke, VA (www.tidesandcurrents.noaa.gov), the Melfa/Accomack Airport

station (Station ID: 03716), or the National Weather Service site at Wallops Island (<http://w1.weather.gov/obhistory/KWAL.html>) were used. Comparison of water level measurements from Wachapreague station and the RBR wave gauges was generally in good agreement and excellent agreement at high water levels (Figure 3.10). There was a time lag in water level evident at lower water levels.

RBR wave analysis software (Ruskin) was used to obtain significant wave height and period for each wave record based on the variance of the depth-corrected water-surface elevation time series recorded at each site (Wiberg et al. *in revision*). Changes in wave height between pairs of sensors across each constructed oyster reef (outer and inner stations) and across a marsh transect were used as an indicator of wave attenuation. Analysis of wave data was limited to flood conditions (i.e., all wave gauges along a transect were covered by water). Table 3.3 summarizes the hours flooded for each site deployment.

Wind speed, wind direction, water depth, and significant wave height (H_s) time series were developed for each site to visualize conditions contributing to the greatest wave heights and wave height differences. Comparisons were made of water depth recorded at the outer vs. inner stations to verify that the wave gauges were measuring the same signal.

Statistical analyses were performed using the statistical software, “R” 3.4.4. Vegetation stem width data were not normally distributed even after transformation; therefore, a nonparametric test, the Mann-Whitney U test, was used to compare stem height and stem width by species. When ANOVA assumptions were not met, log₁₀ transformations were used to satisfy those assumptions. A one-way ANOVA was used to compare vegetation stem height and stem density by marsh site. Post-hoc comparisons were made with Tukey-Kramer (unequal sample sizes) tests. A nonparametric test, the Kruskal-Wallis rank sum test, and a post-hoc comparisons test,

the Dunn's Test of Multiple Comparisons, were performed to compare stem width by marsh site. Significant wave height measurements at each reef site were separated into shallow (< mean water depth) and deep (> mean water depth) water conditions. Mean water depth was based on the sensor placed at the outermost (bay) station. A linear trendline was fit to the data to determine the strength of the relationship. A slope less than 1 suggests a decrease in wave height from outer to inner sampling stations. Wave data were not normally distributed even after transformation; therefore, the Kruskal-Wallis rank sum test and Dunn's test were performed to investigate the change in wave height at three comparison sites.

3.4. Results

Site characteristics

Water depth, wind statistics, and waves

Time series for water depth, wind speed, wind direction, and significant wave height (H_s) are presented in Figures 3.11 – 3.19 (organized from the northernmost to southernmost site) and summarized in Table 3.4. RBR wave gauge-measured water depths at outer and inner stations were very well correlated at all study sites (Table 3.5). Winds at the northern end of the study area (Wallops Island) during the year 1 July 2016 – 30 June 2017 tended to most frequently blow from the south and northwest, with less frequent but occasionally strong winds from the northeast (Figure 3.20). Wind data from the National Weather Service site at Wallops Island were used because it offered the most complete record spanning the duration of field deployments throughout this study.

Vegetation characteristics

A summary of vegetation characteristics for each marsh site is presented in Table 3.6. Stem height, width, and density recorded for this study were consistent with other studies for *Spartina alterniflora* and *Salicornia europaea* (Table 3.7). Overall, *Spartina alterniflora* stems were significantly taller and wider than *Salicornia europaea* stems (Figure 3.21). Stem density by species was not calculated because density counts included both species indiscriminately

Significant differences in stem height and width existed across all three marsh sites (Figure 3.22). BTI-16 was dominated by *Spartina alterniflora* and had the greatest mean stem height and width; FP-16 was dominated by *Salicornia europaea* and presented the lowest mean stem height and width. Stem density was significantly higher at FP-16 than MBE-17, but no significant difference was detected between MBE-17 and BTI-16. This difference is consistent with *Spartina alterniflora* versus *Salicornia europaea*-dominated marsh sites (i.e., higher density was expected at the *Salicornia europaea*-dominated sites) (Table 3.7).

Wave summary – constructed oyster reefs

Mean significant wave heights during the reef deployments ranged from 0.01 – 0.10 m, with the 90th percentile of wave heights reaching 0.22 meter at site MBE in 2017 (Table 3.8).

Regressions of scatter plots of inner vs. outer significant wave heights during each deployment yielded slopes <1 for all cases, indicating some degree of wave attenuation (Figure 3.23 – 3.29).

Separating deep ($>$ mean water depth) and shallow ($<$ mean water depth) conditions yielded regression slopes that were smaller for shallow water conditions than deep water conditions. The average reduction in wave heights across all reef sites when water depths were greater than mean

site depth was 8%, whereas for shallow depths the average wave height reduction was 46%. These results are consistent with the findings of Wiberg et al. (*in revision*).

Note on Box Tree Idaho 2016

Meteorological observations (wind speed, wind direction, atmospheric pressure) and water levels from the NOAA Wachapreague station were not available for the full period of this deployment. Wind speed and direction were obtained from the NOAA station (Station ID: 8632200) at Kiptopeke, VA as it provided the nearest, most complete record. Atmospheric pressure records from Melfa/Accomack Airport (Station ID: 03716) were adjusted to fit Wachapreague atmospheric pressure records and used to fill the gaps in the Wachapreague record.

Wave summary – marsh vegetation

Mean significant wave heights during the marsh deployments ranged from 0.01 – 0.06 m, with the 90th percentile of wave heights reaching 0.13 meter at site BTI in 2016 and 2017 (Table 3.9). Figures 3.30 - 3.32 show wave transformation (% reduction or growth of wave height) over each marsh transect as a percentage of the initial wave height recorded at the outermost (bay) station. For each site, excluding BTI-17, the greatest % decrease in wave height occurred as waves propagated over the marsh platform between the outer and inner edge stations. Wave height initially increased at FP-16 (Figure 3.30) as waves propagated landward and encountered a tidal flat, inducing a shoaling effect; but, as the waves passed over the marsh platform, they were rapidly attenuated. At BTI-17 (Figure 3.32), the greatest reduction in wave height occurred between the tidal flat and outer edge station.

Reefs versus marsh vegetation

A comparison was made to examine the wave-dampening effects of marsh vegetation compared to constructed oyster reefs at Tom's Cove (Figure 3.5). At TCV-16 (Figure 3.33), significant wave height was 49% less at the vegetated station (TCV) than the non-vegetated (TC10) station. During deep water conditions, significant wave height was 47% less at the vegetated station than the non-vegetated station. During shallow water conditions, significant wave height at the vegetated station was 95% less than the non-vegetated station. From these results, it is clear that marsh vegetation had a greater effect on attenuating waves than any of the constructed reef sites.

3.5 Discussion

Wave attenuation by marsh vegetation

Percent reduction of wave height at FP-16 and MBE-17 was compared to define marsh buffer widths over which waves were substantially attenuated (Figure 3.34). FP-16 and MBE-17 were chosen for this analysis because their transect configurations (length and placement of sampling stations) were the most similar (Figure 3.6 and Figure 3.8, respectively). Percent reduction of wave height was calculated as a percentage of wave height recorded at the outer edge station. Values for % reduction at distances of 10, 20, and 30 meters over the marsh platform were linearly interpolated (Table 3.10). At approximately 10 meters, the average % reduction across both sites was 60%. The mean % reduction increased to 78% by 20 meters; and, waves were reduced by an average of 82% at 30 meters. The rapid change in % reduction of wave height from 10 to 30 meters suggests a nonlinear relationship; consistent with findings by Barbier et al. (2008). Average % reduction in wave height was similar to findings in the United

Kingdom (UK) where salt marshes reduced wave height by up to 50% over 10-20 meters (Möller et al. 2002; Möller et al. 1999). However, it can be challenging to compare values between studies due to factors like vegetation characteristics, marsh topography, water depth, and incoming wave height.

Influence of vegetation characteristics on wave attenuation

Vegetation characteristics and % reduction in wave height were compared to determine the effect on wave attenuation at three sites where vegetation was sampled: FP-16, BTI-16, and MBE-17 (Figure 3.35). Percent reduction in wave height across the marsh platform was calculated for each site as a percentage of wave height recorded at the outer edge station compared to the inner marsh station. Change in significant wave height (ΔH_s) was calculated as the difference between the outer edge and inner marsh stations and was found to be significantly lower at BTI-16 than FP-16 and MBE-17. Percent reduction in wave height was greatest at FP-16 where stem height and width were the lowest, but density was the highest. BTI-16 was characterized by the lowest % reduction in wave height, yet reported the highest stem height and width. MBE-17 fell between FP-16 and BTI-16 for % wave reduction, stem height, and stem width; and, recorded the lowest stem density. These findings are consistent with measurements made by Möller (2006) that reported the highest wave attenuation over a transect with the highest vegetation density. These results suggest that stem density may be a controlling factor in wave attenuation measured at these three sites; although, physical properties not considered here (e.g., nearshore bathymetry, incoming wave height) may also play an important role.

Wave attenuation by oyster reefs

Wave and water-level measurements collected across five constructed oyster reefs in the Virginia Coast Reserve suggest that reefs can be effective at reducing wave energy, but that this efficacy is limited to shallow water depth conditions. The strong difference in wave attenuation capacity of the reefs as a function of water depth is consistent with previous findings by Wiberg et al. (*in revision*). The average reduction in wave heights across all reef sites when water depths were greater than mean site depth was 8%, whereas for shallow depths the average wave height reduction was 46%.

When water depths are great enough that waves can pass over a constructed oyster reef unmodified, wave energy will dissipate either at the marsh edge (tending to drive marsh retreat) or within the marsh platform, depending on the elevation of the marsh relative to mean sea level. Thus, the potential benefits for reef-associated wave attenuation are dependent on water depth and marsh edge elevation (Wiberg et al. *in revision*). Since the largest waves generally accompany high wind and deep water conditions, constructed oyster reefs with a crest elevation below mean sea level are unlikely to be effective at wave attenuation under the highest wave conditions. However, as seen at the Tom's Cove site (TCV-16), which compares waves at a vegetated and non-vegetated station, marsh vegetation is effective at attenuating waves even during deeper water conditions. Thus, combining constructed oyster reefs with vegetated treatments may be an effective and sustainable long-term shoreline stabilization technique in which the reef helps to stabilize the marsh edge while expansive marsh vegetation attenuates wave energy that passes over the fringing reef.

Figures

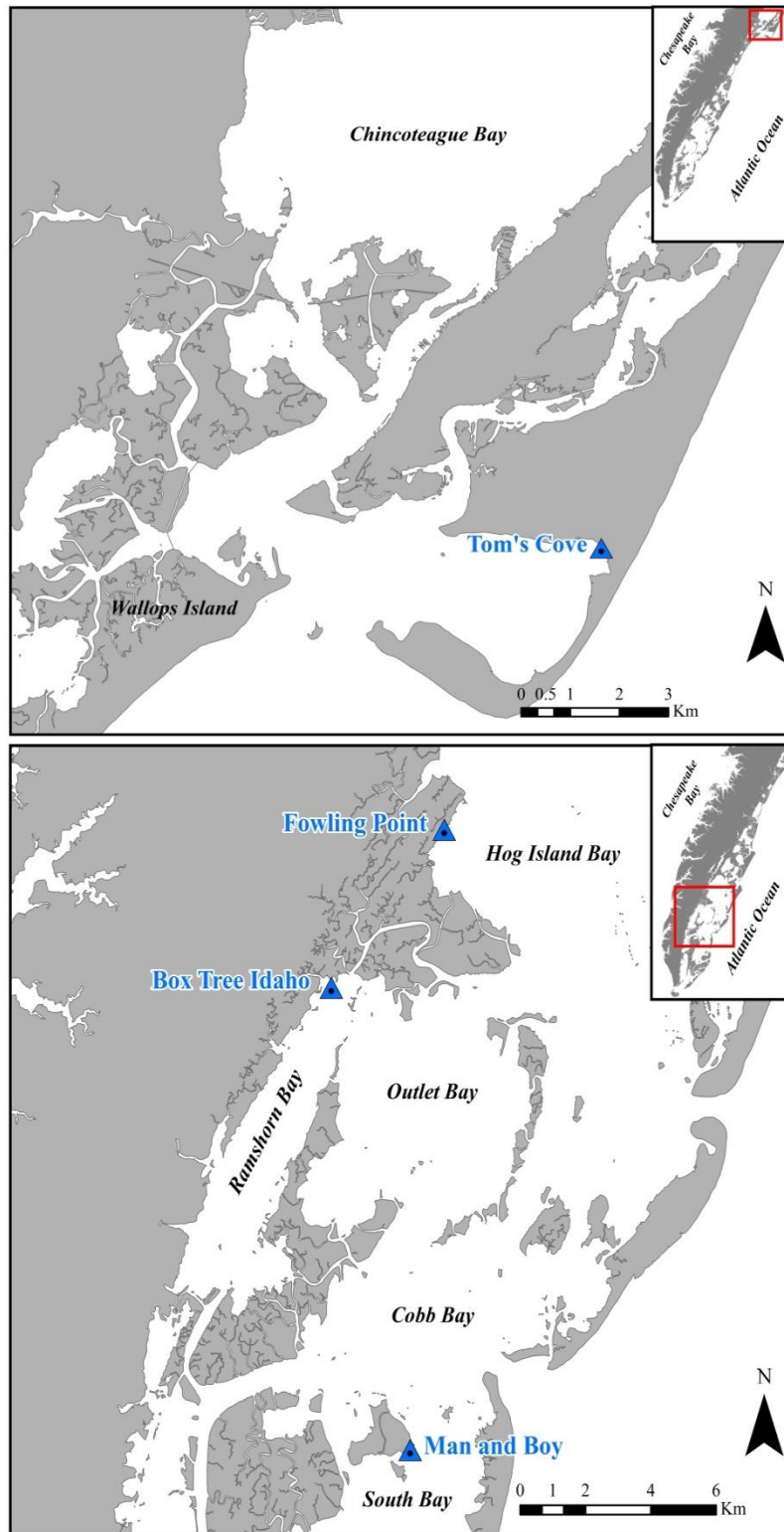


Figure 3.1. Locations of the four marsh sampling sites: Tom's Cove, Fowling Point, Box Tree Idaho, and Man and Boy.



Figure 3.2. Photographs of the study sites. Tom’s Cove (a), Fowling Point (b), Box Tree Idaho marsh and reef (c), and Man and Boy East (d) and South (e).

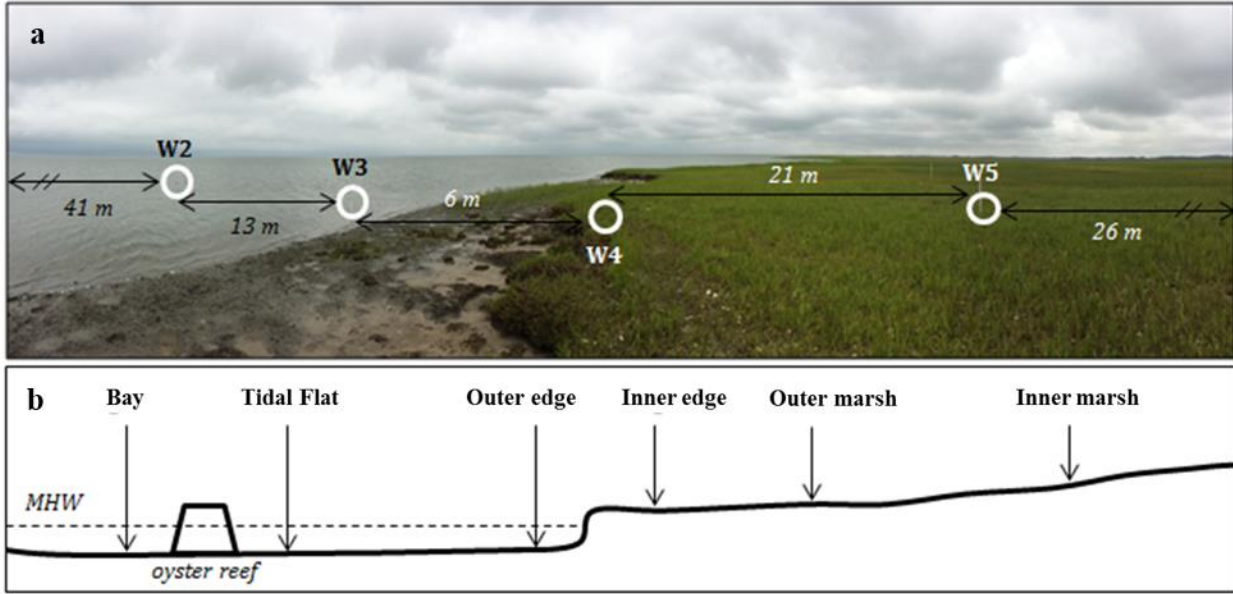


Figure 3.3. (a) Transect configuration at Fowling Point marsh showing wave gauges (W2, W3, W4, W5). W1 and W6 are not visible in the frame. (b) Schematic cross-section of generalized transect.

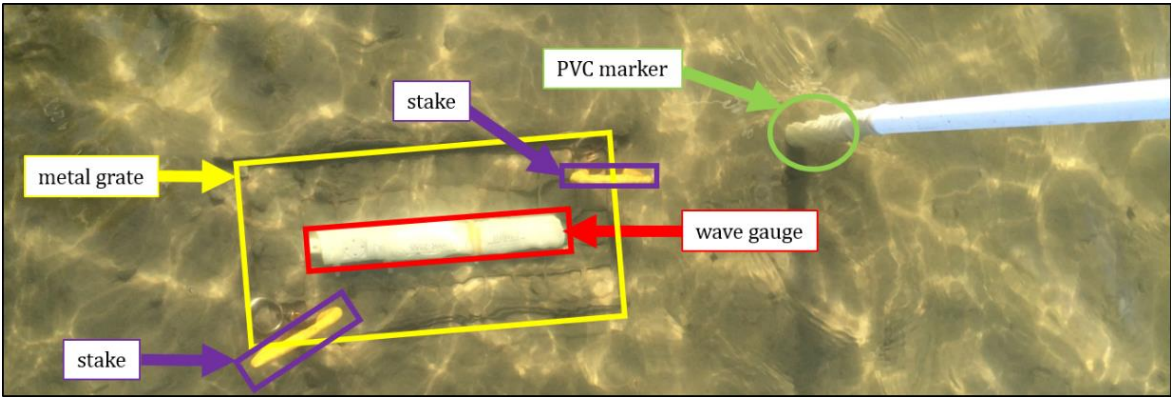


Figure 3.4. Wave gauge secured to metal grate with zip ties and staked into ground. PVC pipe placed to mark location.



Figure 3.5. TC1-16/TC2-16/TCV-16 study site with sampling stations.



Figure 3.6. FP-16 study site with sampling stations.



Figure 3.7. BTI-16/BTI-17 study site with sampling stations.

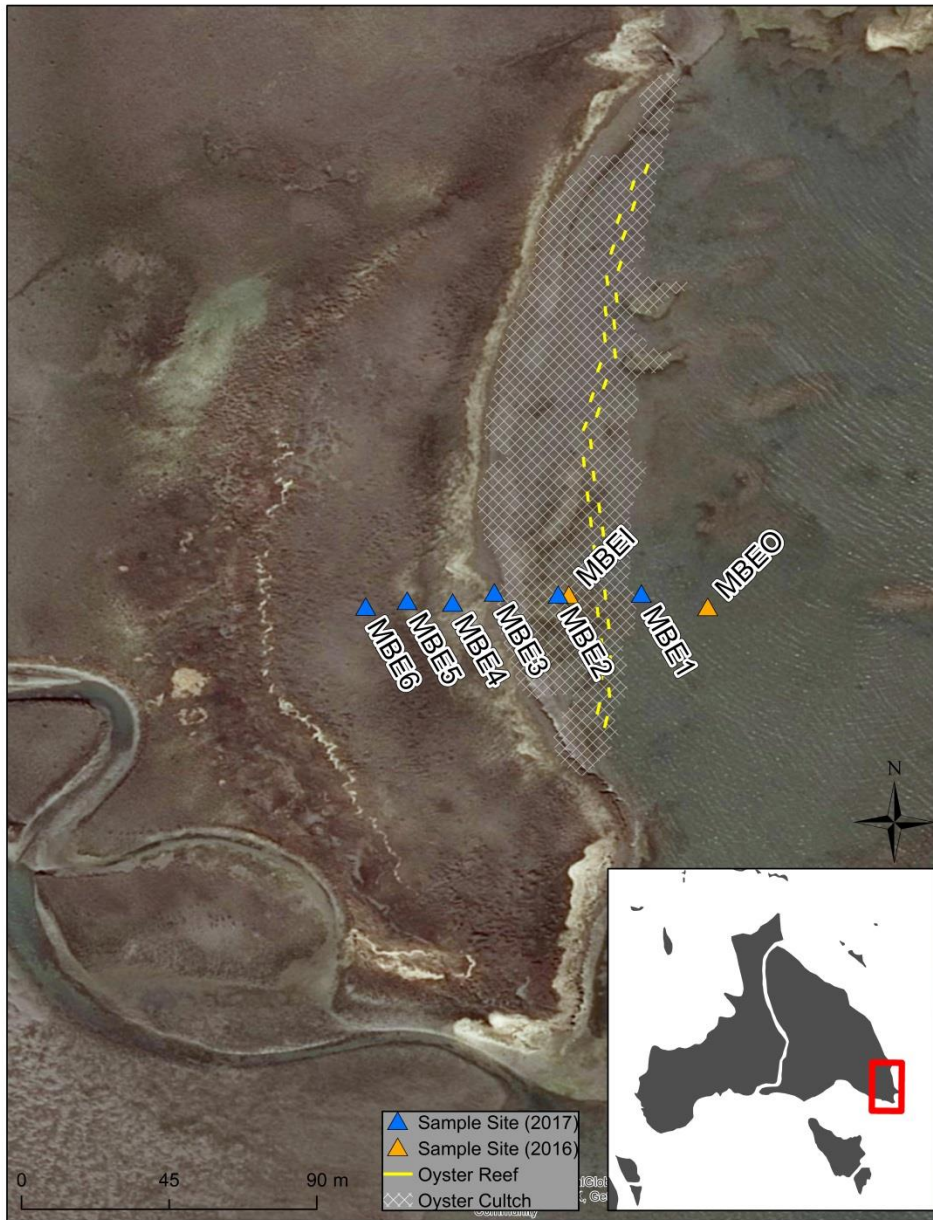


Figure 3.8. MBE-16/MBE-17 study site with sampling stations.

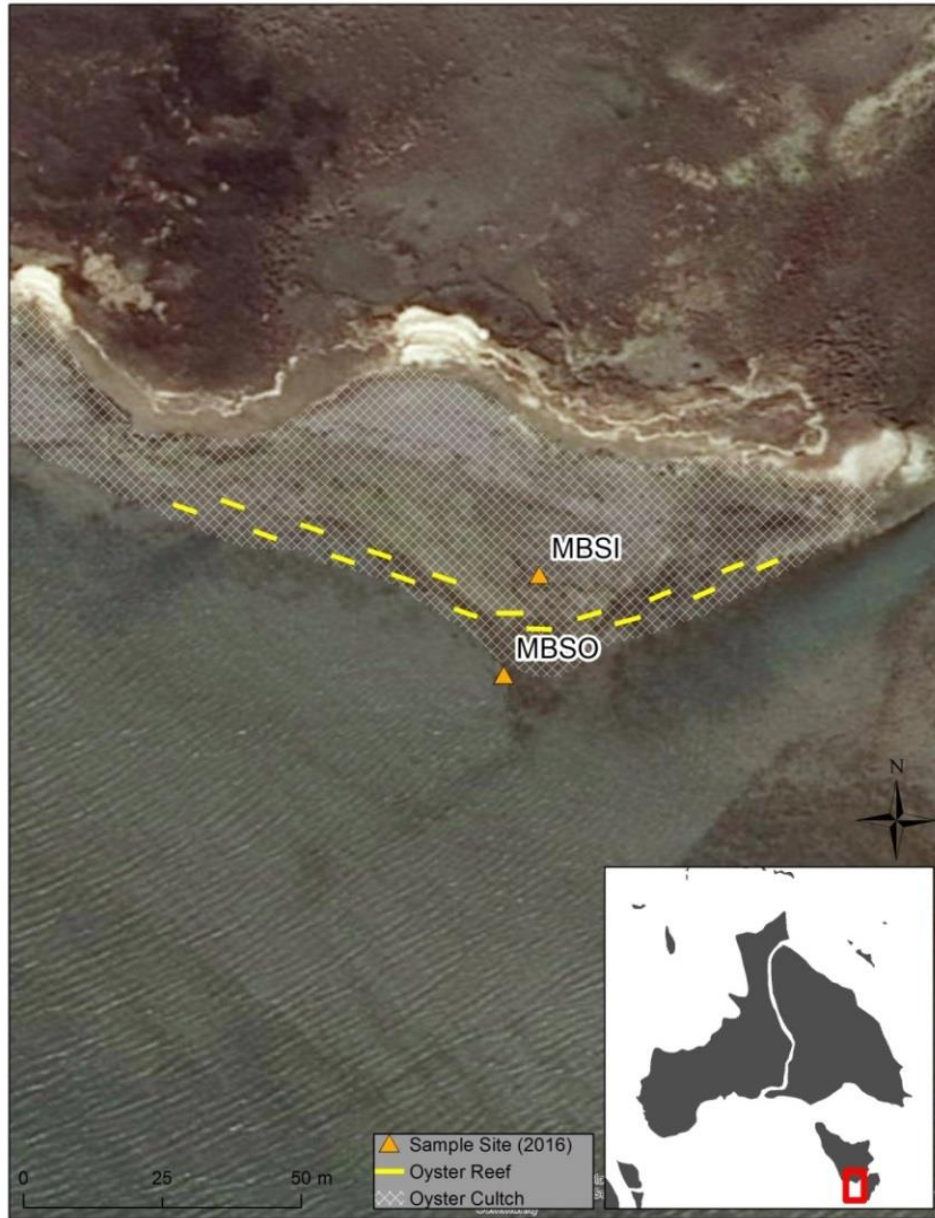


Figure 3.9. MBS-16 study site with sampling stations.

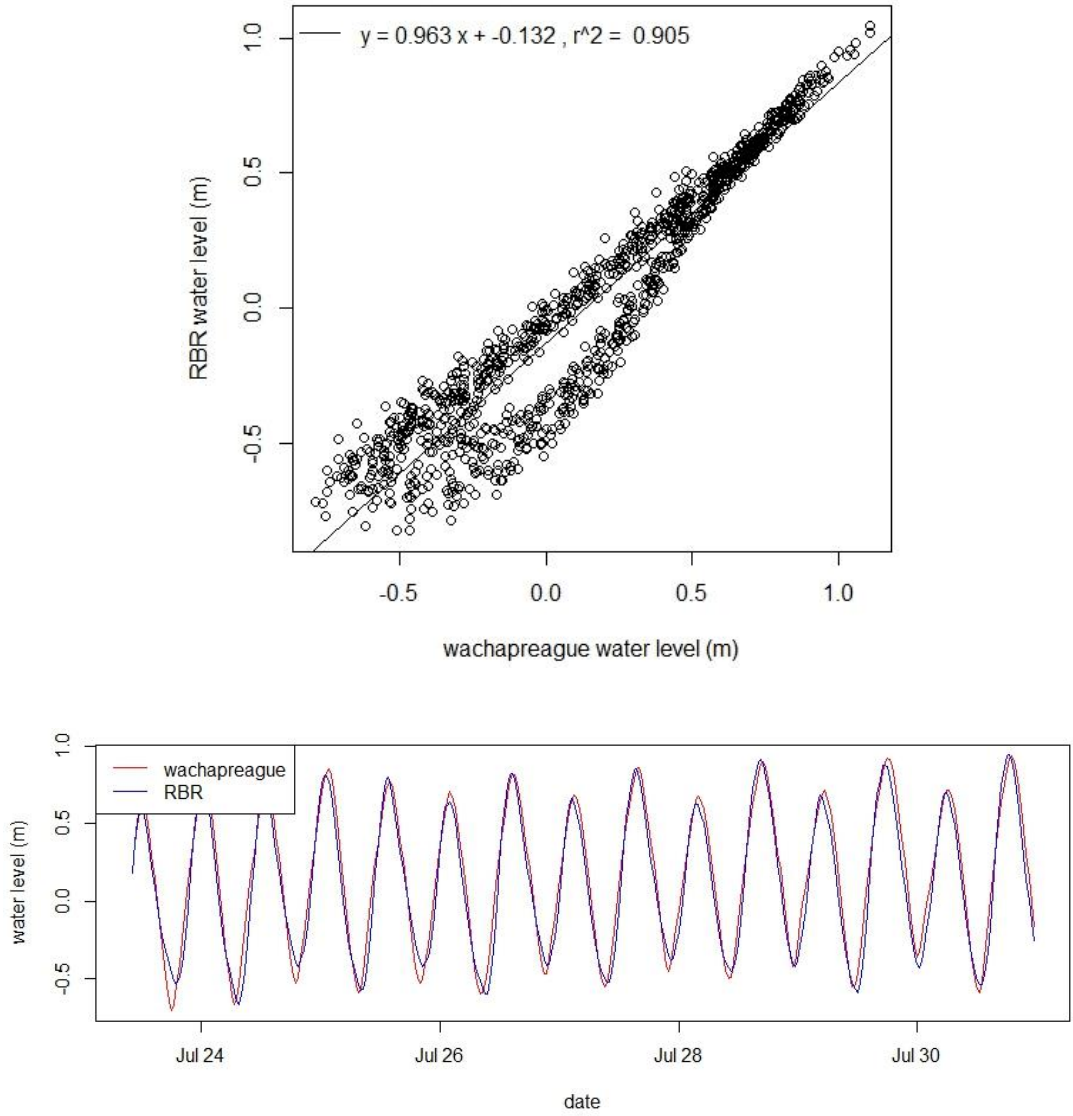


Figure 3.10. Wachapreague station (WAHV2) water level measurements compared to RBR water level measurements from BTI-16.

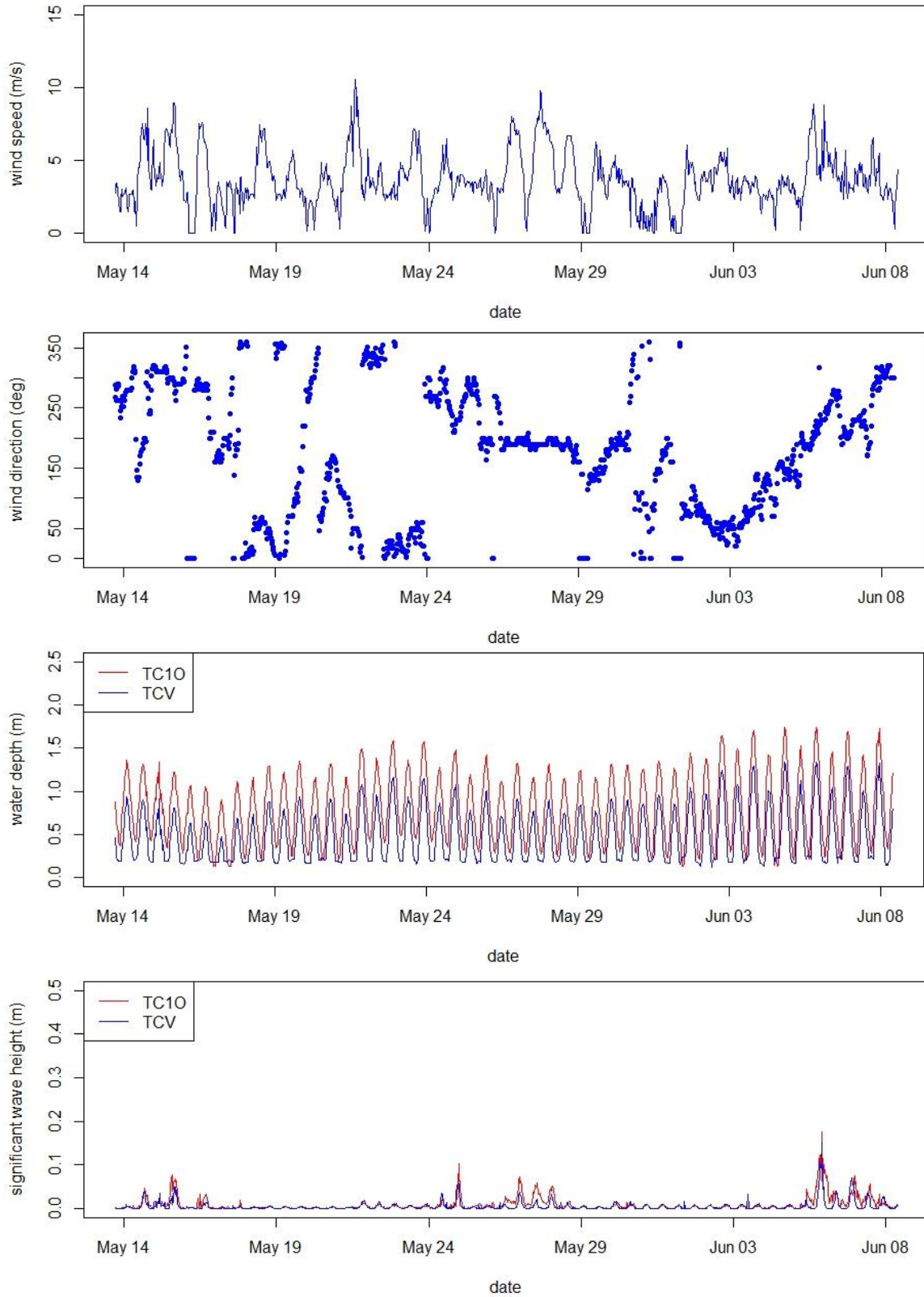


Figure 3.11. Wind speed, wind direction, water depth, and H_s time series from TC1-16.

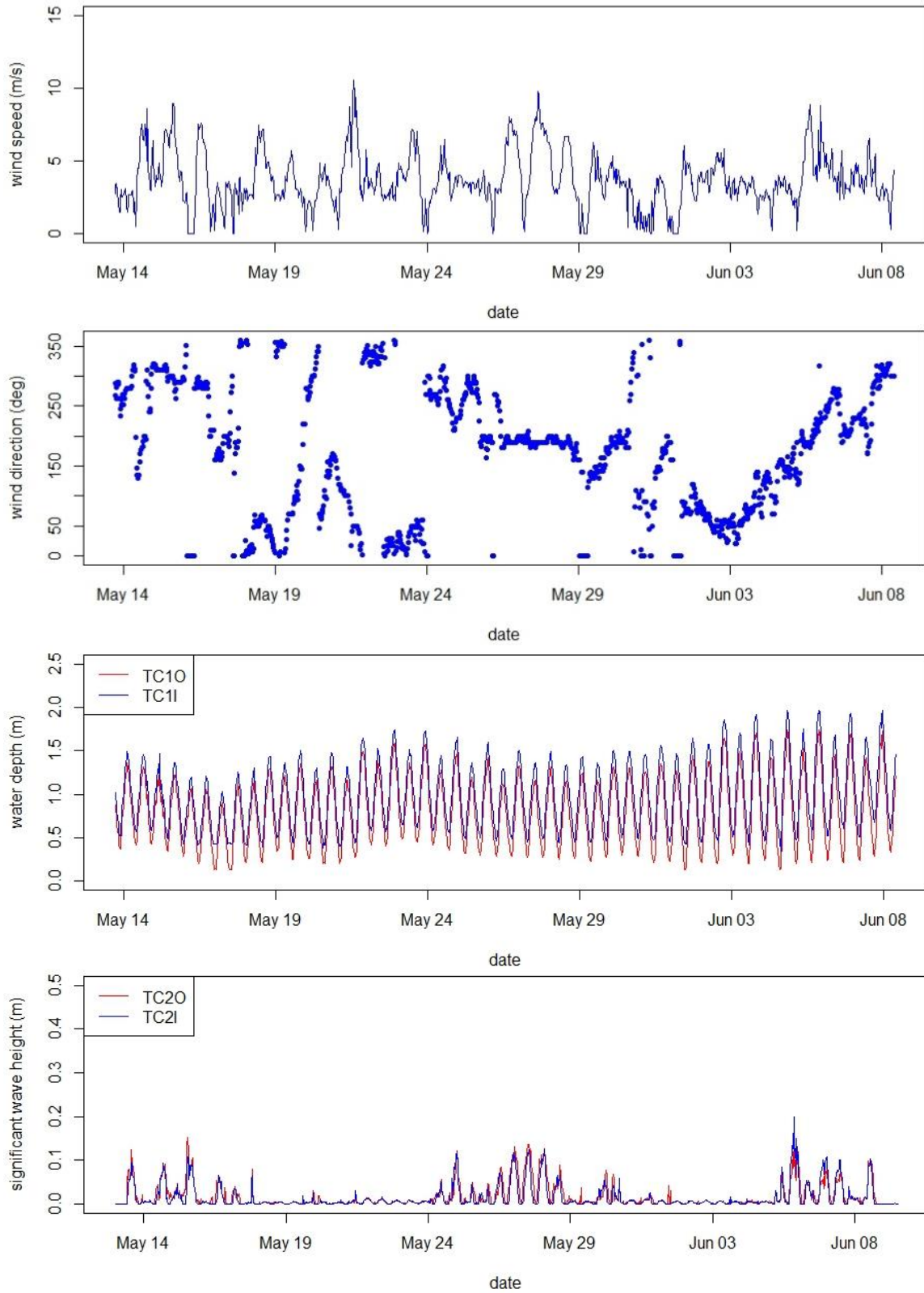


Figure 3.12. Wind speed, wind direction, water depth, and H_s time series from TC2-16.

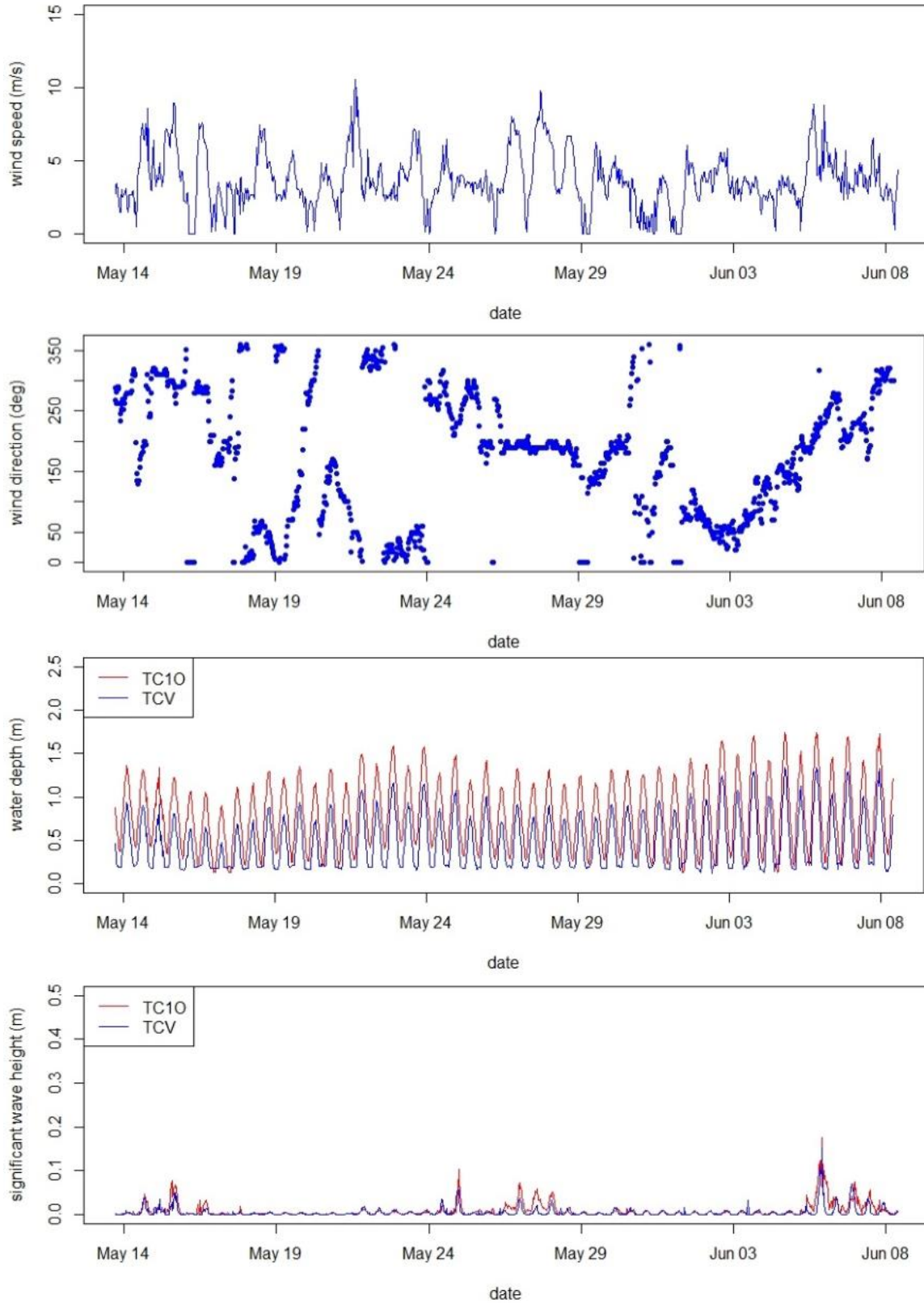


Figure 3.13. Wind speed, wind direction, water depth, and H_s time series from TCV-16.

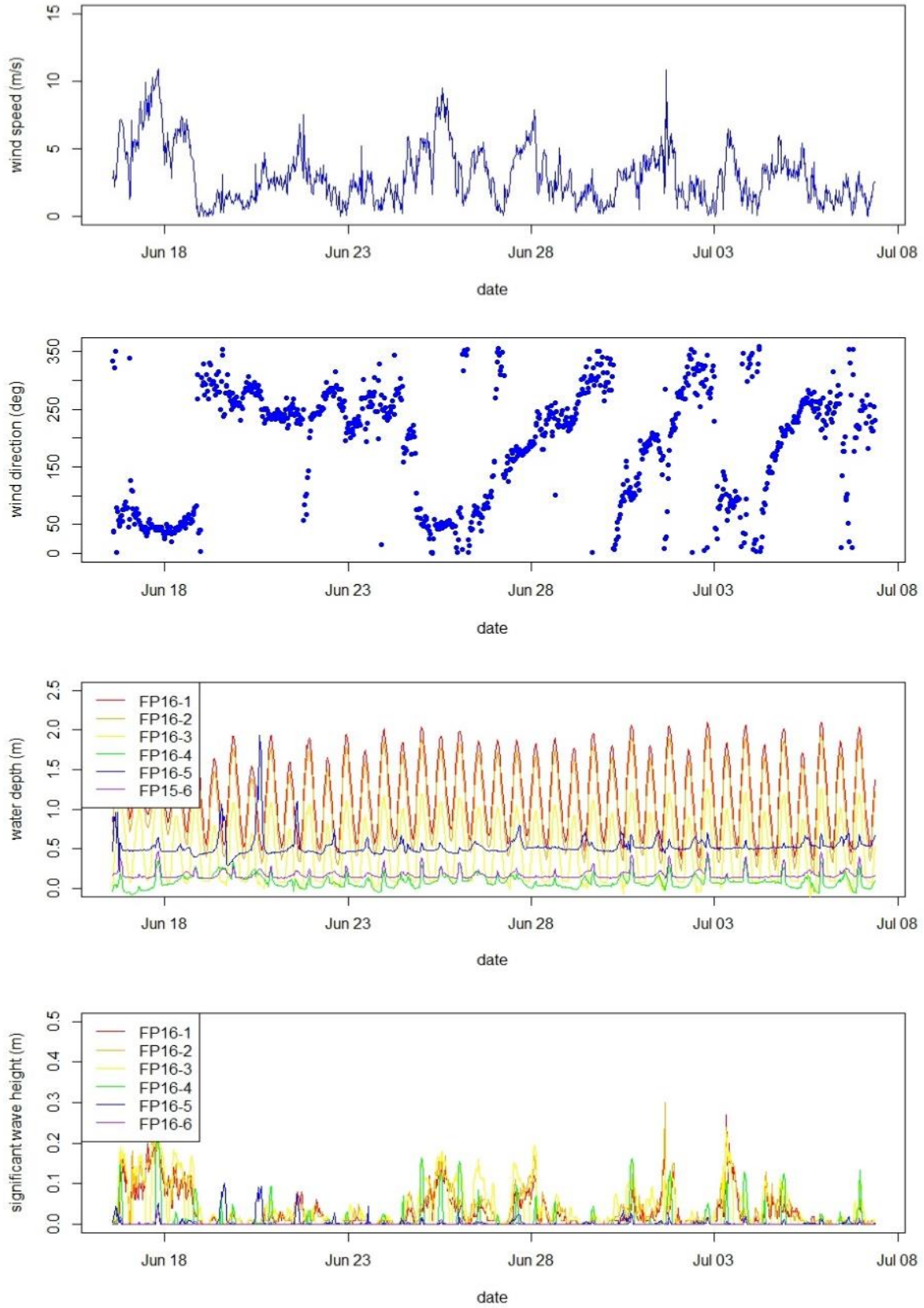


Figure 3.14. Wind speed, wind direction, water depth, and H_s time series from FP-16.

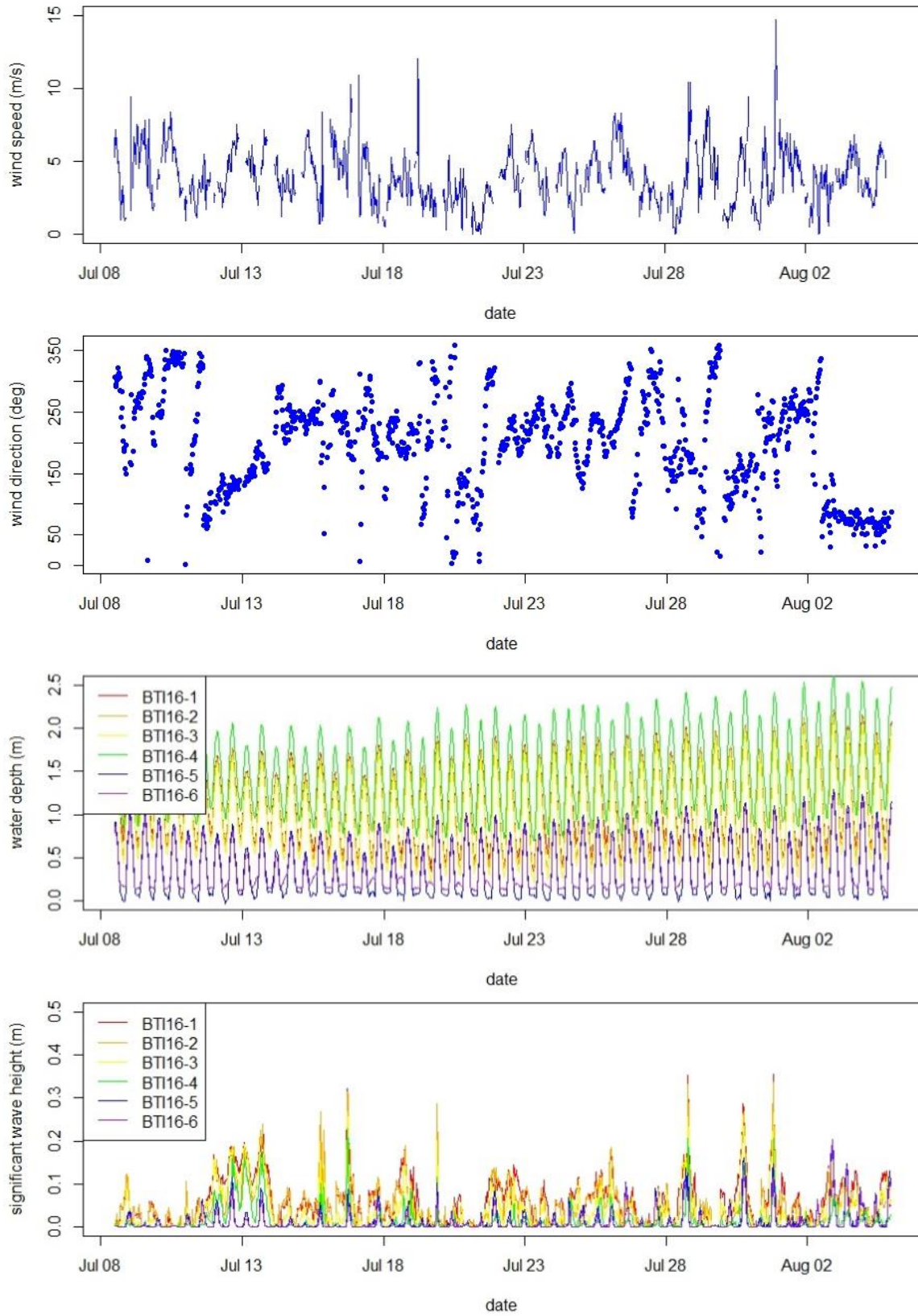


Figure 3.15. Wind speed, wind direction, water depth, and H_s time series from BTI-16.

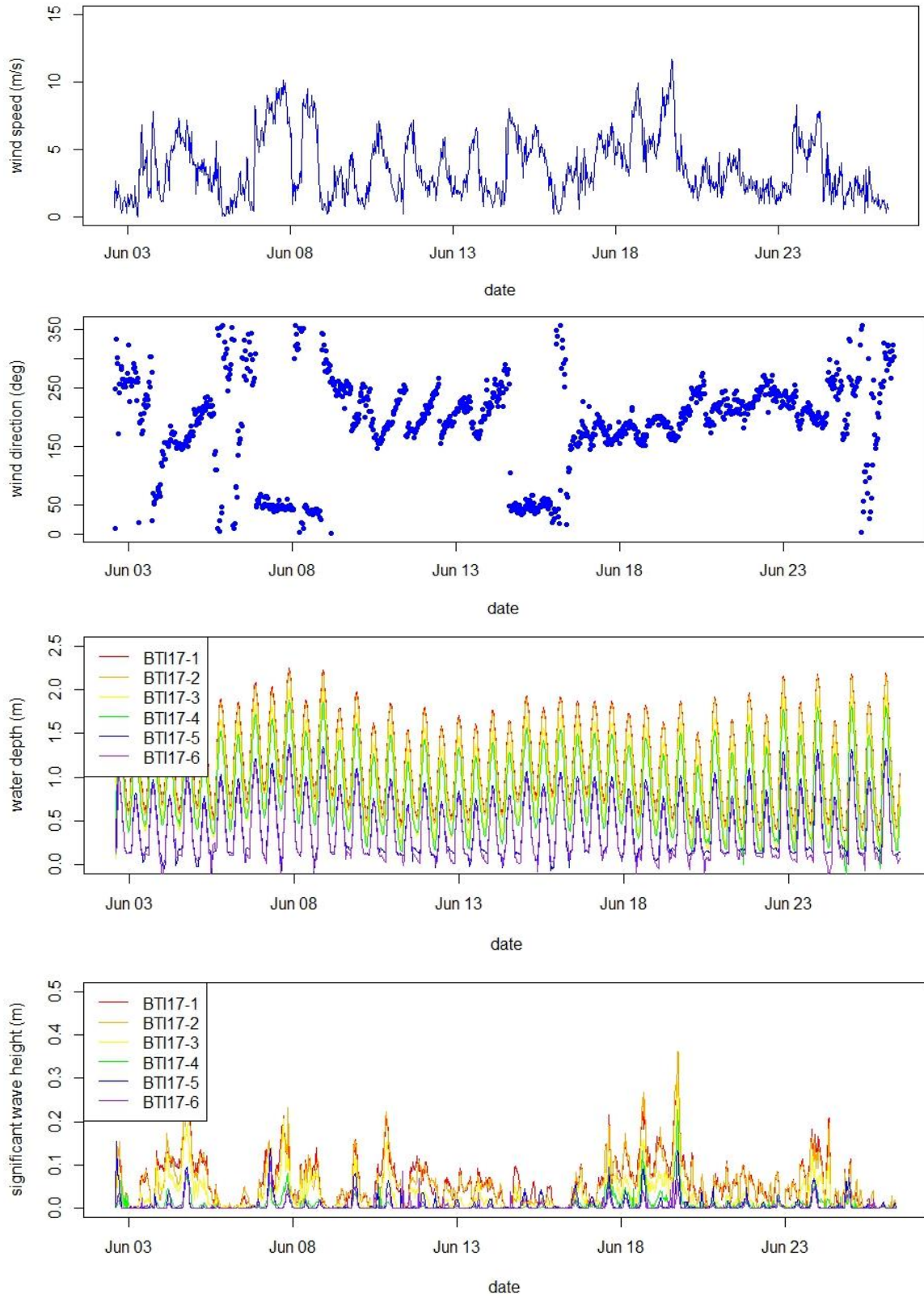


Figure 3.16. Wind speed, wind direction, water depth, and H_s time series from BTI-17.

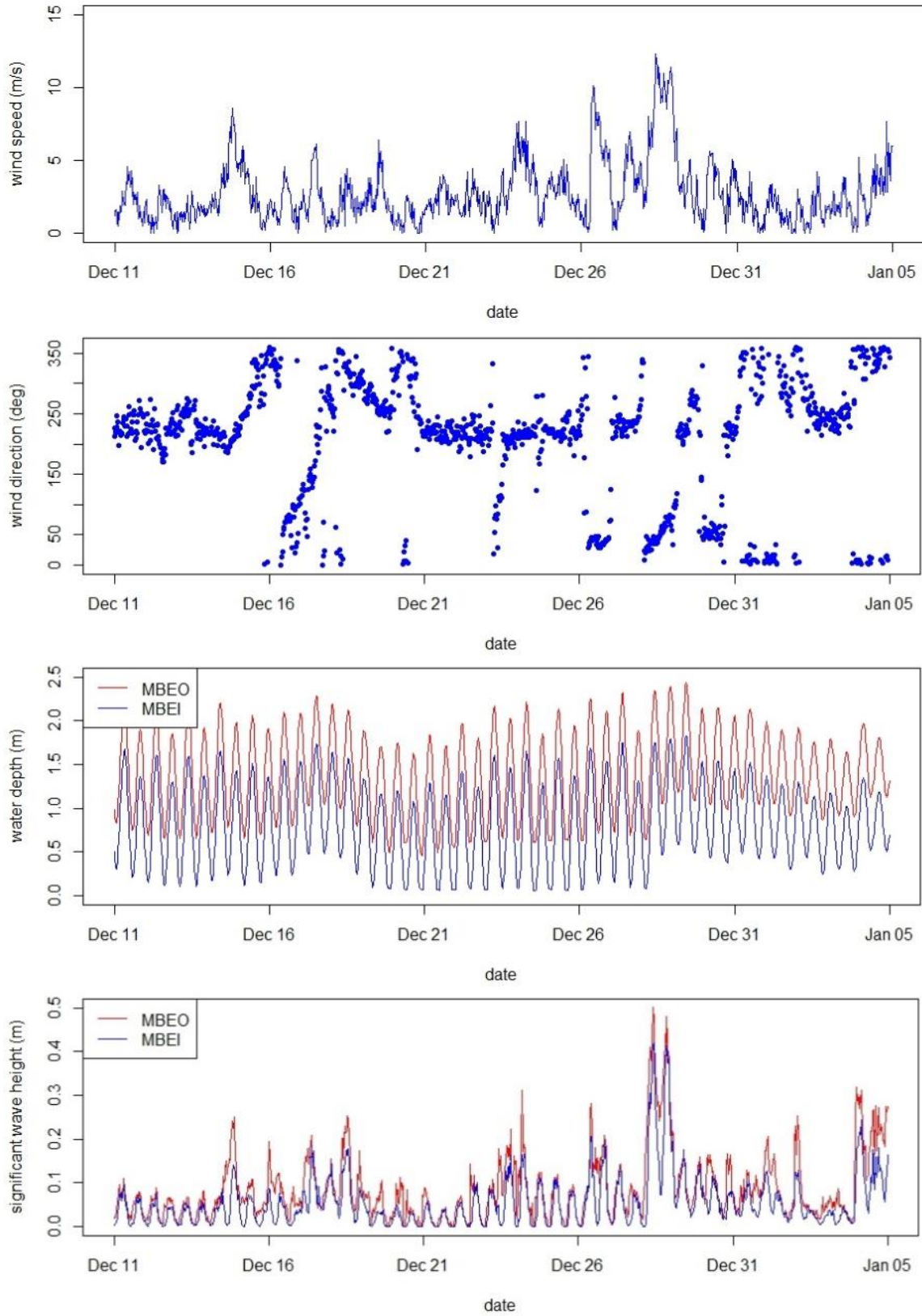


Figure 3.17. Wind speed, wind direction, water depth, and H_s time series from MBE-16.

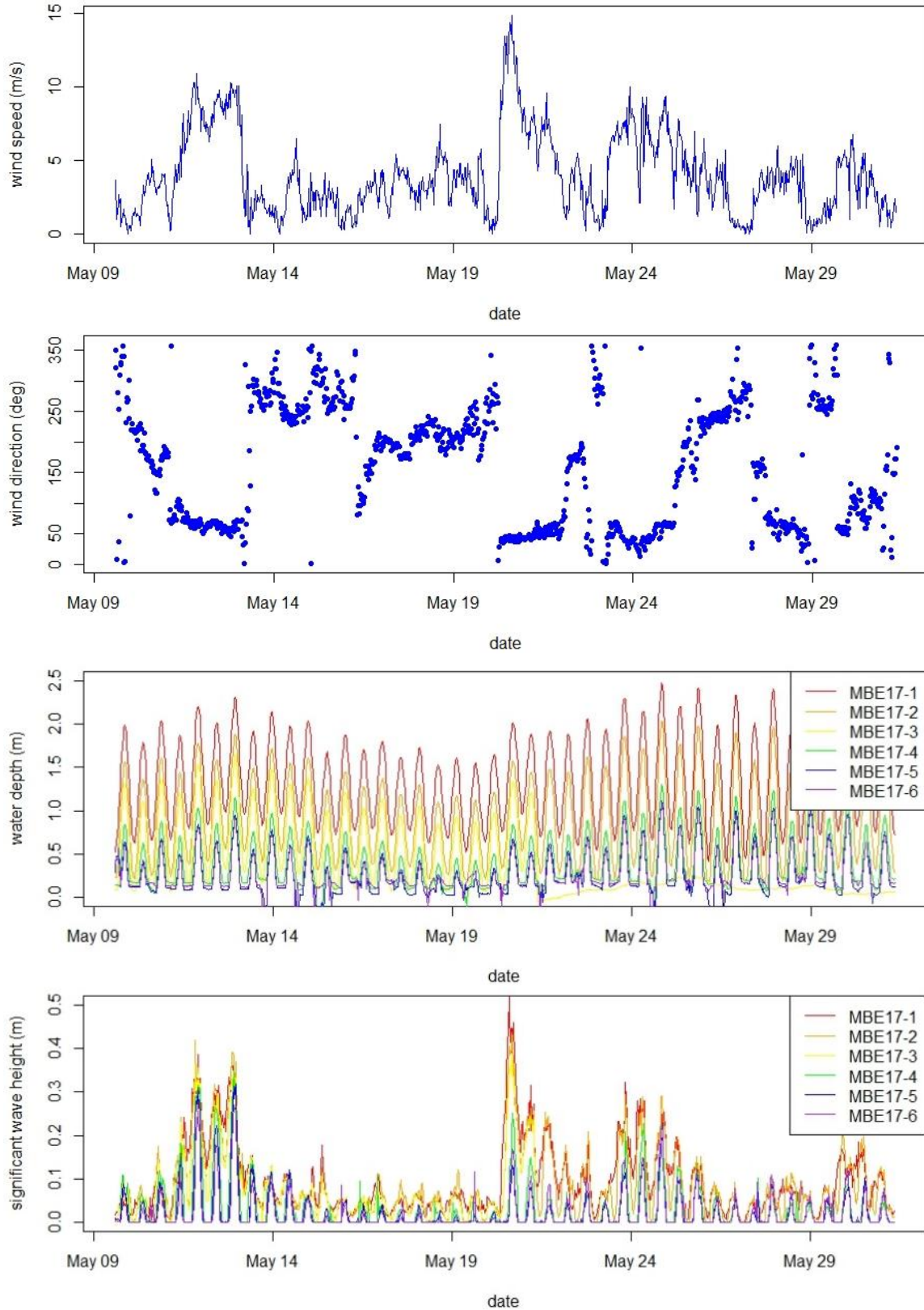


Figure 3.18. Wind speed, wind direction, water depth, and H_s time series from MBE-17.

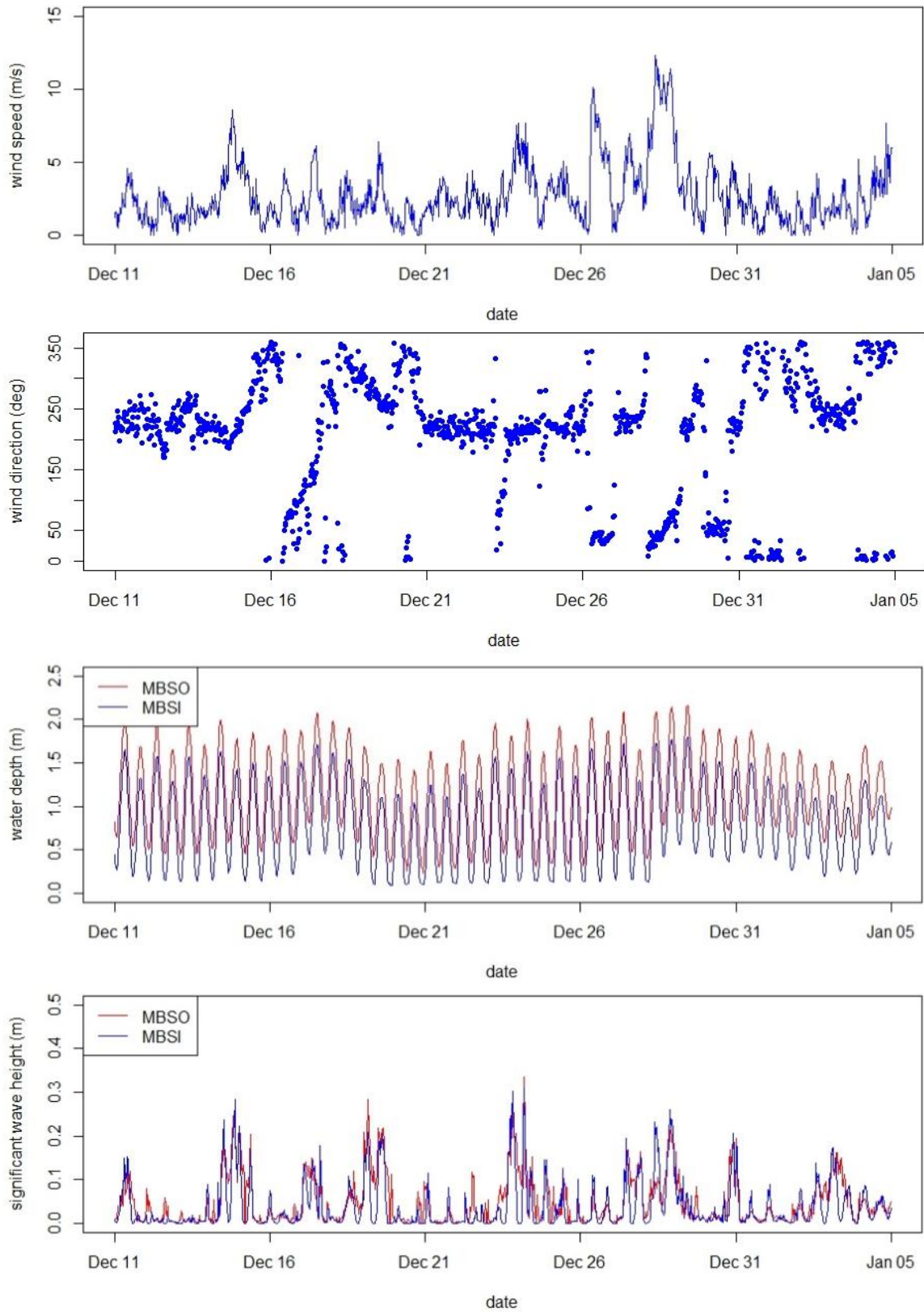


Figure 3.19. Wind speed, wind direction, water depth, and H_s time series from MBS-16.

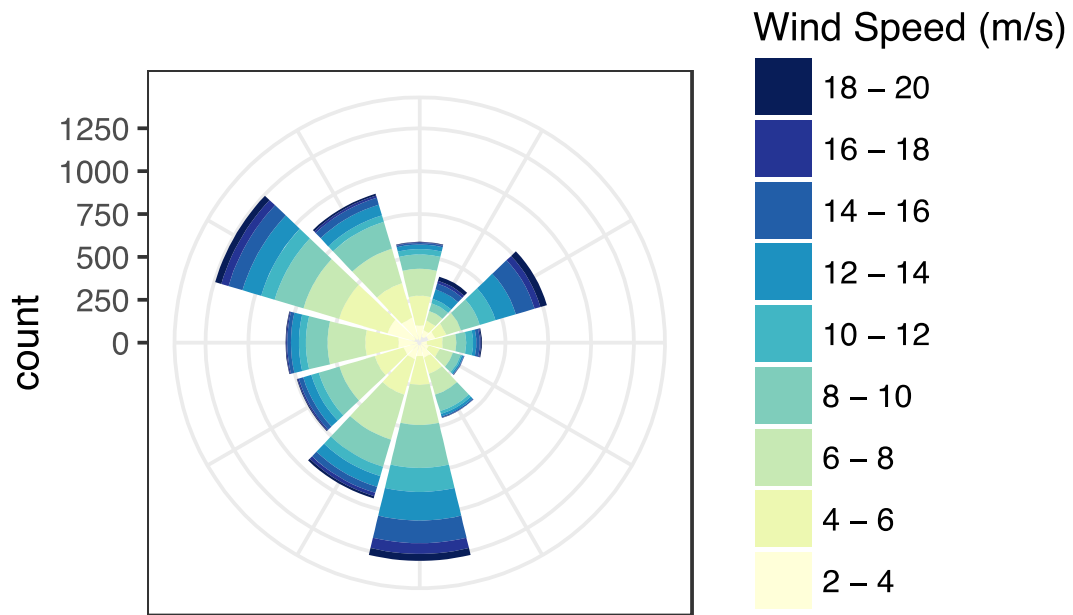


Figure 3.20. Wind rose of winds recorded at the National Weather Service site at Wallops Island, VA 1 July 2016 - 30 June 2017.

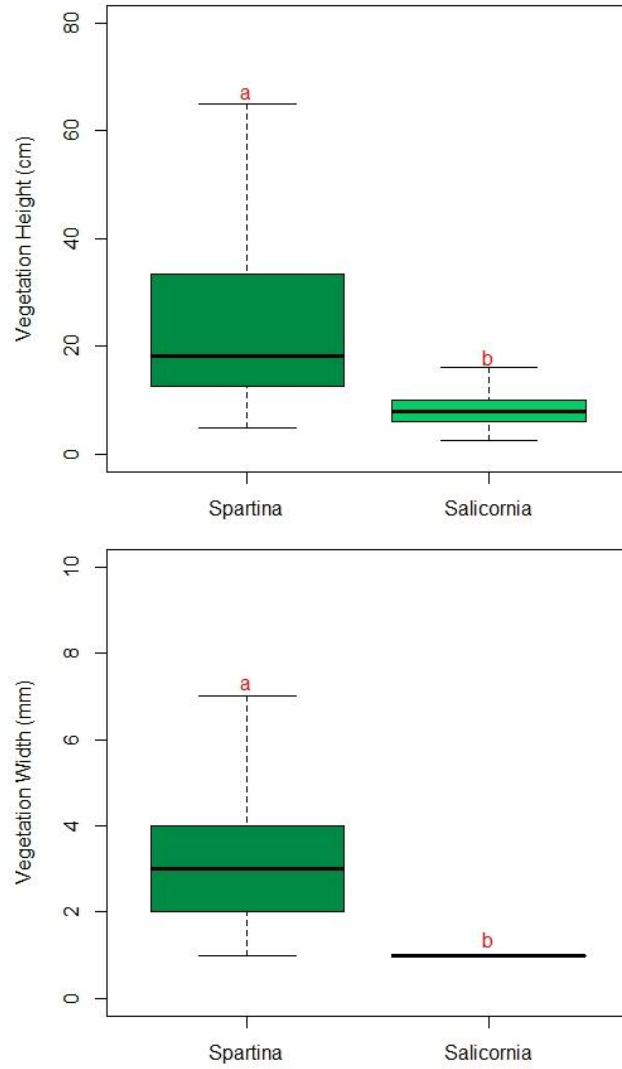


Figure 3.21. Stem height (*upper*) and stem width (*lower*) for *Spartina alterniflora* and *Salicornia europaea* at three marsh sites. Letters indicate significant differences between species ($p < 0.05$). Results from Mann-Whitney U test can be found in Appendix A (16-17).

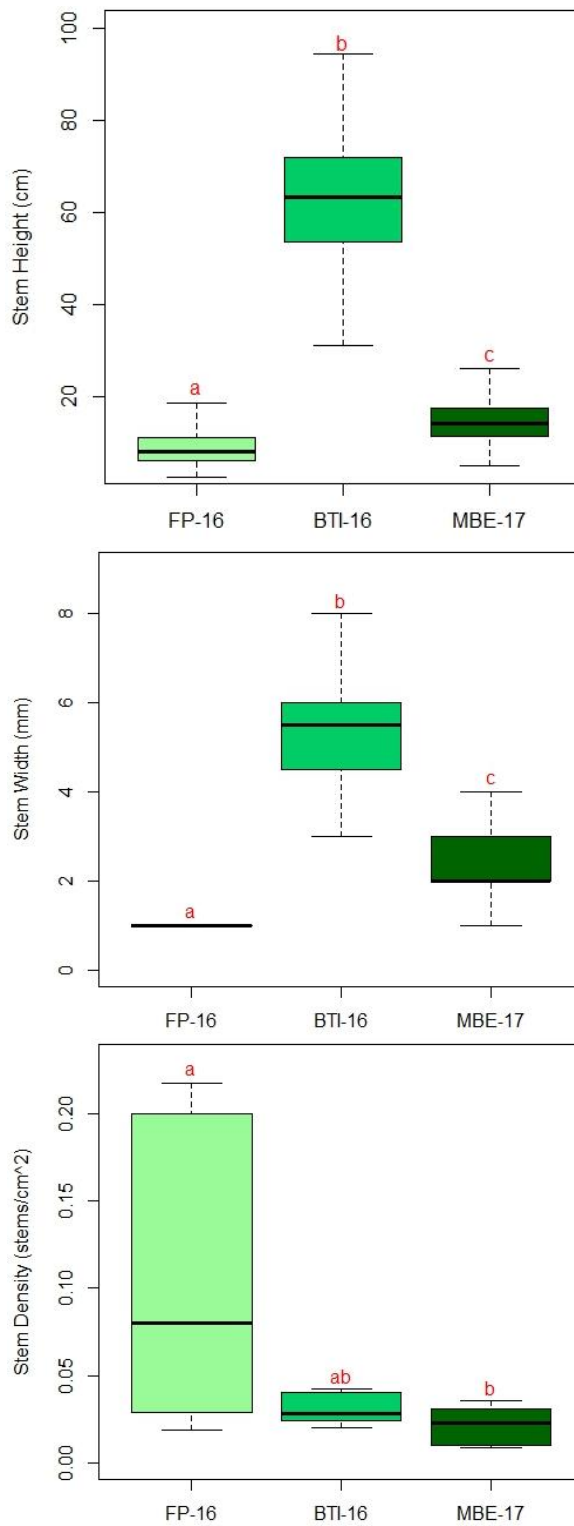


Figure 3.22. Stem height (*upper*), stem width (*middle*), and stem density (*lower*) at three marsh sites. Letters indicate significant differences between sites ($p < 0.05$). Results from 1-way ANOVA, Tukey multiple comparisons, Kruskal-Wallis rank sum, and Dunn's test can be found in Appendix A (18-20).

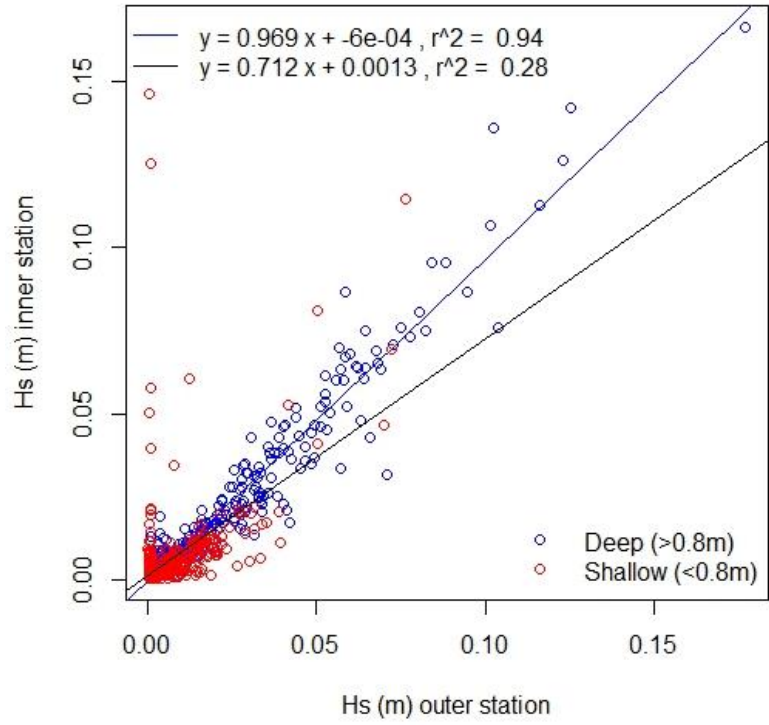


Figure 3.23. Regression analysis of waves on both sides of reef at TC1-16.

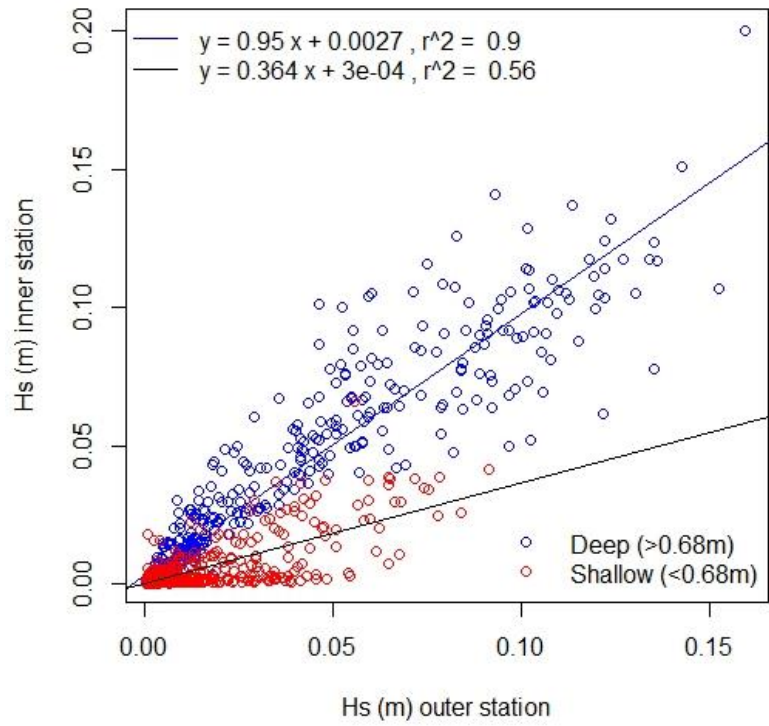


Figure 3.24. Regression analysis of waves on both sides of reef at TC2-16.

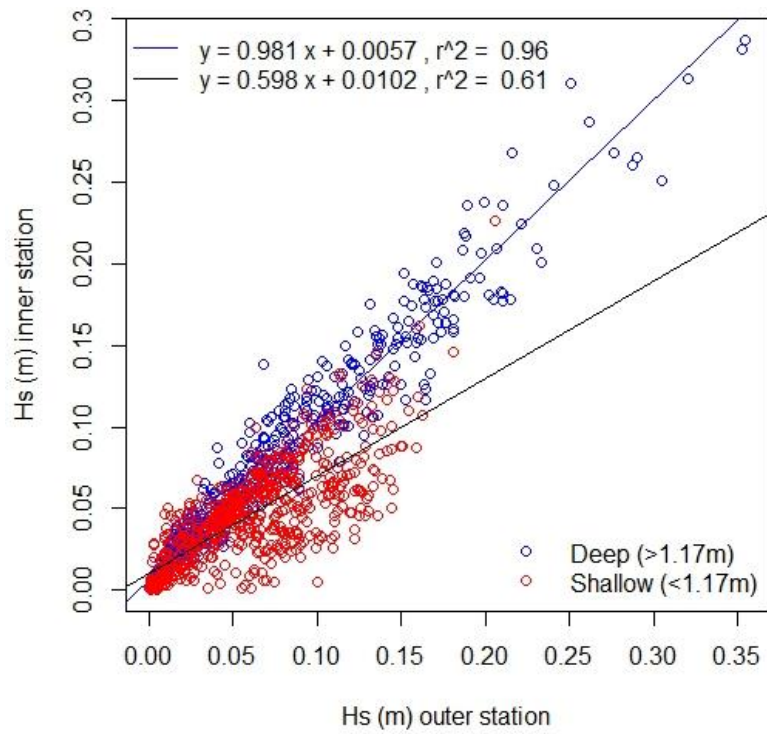


Figure 3.25. Regression analysis of waves on both sides of reef at BTI-16.

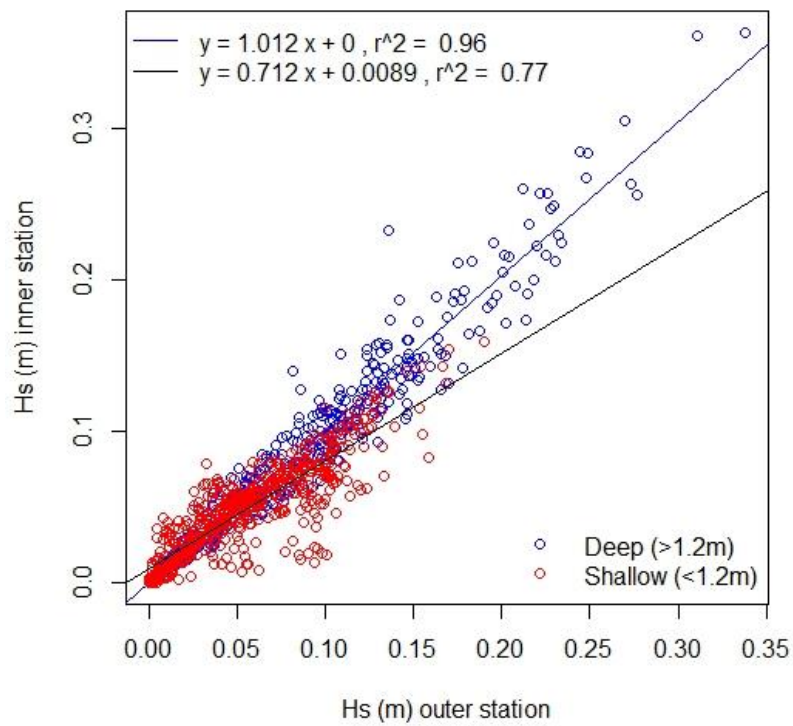


Figure 3.26. Regression analysis of waves on both sides of reef at BTI-17.

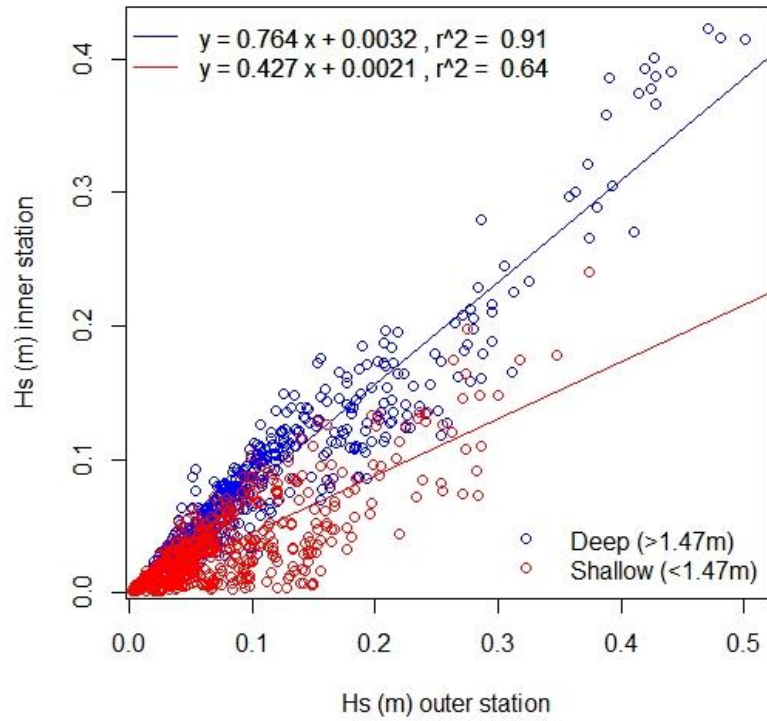


Figure 3.27. Regression analysis of waves on both sides of reef at MBE-16.

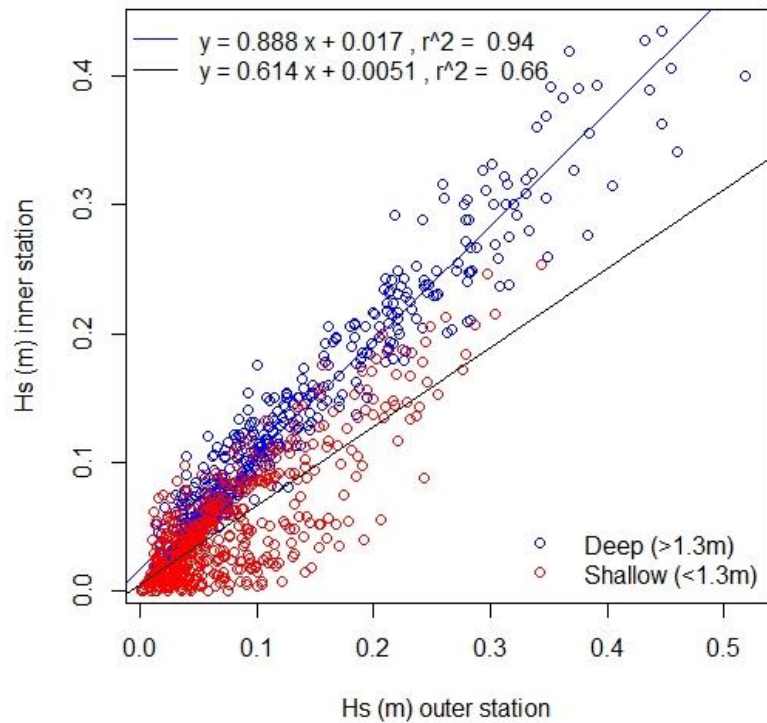


Figure 3.28. Regression analysis of waves on both sides of reef at MBE-17.

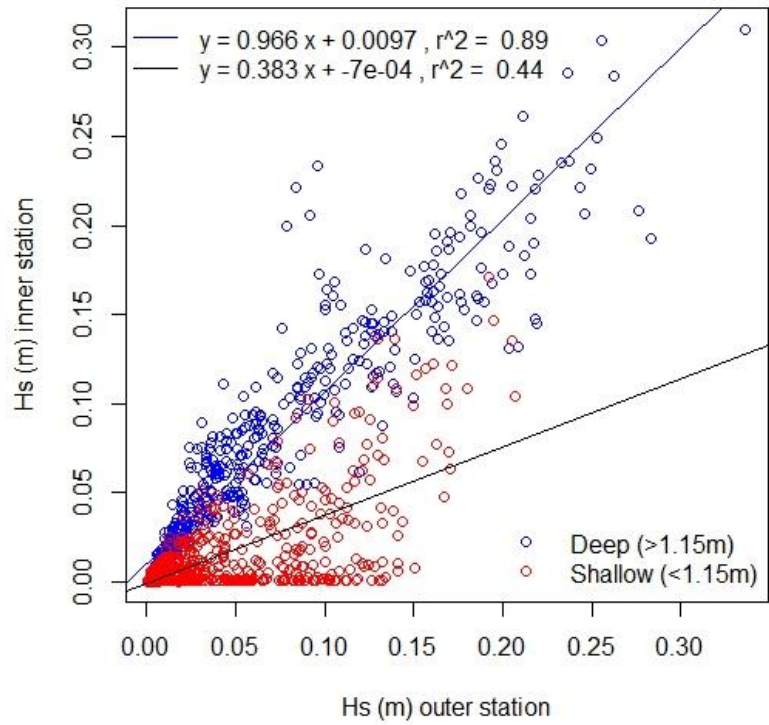


Figure 3.29. Regression analysis of waves on both sides of reef at MBS-16.

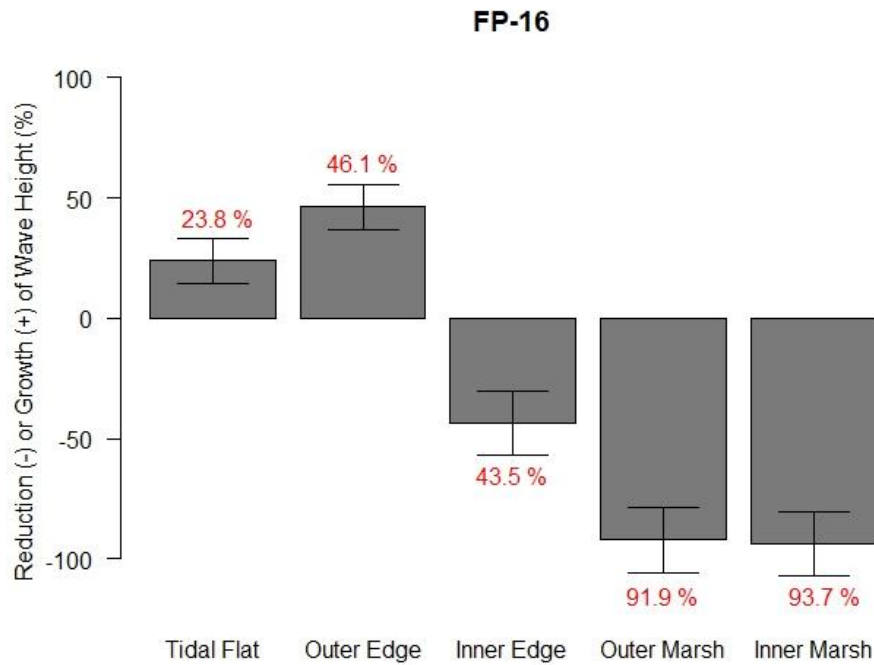


Figure 3.30. Average growth or reduction (%) in significant wave height (± 1 SE) recorded at FP-16 as waves propagated from outer to inner stations, shown as a percentage of the initial height recorded at the outermost station. The full transect length at FP-16 was 108 meters.

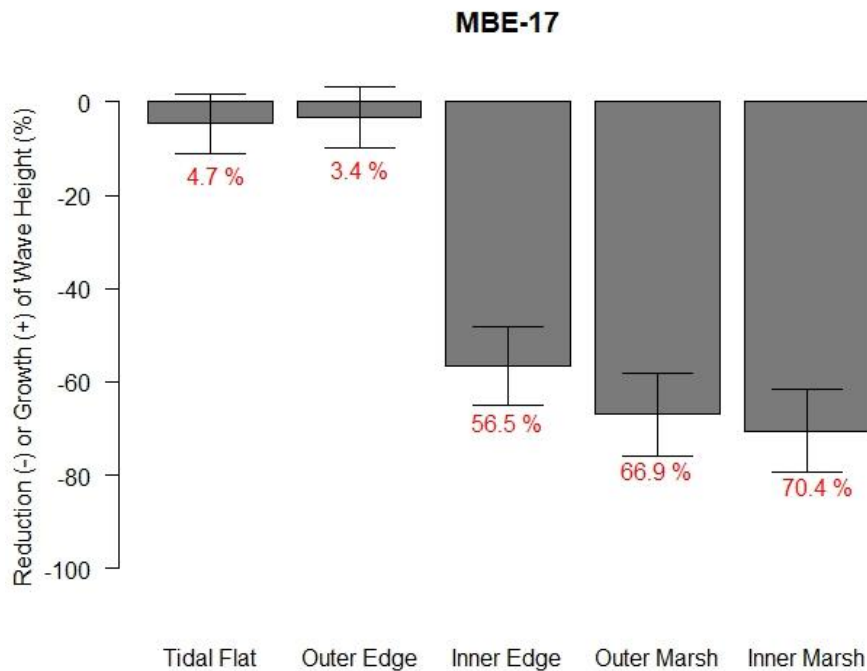


Figure 3.31. Average growth or reduction (%) in significant wave height (± 1 SE) recorded at MBE-17 as waves propagated from outer to inner stations, shown as a percentage of the initial height recorded at the outermost station. The full transect length at MBE-17 was 68 meters.

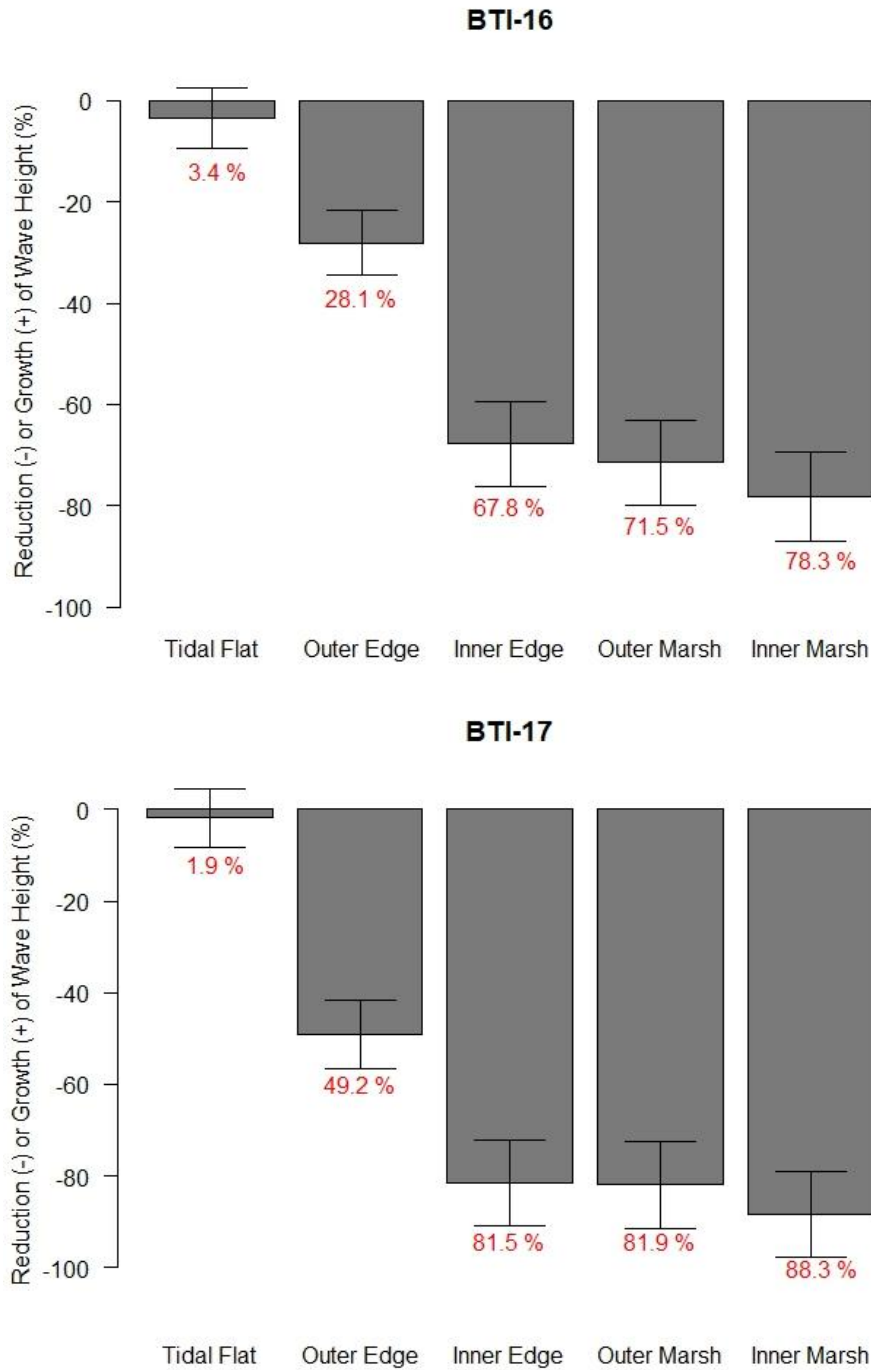


Figure 3.32. Average growth or reduction (%) in significant wave height (± 1 SE) recorded at BTI-16 (*upper*) and BTI-17 (*lower*) as waves propagated from outer to inner stations, shown as a percentage of the initial height recorded at the outermost station. The full transect length at BTI-16 and BTI-17 was 673 meters.

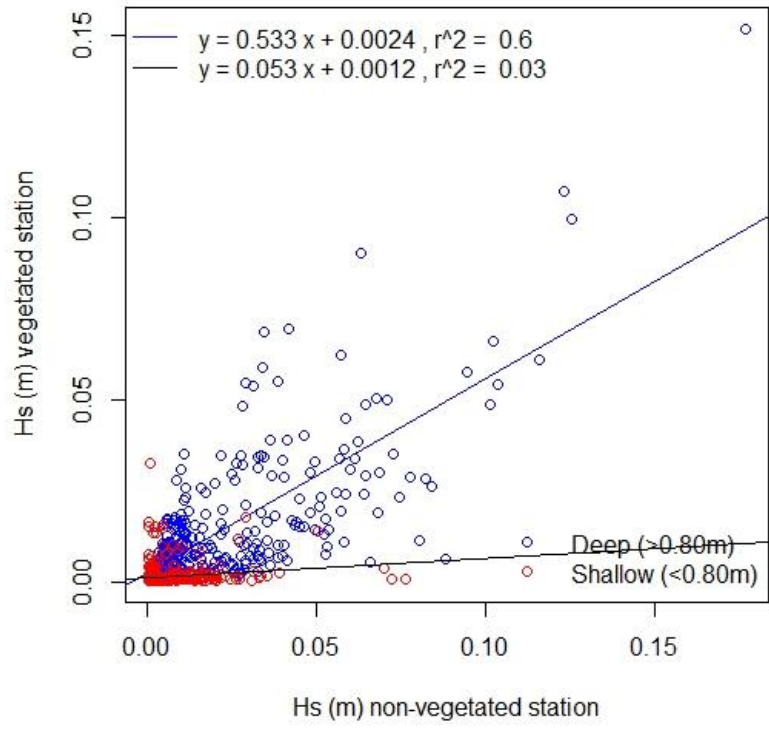


Figure 3.33. Regression analysis of waves for vegetated and non-vegetated stations at TCV-16.

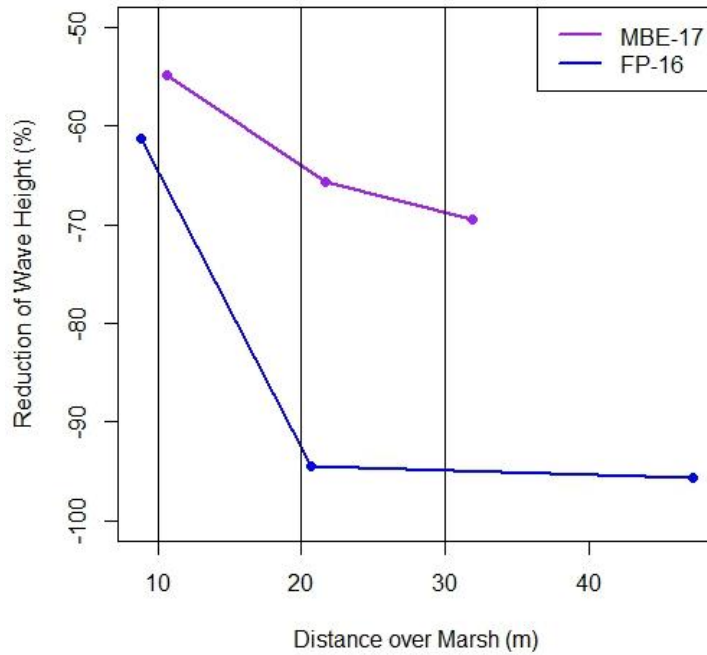


Figure 3.34. Average reduction (%) in significant wave height recorded for inner edge, outer marsh, and inner marsh stations at MBE-16 and FP-16, calculated as a percentage of wave height recorded at the outer edge station. Vertical lines represent 10, 20, and 30 meter transects (See Table 3.10).

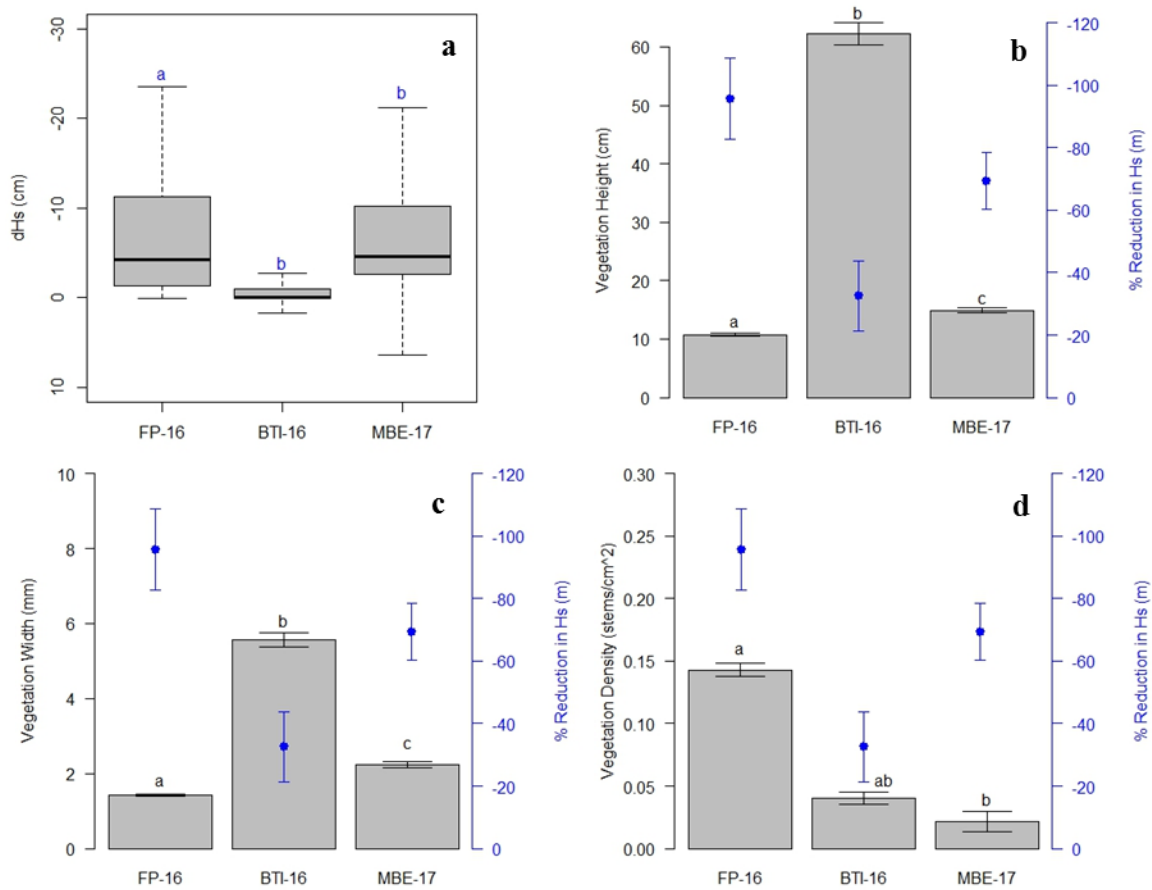


Figure 3.35. (a) Change in wave height (ΔH_s) from the outer edge station to the inner marsh station. Letters indicate significant differences between sites ($p < 0.05$). Kruskal-Wallis rank sum and Dunn's test can be found in Appendix A (21). (b-d) % reduction in significant wave height (± 1 SE) recorded at FP-16, BTI-16, and MBE-17 compared to vegetation height (b), vegetation width (c), and vegetation density (d). % reduction shown as a percentage of the initial height recorded at the outer edge station.

Tables

Site	Reef design	Reef height (m)	Reef distance to shoreline (m)	Marsh orientation	Total transect length (m)
TC1-16	Staggered	0.46	4	S	15
TC2-16	Staggered	0.46	14	S	17
TCV-16	NA	NA	NA	S	NA
FP-16	NA	NA	NA	NE-SW	108
BTI-16	Continuous	0.7	620	NE-SW	673
BTI-17	Continuous	0.7	620	NE-SW	673
MBE-16	Staggered	0.46	26	NW-SE	35
MBE-17	Staggered	0.46	26	NW-SE	68
MBS-16	Staggered	0.46	30	S	19

Table 3.1. Summary of constructed oyster reef and marsh characteristics.

Site	Measuring	Start date	End date
MBE-16	W	12/10/2015	1/6/2016
MBS-16	W	12/10/2015	1/6/2016
TC1-16	W	5/13/2016	6/8/2016
TC2-16	W	5/13/2016	6/8/2016
TCV-16	W	5/13/2016	6/8/2016
FP-16	W, V	6/16/2016	7/7/2016
BTI-16	W, V	7/8/2016	8/5/2016
MBE-17	W, V	5/9/2017	5/31/2017
BTI-17	W	6/2/2017	6/26/2017

Table 3.2. Sampling schedule of deployments at study sites. W = wave measurements, V = vegetation samples.

Site	Hours flooded	Total hours	% flooded
TCV-16	597	660	90.5
FP-16	203.5	499.5	40.7
BTI-16	524	659	79.5
BTI-17	464	570.5	81.3
MBE-17	189	282	67.0

Table 3.3. Summary of hours flooded during field deployments at marsh sampling sites.

Site	Mean water depth (m)	90 th %tile	Mean wind speed (m/s)	90 th %tile	Mean H_s (m)	90 th %tile
TC1-16	0.80	1.31	3.67	6.57	0.01	0.03
TC2-16	0.80	1.31	3.67	6.57	0.02	0.06
TCV-16	0.80	1.31	3.67	6.57	0.01	0.03
FP-16	1.22	1.85	3.00	5.81	0.03	0.09
BTI-16	1.17	1.77	3.94	6.40	0.06	0.13
BTI-17	1.20	1.82	3.66	6.90	0.06	0.13
MBE-16	1.39	2.01	2.72	5.40	0.09	0.19
MBE-17	1.34	2.00	3.98	8.00	0.10	0.22
MBS-16	1.15	1.78	2.72	5.40	0.05	0.13

Table 3.4. Summary of water depth, wind speed, and mean significant wave height (H_s) measurements during field deployments at sampling sites.

Site	Slope	R ²
TC1-16	0.997	0.986
TC2-16	0.921	0.980
TCV-16	0.996	0.998
FP-16	0.997	1.0
BTI-16	1.031	0.997
BTI-17	1.0	1.0
MBE-16	0.998	0.995
MBE-17	0.997	1.0
MBS-16	0.996	0.999

Table 3.5. Comparison between water depth measurements from RBR wave gauges placed at inner and outer stations at each study site.

Site	Mean Veg Height (cm)	SE	Mean Veg Width (mm)	SE	Density (stems/cm ²)	<i>Spartina</i> %: <i>Salicornia</i> %
FP-16	10.74 ^a	0.25	1.43 ^a	0.03	0.14 ^a	18.5% : 81.5%
BTI-16	62.22 ^b	1.90	0.622 ^b	0.02	0.04 ^{ab}	100% : 0%
MBE-17	14.93 ^c	0.38	2.24 ^c	0.05	0.02 ^b	100% : 0%

Table 3.6. Vegetation characteristics at three marsh sites. Letters indicate significant differences between sites ($p < 0.05$). Results from Results from 1-way ANOVA, Tukey multiple comparisons, Kruskal-Wallis rank sum, and Dunn's test can be found in Appendix A (18-20).

Study	<i>Spartina</i> height (cm)	<i>Spartina</i> width (mm)	<i>Spartina</i> density (stems/cm ²)
Blum, 1993	40 – 100 ^s	–	–
Anderson and Treshow, 1980	50 – 80 ^s ; 100 – 250 ^t	–	–
Valiela et al. 1978	10 – 40 ^s ; 200 – 300 ^t	2 – 9 ^s	0.04 – 0.11 ^t
Ellison, 1987	15.2 – 18.8 ^s	2.24 – 2.56 ^s	–
	<i>Salicornia</i> height (cm)	<i>Salicornia</i> width (mm)	<i>Salicornia</i> density (stems/cm ²)
Ellison, 1987	9.5 – 25.6	0.2 – 1.8	0.16 – 0.96

Table 3.7. Studies reporting stem height, width, and density for *Spartina alterniflora* and *Salicornia europaea*. *t* and *s* superscripts indicate tall-form or short-form *Spartina alterniflora*, respectively.

Reef Site	Mean <i>H_s</i> (m) Outer	90 th Percentile	Slope (all)	R ²	Slope (deep)	R ²	Slope (shallow)	R ²
TC1-16	0.01	0.03	0.926	0.79	0.969	0.94	0.712	0.28
TC2-16	0.02	0.06	0.893	0.81	0.950	0.90	0.364	0.56
BTI-16	0.06	0.13	0.868	0.83	0.981	0.96	0.598	0.61
BTI-17	0.06	0.13	0.937	0.90	1.012	0.96	0.712	0.77
MBE-16	0.09	0.19	0.683	0.77	0.764	0.91	0.427	0.64
MBE-17	0.10	0.22	0.867	0.84	0.888	0.94	0.614	0.66
MBS-16	0.05	0.13	0.807	0.67	0.966	0.89	0.383	0.44

Table 3.8. Comparison of waves across reefs for water depths deeper and shallower than mean water depth at each sampling site.

Marsh Site	Mean H_s (m) Outer	90 th Percentile
TCV-16	0.01	0.03
FP-16	0.03	0.09
BTI-16	0.06	0.13
BTI-17	0.06	0.13

Table 3.9. Summary of wave characteristics at marsh sites.

Station	FP-16		MBE-17	
	Distance over marsh (m)	% H_s reduction	Distance over marsh (m)	% H_s reduction
Inner edge	8.8	61.3	10.6	54.9
LERP	10	64.7	-	-
LERP	20	92.6	20	63.9
Outer marsh	20.7	94.5	21.7	65.7
LERP	30	94.9	30	68.7
Inner marsh	47.2	95.6	31.9	69.4

Table 3.10. Marsh buffer width interpolation and percent reduction in significant wave height (% H_s) at FP-16 and MBE-17. LERP = linear interpolation.

CHAPTER 4

MODELING SITE SUITABILITY FOR LIVING SHORELINES

4.1 Objective

The final objective of this study was to design a site suitability model to suggest appropriate placement of living shorelines given shoreline-specific characteristics. Using remote sensing data and GIS, a system-wide binary model called the Living Shoreline Explorer Model (LSEM) was developed for the Virginia Coast Reserve (VCR). The LSEM is a spatial modeling tool that considers conditions suitable for the use of living shoreline stabilization methods. Data from this research is available to the public via the Living Shoreline Explorer (LSE) app on the TNC *Coastal Resilience* web mapping decision-support tool which provides nature-based shoreline stabilization recommendations to support coastal management decisions.

4.2 Methods

Selection of suitability variables

Living shoreline placement is sensitive to wave climate (Hardaway et al. 2010); therefore, five suitability variables related to wave energy impacting the shoreline were selected: wave exposure, distance to boat activity, elevation, slope, and vegetation buffer width (Table 4.1). Wave exposure more comprehensively captures fetch and bathymetry variables used in previous site suitability assessments (e.g., Zylberman, 2016; Boyd et al. 2014; Carey, 2013; Berman and Rudnicky, 2008) by incorporating wind statistics to generate a representative measure of wave energy experienced at the shoreline. Distance to boat activity was used in a previous site suitability assessment by Carey (2013) and considers short-term wave attack along a shoreline by boat wake. Elevation is commonly used in suitability assessments and was used for this study as

a measure of marsh stability under wave attack. Slope was used by Boyd et al. (2014) and serves as an additional measure of marsh stability. Elevation and slope together allow for an alternative characterization of the “bank condition” variable used by Berman and Rudnicki (2008) that considers shoreline erodibility. Vegetation characteristics have been considered in previous site suitability assessments but were measured using a different metric. For example, Berman and Rudnicki (2008) considered marsh presence/absence, but not the physical characteristics of the marsh that contribute to wave-dampening capacity (i.e., buffer width).

Design outputs

The LSEM analyzed shoreline conditions suitable for soft and hybrid shoreline stabilization methods. The soft stabilization technique considered for this study was marsh enhancement (i.e., marsh plantings); the hybrid stabilization treatment was marsh enhancement with structures (e.g., rock sill or constructed oyster reef). The model also considered areas where nature-based solutions were not suitable and traditional hardened structures would be more appropriate. A description of each of the design outputs – soft stabilization, hybrid stabilization, and unsuitable – is outlined in the succeeding paragraphs. The LSEM does not consider a “no action needed” approach; therefore, the model is conservative in recommending action.

Soft stabilization

Marsh enhancement is a soft stabilization method that involves restoring or enhancing native marsh grass along intertidal substrate (Hardaway et al. 2010). Marsh enhancement techniques include seeding, transplanting sprigs (roots and rhizomes, little substrate), transplanting plugs (roots and rhizomes, intact substrate), and planting nursery-grown seedlings (Broome et al. 1988). The LSEM was designed for shorelines dominated by salt marshes; in the event that there

was a sandy shoreline, beach nourishment should replace marsh enhancement as the soft stabilization recommendation. Beach nourishment involves replenishing an existing beach with additional sand (Hardaway and Byrne, 1999) and must be composed of grain sizes that are comparable to the existing beach (Hardaway et al. 2010). Shorelines with low wave exposure, no exposure to boat wake, stable edges (i.e., low elevation, gentle slope), and an existing marsh buffer were considered suitable for marsh enhancement or beach nourishment.

Hybrid stabilization

Marsh enhancement with a rock sill or constructed oyster reef is a hybrid stabilization method that combines soft and hardened design elements. Rock sills and constructed oyster reefs are low profile structures (~30 centimeters above high water level) placed offset from and parallel to a shoreline (ASMFC, 2010). They are designed with spacing and gaps that maintain terrestrial-marine connectivity by allowing water and sediment to flow between the structures (ASMFC, 2010). Rock sills and constructed oyster reefs facilitate marsh establishment by breaking waves present in low to moderate water depths before they reach the marsh edge (Miller et al. 2016). This wave buffering facilitates a lower wave energy environment immediately behind the structures and encourages the accumulation of sediment and expansion of the existing marsh (Miller et al. 2016). Shorelines with moderate wave energy; some exposure to boat wake activity; and, an existing marsh buffer were considered suitable for marsh with structures.

Unsuitable

Shorelines with high wave energy, exposure to boat traffic, and degraded or non-existent marsh buffers were considered unsuitable for nature-based stabilization techniques. Instead,

these shorelines may be better protected by traditional stabilization methods like seawalls, bulkheads, or riprap revetments. Sea walls and bulkheads are vertical structures designed to withstand high wave energy and stabilize upland sediment (Hardaway et al. 2010). Riprap revetments are constructed of large, irregular, broken stones and designed with a sloped surface to break waves more gradually than seawalls and bulkheads (ASMFC, 2010).

Model development

Site suitability assessments are often conducted using one of two GIS-based modeling approaches: index (e.g., Dobbs et al. 2017; Carey, 2013) or binary (e.g., Zylberman, 2016; Boyd et al. 2014; Berman and Rudnicki, 2008) (Glennon, 2011). An index model ranks sites on a continuous scale according to specified criteria; the Marsh Vulnerability Index (MVI) from Chapter 2 of this study is an example of an index model. A binary model provides a straightforward “yes” or “no” assessment of a site according to specified design output criterion. Because successful living shoreline design and placement requires site-specific parameters to be satisfied, the LSEM was developed using the binary model approach to identify suitable/unsuitable locations for shoreline treatments.

All geospatial processing for the LSEM was done within the Esri ArcGIS 10.5 platform. Data layers for each suitability variable were processed and available for use after the development of the MVI described in Chapter 2 of this study and are summarized in Table 4.2. Suitability variables were reclassified according to criteria outlined in Table 4.3. A description of how criteria thresholds were developed is described in subsequent sections. Living shoreline design outputs (i.e., soft, hybrid, and unsuitable) were defined using combinations of reclassified suitability variables (Table 4.4). All possible combinations of each design output were generated using “R” statistical software, and GIS-based attribute queries were generated to identify and

select shoreline segments that satisfied these definitions (Table 4.5). Softer stabilization methods were prioritized; attribute queries were run in sequence to overwrite harder stabilization methods. The LSEM output is a 30-meter resolution feature class dataset for VCR shorelines. Each coastal grid cell (900 m²) contains a shoreline stabilization recommendation for the underlying shoreline segment. Figure 4.1 provides a general schematic of the methodology described above.

The LSEM is designed to offer nature-based solutions for tidal salt marshes in shallow estuarine environments; therefore, it cannot reliably model the deeper estuarine environment of the Chesapeake Bay, the ocean-facing shoreline of the barrier islands, or tidal channels. Consequently, tidal channels and the Chesapeake Bay and Atlantic Ocean-facing shorelines were excluded from the analysis. Stabilization recommendations were only made for mainland marshes, the portion of the study area most likely to be targeted for shoreline protection; thus, the total length of shoreline considered was 278 kilometers.

Data collection and reclassification

A description of how each of the five suitability variables was classified for use in the development of the LSEM is outlined in the succeeding paragraphs. Figures 4.2 – 4.6 depict each suitability variable in raw form extracted to a coastal grid; however, with the exception of wave exposure (which was calculated for discrete points along the shoreline), each dataset is also available for the entire system. Detailed information on the processing and validation of these data layers is available in Chapter 2 of this study.

Wave exposure

Significance

Shorelines that are regularly exposed to high wave energy are not suitable for living shorelines (Berman and Rudnicky, 2008). Established marshes can be undercut and toppled by persistent high wave energy (McLoughlin et al. 2015); marsh transplants and seeds cannot establish under severe wave climate conditions (Broome et al. 1988). Living shorelines are best suited for low wave energy environments (Hardaway et al. 2010). Low energy is characterized as shorelines with average fetch exposure of <800 meters (Hardaway and Byrne, 1999).

Reclassification

Shorelines with high wave exposure values were considered less suitable for living shoreline designs. Theuerkauf et al. (2016) suggest a threshold for high energy environments through observations that natural oyster reefs did not persist at wave exposure values over $500 \text{ J}\cdot\text{m}^{-1}$. This value was used to define the high (0) class; wave exposure values decreased linearly by subsequent class for the LSEM reclassification scheme (Table 4.3).

Distance to boat activity

Significance

Boat-generated waves can increase wave energy impacting the shoreline (Miller et al. 2016; Houser, 2010) and may increase shoreline erosion in sheltered, low wave energy environments (Hardaway et al. 2010). The VCR is minimally impacted by boating activity due to low population density (McLoughlin et al. 2015); however, areas along mainland marshes near public

boat ramps may experience wake-induced erosion (Duhring et al. 2006) and should be considered in living shoreline design projects (Miller et al. 2016; Carey, 2013).

Reclassification

Visual analysis of the water access sites throughout the study area indicated that most inlets and harbors extended no more than 800 meters inland. Therefore, the distance to boat activity threshold was defined by less than 800 meters as present (0) and greater than 800 meters as absent (2) for the LSEM reclassification scheme (Table 4.3).

Elevation

Significance

Lower elevation marsh edges are better protected than higher marsh edges by structures like rock sills or constructed oyster reefs under a variety of water conditions. In low and moderate water depths, structures break waves before they reach the marsh edge. Waves generated during deeper water conditions propagate over the structures onto the marsh platform without breaking on the vulnerable marsh edge. However, marshes with higher elevation are exposed to wave attacks under these deeper water conditions. In addition, marsh edges with a lower elevation tend to be more stable than marsh edges with higher elevation (McLoughlin et al. 2015).

Reclassification

McLoughlin et al. (2015) found for marshes in the study area that lower elevation marshes were more stable than those with higher elevations. Thus, elevation values measured for the McLoughlin et al. (2015) study at a high, unstable marsh (Matulakin Marsh; 0.39 ± 0.01 m) and

a low, stable marsh (Fowling Point; 0.09 ± 0.03 m) were used to define the range of values from high (0) to low (2), respectively, for the LSEM reclassification scheme (Table 4.3).

Slope

Significance

Gently sloping marshes maximize plantable area (Priest, 2006) and provide ideal growing conditions for marsh vegetation (Duhring, 2006). Additionally, a gently sloping marsh is indicative of a stable marsh edge (McLoughlin et al. 2015).

Reclassification

McLoughlin et al. (2015) found for marshes in the study area that steep or vertical scarps were characteristic of unstable marsh edges. Thus, slope values measured from a steep, unstable marsh site (Matulakin Marsh; 24°) and a gentle, stable marsh site (Fowling Point; 12°) were used to define the range of values from high (0) to gentle (2), respectively, for the LSEM reclassification scheme (Table 4.3). A loss of marsh edge resolution caused by resampling this dataset was not discovered until after the LSEM was fully developed; therefore, the range values were defined at a local-slope level. Future iterations of the LSEM should incorporate landscape-level slope values for range divisions.

Vegetation buffer width

Significance

The existence of a substantial marsh buffer indicates a stable marsh (Dobbs et al. 2017) and favorable conditions for marsh planting viability (Berman and Rudnicky, 2008).

Reclassification

Field measurements indicate salt marshes can reduce wave energy by up to 50% over 10-20 meters (Möller, 2006; Möller et al. 1999). Therefore, 20 meters was used to define a marsh buffer as wide (2), and a minimum value of 10 meters was used as narrow (0) for the LSEM reclassification scheme (Table 4.3).

Statistical analysis

Statistical analyses were performed using the statistical software, “R” 3.4.4. Suitability datasets were not normally distributed even after transformation; therefore, a nonparametric test, the Kruskal-Wallis rank sum test, followed by a post-hoc comparisons test, the Dunn’s Test of Multiple Comparisons, were performed to investigate differences between suitability variables at three comparison sites.

4.3 Results

The results of the LSEM are shown in Figure 4.7. The LSEM designated 85% (237 km) of shoreline along Virginia’s coastal bays as suitable for nature-based shoreline stabilization projects. 59% (164 km) of the shoreline was determined to be suitable for soft stabilization, 26% (73 km) was found to be suitable for hybrid stabilization, and 18% (41 km) were unsuitable for living shorelines. Figure 4.8 shows the percentage and total length of shoreline in the study area for each shoreline stabilization technique.

Model validation

To assess the performance of the LSEM as a spatial modeling tool, LSEM recommendations were compared to: 1) a suitability assessment model developed by the Virginia Institute of

Marine Science (VIMS) Coastal Center for Coastal Resources Management (CCRM) known as the Living Shoreline Suitability Model (LSSM) and 2) habitat management permit applications submitted to the Virginia Marine Resources Commission (VMRC).

LSEM and LSSM

In 2016, VIMS CCRM published an online comprehensive map viewer for Accomack and Northampton Counties of the Virginia Eastern Shore with map contents that include Preferred Best Management Practices (BMP) depicting shoreline stabilization recommendations based on LSSM output (CMAP, 2017). The criteria used to quantify suitability for the LSSM included fetch, bathymetry, marsh presence, beach presence, bank condition, and tree canopy presence (Berman and Rudnický, 2008). While the criteria used for the LSSM were different than the LSEM, the objective of the two models was the same: to recommend the most appropriate shoreline stabilization techniques to coastal stakeholders. The LSSM was validated against field assessments resulting in a 58% accuracy rate in predicting suitability (Berman and Rudnický, 2008). The validation process involved the comparison between model results, permit reviews, and field determinations made during site visits.

LSEM and LSSM stabilization recommendations were examined at three comparison sites. Sites were selected based on increasing levels of human impact: Box Tree Idaho (BTI), Upshur Neck (UN), and Oyster (OY) (Figure 4.9). A summary of suitability variables for the three comparison sites is provided in Table 4.6. There were significant differences between wave exposure, distance to boat activity, elevation, and vegetation buffer width at all three sites. Slope was significantly higher at UN and OY compared to BTI. Table 4.7 shows the percentage and total length of shoreline at the three sites for each stabilization technique.

Box Tree Idaho

BTI is an undeveloped mainland marsh in Northampton County located in Ramshorn Bay (Figure 4.9). This site experienced low exposure to wind- and boat-generated waves; had characteristics of a stable edge (low elevation, gentle slope); and, supported a wide marsh buffer. Visual analysis of BTI suggested that, in general, the LSEM recommended softer stabilization methods than the LSSM (Figure 4.10). The LSEM recommends soft stabilization for 97% of the shoreline with the remainder stabilized with hybrid techniques. The LSSM only recommended 18% of the shoreline for soft stabilization and 82% for hybrid methods. The larger proportion of shoreline recommended by the LSSM for hybrid stabilization was likely due to a difference in defining the location of the shoreline; the LSEM used the mean high water shoreline, while the LSSM shoreline was located in the marsh upland region.

Upshur Neck

UN is a developed mainland marsh in Accomack County located in Hog Island Bay featuring private residences, roads, docks, agriculture plots, and hardened structures (i.e., bulkhead and riprap) (Figure 4.9). UN experienced the highest exposure to waves of the three sites; had the most unstable edge characteristics (high elevation, sections of steep slope); and, some segments of shoreline included a moderate to narrow marsh vegetation buffer. Visual analysis of the UN shoreline suggested there was more variation in shoreline stabilization recommendations offered by the LSEM than the LSSM (Figure 4.10). Both models designated the majority of the shoreline as suitable for hybrid stabilization. The LSSM designated 91% of the shoreline as suitable for hybrid stabilization, with the remaining 9% suitable for soft stabilization. The LSEM recommended hybrid stabilization for 74% of the shoreline, 19% for soft stabilization, but also identified 7% as unsuitable for nature-based solutions. Two shoreline

segments were designated as unsuitable by the LSEM because the marsh vegetation buffer width present there was <10 meters.

Oyster

Oyster (OY) is a highly developed harbor community in Northampton County made up of private residences, commercial and non-profit aquaculture facilities, a public boat ramp, and the Anheuser-Bush Coastal Research Center (Figure 4.9). While this site was the most sheltered from wind-waves, its shorelines were the closest to concentrated boat activity (<800 meters) and included sections with narrow vegetation buffer widths (<10 meters). As a result, the LSEM suggested that the entire inner harbor was unsuitable for living shorelines, while the shorelines immediately outside were suitable for soft stabilization. LSSM recommendations were more variable within the harbor; recommendations alternated between segments of soft and hybrid techniques and areas of special concern. Select shorelines were designated by the LSSM as areas of special concern due to marsh development and navigation access restrictions. The recommended shoreline stabilization technique for areas of special concern includes vegetation buffers where possible, revetments where protection from erosion is necessary, and limited use of bulkheads (CCRM, 2018). Shorelines determined to be areas of special concern were most comparable to the unsuitable design output for the LSEM, which recommends more traditional stabilization methods.

VMRC Habitat Management Permit Applications

The VMRC maintains a Habitat Management Permits and Applications webpage (<https://webapps.mrc.virginia.gov/public/habitat/>) that can be queried for living shoreline projects beginning in 2010. Since 2010, five living shoreline permits were issued to property

owners on the Atlantic side of the Virginia Eastern Shore (Figure 4.11). Of these five, two (Site 1 and 5; Figure 4.11) received official VIMS Tidal Shoreline Management Recommendations (TSMR) and were constructed as approved (Table 4.8). The remaining three did not receive official recommendations, or this data was otherwise unavailable. VIMS TSMR recommendations used a coastal management tool called the Decision Tree Coastal Management Decision Tool (<http://ccrm.vims.edu/decisiontree/>) which guides users through a series of questions about shoreline characteristics to produce a recommendation. Shoreline characteristics used to arrive at a recommendation were similar to those used by the LSSM and included: erosion presence, forested shoreline, bank height, grading inhibitors, beach presence, marsh presence, fetch, and nearshore water depth (CCRM, 2018).

Site 1 is located on the mainland side of Chincoteague Bay (Figure 4.12). The LSEM and VIMS decision tree suggested a hybrid approach for this stretch of shoreline. The final project included beach nourishment with marsh plantings and a sill (Table 4.8). Site 5 is located on Chincoteague Island (Figure 4.12). Here, the shoreline is split between two LSEM recommendations: soft stabilization and unsuitable. The western portion of the shoreline supports an existing marsh and is designated as suitable for soft stabilization while the eastern portion is modified with a bulkhead and pier structures, resulting in the designation of unsuitable due to high elevation/slope and the absence of a marsh buffer. The VIMS decision tree recommended the removal of a bulkhead and implementation of a hybrid solution for this property. The final project involved an assortment of soft, hybrid, and traditional shoreline stabilization treatments that incorporated marsh enhancement, beach nourishment, a bulkhead, and marsh toe sill (Table 4.8). A marsh toe sill is different than a typical sill in that it is placed immediately at the marsh edge with no offset.

4.4 Discussion

Overall, a comparison between the LSEM and LSSM suggested that shoreline stabilization recommendations did not always agree. Discrepancies between the two models stemmed from disparate shoreline definitions and characterization of variables used to calculate suitability, primarily vegetation buffer width and exposure to boat wake. Ultimately, both spatial models presented strengths and weaknesses in determining living shoreline suitability.

The contrast between the two models at BTI likely stemmed from a difference in defining the shoreline. While the LSEM used the mean high water shoreline, much of the LSSM shoreline was located in the marsh upland region. Thus, for shorelines with fringing intertidal marshes, the LSEM and LSSM modeled different sets of environmental conditions and processes. Shorelines that lacked a substantial intertidal marsh (e.g., UN and OY) considered essentially the same shoreline. The LSSM may have considered the marsh upland region because it closely coincides with parcel boundaries, where landowners make property management decisions. The strength of the LSEM, however, is in its thorough analysis of conditions and processes that shape and sustain the intertidal marsh-bay boundary; thus, the mean high water shoreline was selected as the focus of this suitability analysis.

Recommendations at UN generally agreed between the two models although the LSEM was more sensitive to shoreline segments with narrow marsh buffers which resulted in some segments being identified as unsuitable. The southernmost unsuitable segment at UN is fronted by a series of hardened structures (rip rap, bulkhead, groin field) (Figure 4.13), suggesting that coastal stakeholders decided this stretch of shoreline needed hardened protection. While this shoreline segment could be overprotected by hardened structures, it is possible that this supports the LSEM's determination that this stretch of shoreline is unsuitable for nature-based solutions.

At OY, the LSEM was heavily influenced by proximity to boat activity while the LSSM did not consider this variable. As with UN, portions of the OY shoreline are currently protected with hardened structures (Figure 4.14) which may suggest that this type of infrastructure is necessary to protect the shoreline from boat-generated waves in the active harbor. Analysis of bathymetry conducted as part of this study quantified the nearshore depth of OY shorelines recommended for soft stabilization by the LSSM. This analysis revealed nearshore depth values that are not ideal for successful implementation of living shorelines. Berman and Rudnicky (2008) maintain that the 1-meter bathymetric contour must be less than 10 meters from the shoreline to be suitable for marsh plantings; the average depth fronting these shorelines was approximately 3 meters (Figure 4.14). On the other hand, there are some shorelines determined unsuitable by the LSEM that were likely over-influenced by proximity to boat activity as vessels rarely travel past the ABCRC and aquaculture docks. These shorelines would likely benefit from the use of a living shoreline as the LSSM suggests.

Albeit the sample size was small, the comparison exercise between the LSEM and VMRC Habitat Management Permit Applications suggested that the LSEM, VIMS decision tree, and permit reviews generally agreed. The LSEM and VIMS decision tree recommendations matched at Site 1 and the implementation of the approved permit reflected those recommendations. Site 5 was more complex; the LSEM and VIMS decision tree recommendations did not completely agree; however, the final project reflected components of both recommendations. The scenario at Site 5 illustrates that recommendations and project designs may differ due to professional site determinations and landowner preferences.

Future work

Including additional suitability variables into the generation of the LSEM, especially nearshore depth and existing shoreline protection structures, could improve the final suitability determination. Although bathymetry was included in the calculation of wave exposure, it was not included as an independent nearshore parameter. The nearshore depth (i.e., <10 meters from shoreline) must be relatively shallow for the successful placement of a living shoreline (Berman and Rudnicky, 2008). Understanding what and where hardened structures are used throughout the study area can provide insight into vulnerable shorelines. Some of these hardened shorelines may even benefit from replacement or retrofit of a nature-based shoreline stabilization design.

Geospatial computations are dependent on the quality and resolution of data used; therefore, errors in data layers affect the accuracy of the model output. The distance to boat activity data layer might have provided better resolution on impacted shorelines if it had included information for smaller, private docks and vessel navigation routes. This may prevent the over-classification of unsuitable shorelines as seen at OY. While the alongshore resolution of the LSEM was very high (30 meters), the cross-shore resolution needed to capture slope was poor, resulting in an inability to resolve the marsh edge profile. To accurately capture local slope and account for nearshore bathymetry in future iterations, spatial processing must resolve this cross-shore variability.

A “no action needed” design option was considered during model development but was not pursued. Similar to other suitability assessment models (e.g., Zylberman, 2016; Boyd et al. 2014; Carey, 2013; Berman and Rudnicky, 2008), the LSEM assumes that shoreline stabilization should occur. This is not the case for every shoreline, yet is difficult to determine via spatial modeling; and, there may be public trust or legal liability involved if a shoreline designated as

stable develops an erosion problem. This resulted in an inherently conservative model that always recommended action. A “no action needed” approach should be investigated for future iterations of the LSEM, possibly through the quantification of shoreline change rates across the entire study area. Shorelines designated by the MVI as having low vulnerability and that are not actively eroding could be considered for “no action needed.”

Other future work should include the validation of LSEM output with permit applications and field assessments. The VMRC Habitat Management Permits and Applications webpage can be used to locate living shoreline projects. Coordination with landowners for site visits would allow comparison of LSEM output recommendations with field assessments. Still, an agreement between an LSEM recommendation and living shoreline project does not necessarily confirm that the recommendation was the most appropriate option. A better test of the efficacy of the LSEM is to compare recommendations with long-term living shoreline success/failure criteria. Per the VMRC regulation 4 VAC 20-1300-10 ET SEQ, living shoreline projects require monitoring reports at the end of the first full growing season and after the second year vegetation is established. It would be invaluable to view these monitoring reports to determine success/failure criteria. Because the living shoreline concept is relatively new and 4VAC 20-1300-10 ET SEQ came into effect September 2015, the monitoring reports will likely be sparse. Also, requirements for the monitoring reports are vague and do not appear to be standardized, which may make quantification of success/failure difficult. However, the effort would certainly be worthwhile, given that field validation and success/failure metrics would not only offer insight into the accuracy of the tool but would also provide constructive feedback for improvements to the model.

Coastal management

The LSEM recommended nature-based shoreline stabilization methods for the VCR based on site-specific information. The model represents a streamlined approach that can be used as a screening tool to support landowners, planners, and managers in assessing nature-based shoreline stabilization options, with the acknowledgement that living shoreline design and placement is complex and requires a site visit for a final determination (TNC, 2017). Spatial models can provide information that allows landowners to begin the design process (e.g., contact an environmental engineering firm), but they cannot account for details like designs preferred by particular consultants nor what a landowner is willing to pay and wanting to see (i.e., aesthetics). It is not the intent of the LSEM to replace site-based consulting services, but rather to offer coastal stakeholders context for understanding their shoreline relative to others and a guidepost for selecting an appropriate shoreline stabilization consultant.

As evidenced by the VMRC Habitat Management Permit query, very few coastal landowners have applied for living shoreline permits since 2010. This is likely due in part to a lack of confidence in the efficacy of living shoreline designs (Berman and Rudnicky, 2008). For landowners to seriously consider alternative approaches for shoreline stabilization these options must be monitored for long-term effectiveness (Berman and Rudnicky, 2008) and those results must be communicated to the coastal community. To address the latter, the results of this study are available to the public via the Living Shoreline Explorer (LSE) app hosted on the TNC *Coastal Resilience* web mapping decision-support platform (Figure 4.15). TNC offers free open houses and workshops to teach residents of the Virginia Eastern Shore how to use this innovative mapping tool in making informed coastal management decisions.

Figures

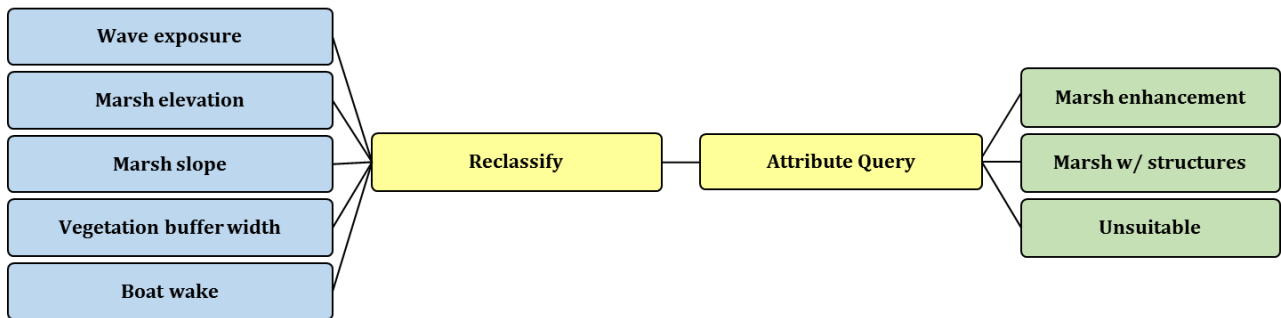


Figure 4.1. LSEM general methodology. Blue = inputs, yellow = processing, green = outputs.

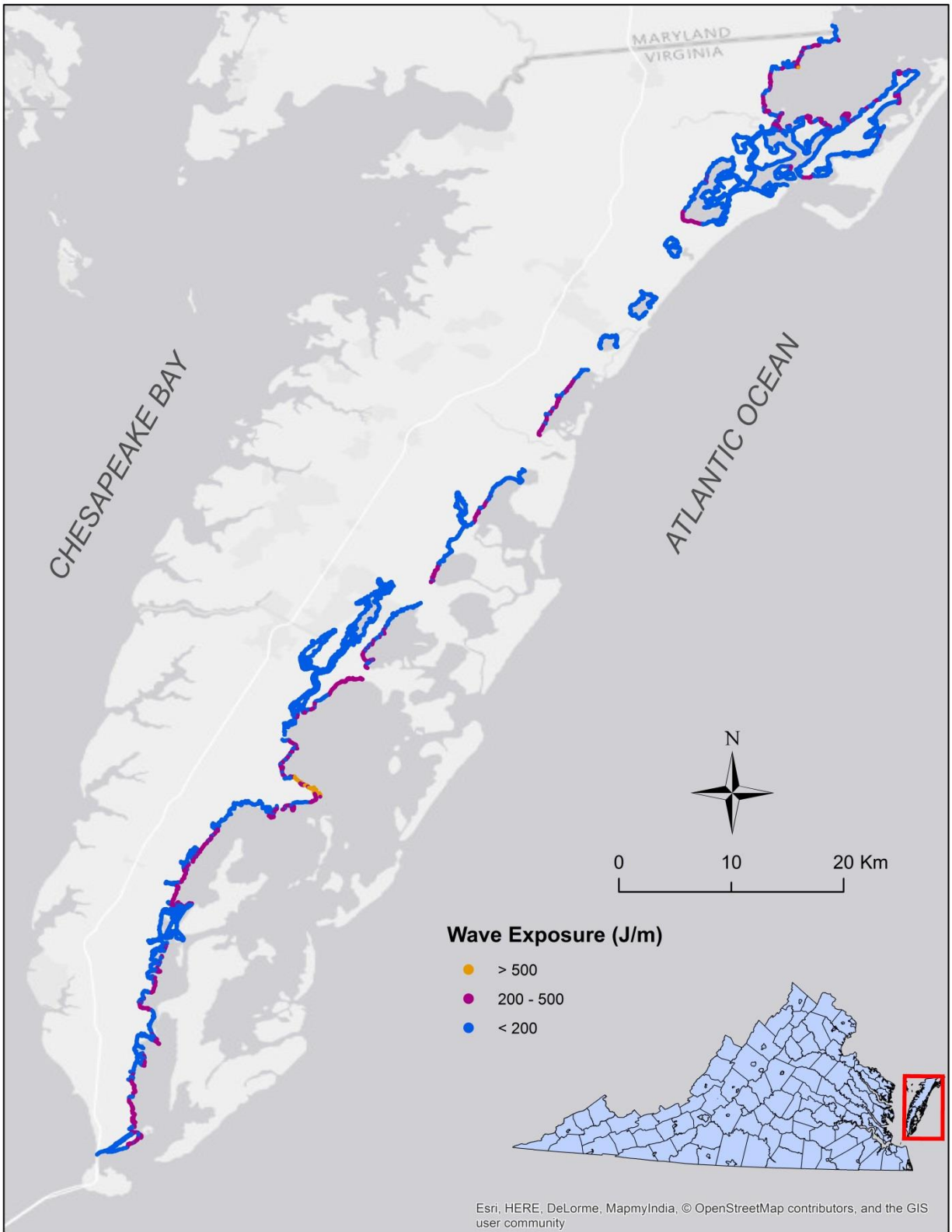


Figure 4.2. Wave Exposure in $J \cdot m^{-1}$ along mainland marshes in the VCR.

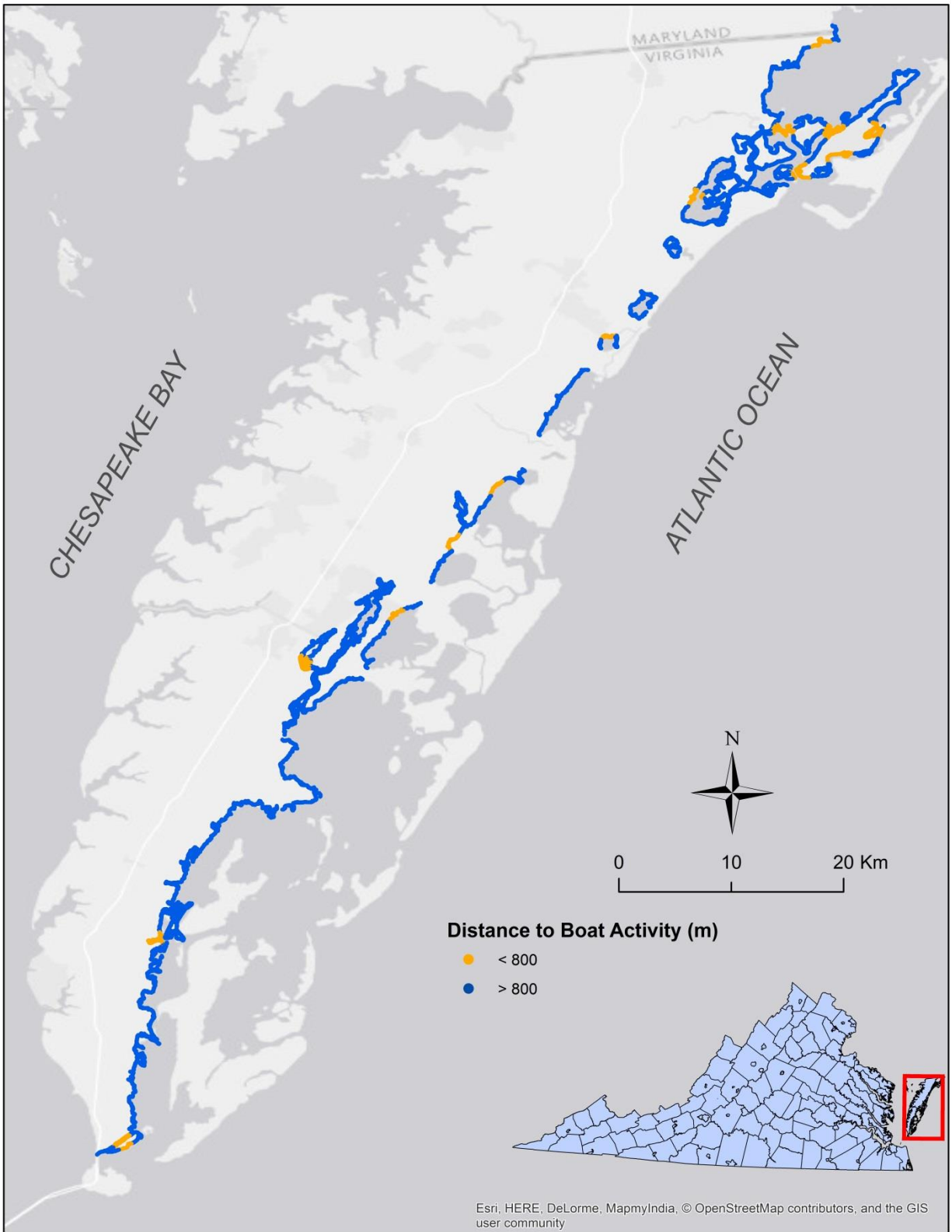


Figure 4.3. Distance to boat activity in meters along mainland marshes in the VCR.

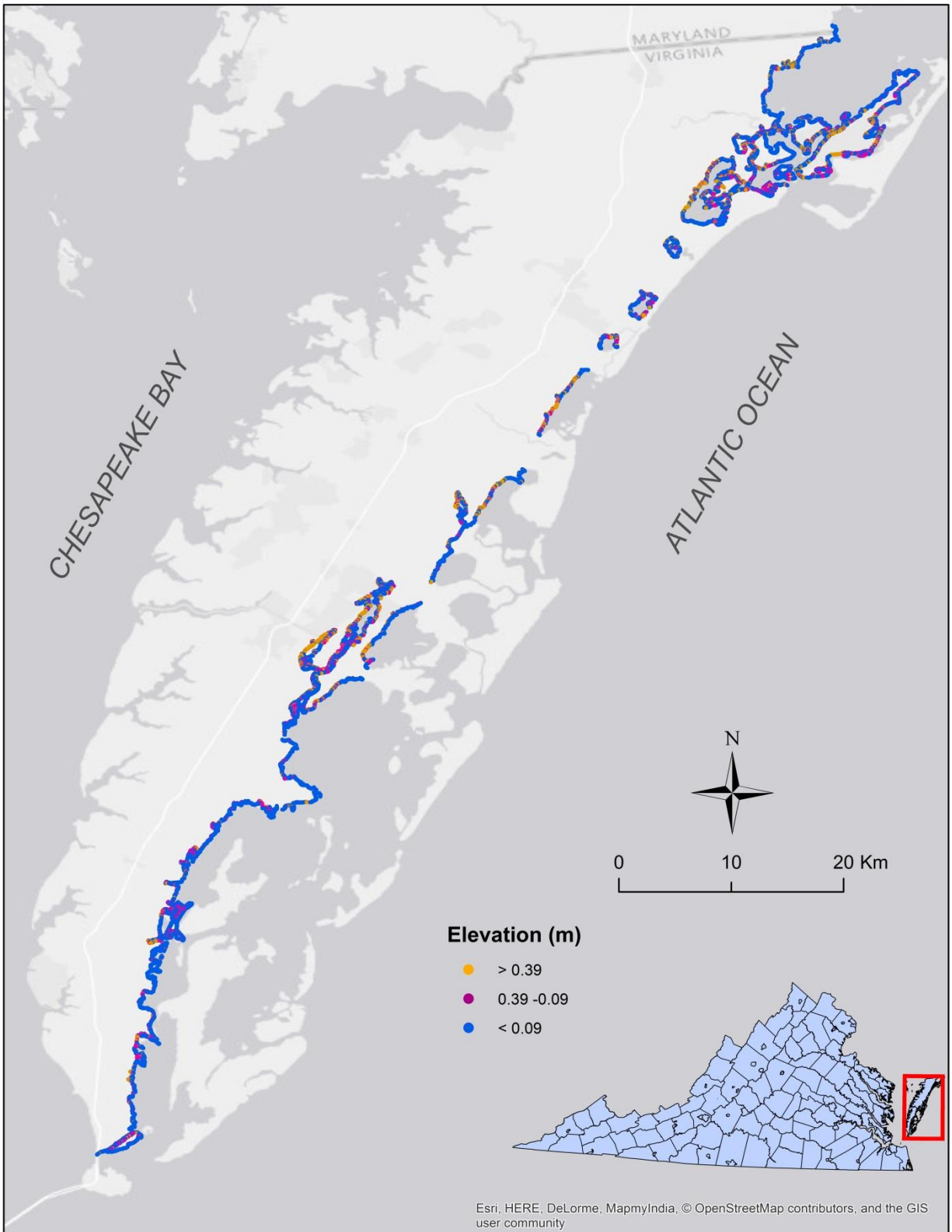


Figure 4.4. Elevation in meters along mainland marshes in the VCR.

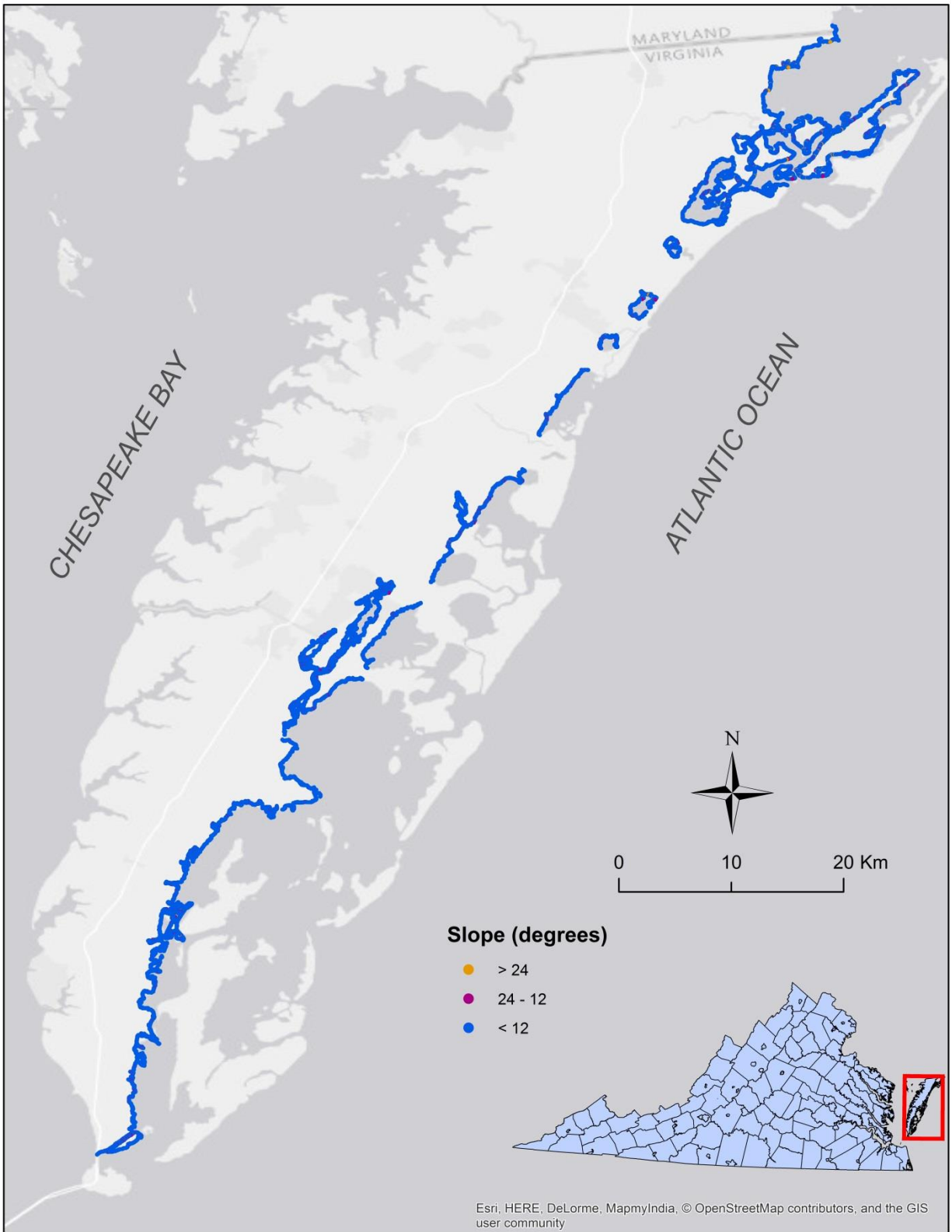


Figure 4.5. Slope in degrees along mainland marshes in the VCR.

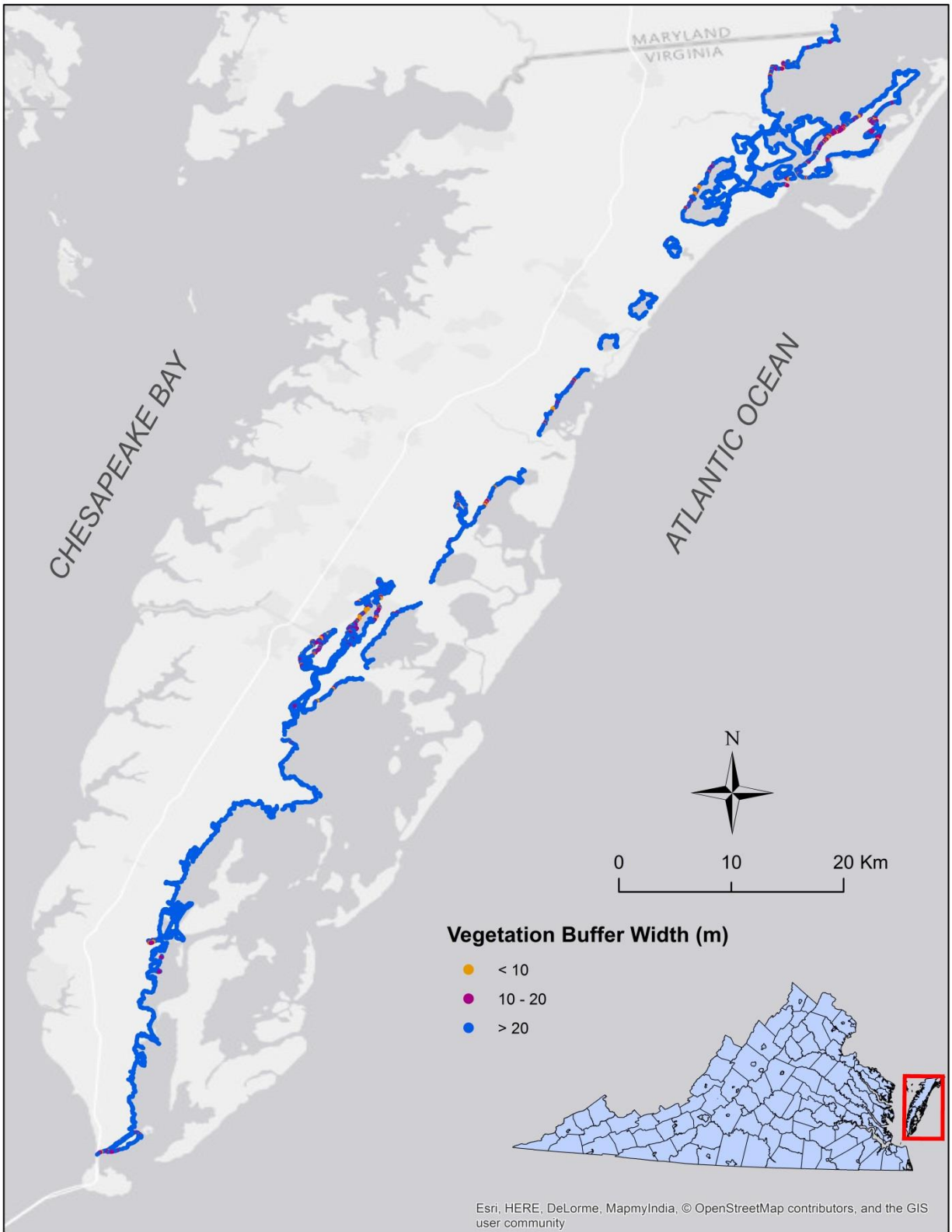


Figure 4.6. Vegetation buffer width in meters along mainland marshes in the VCR.

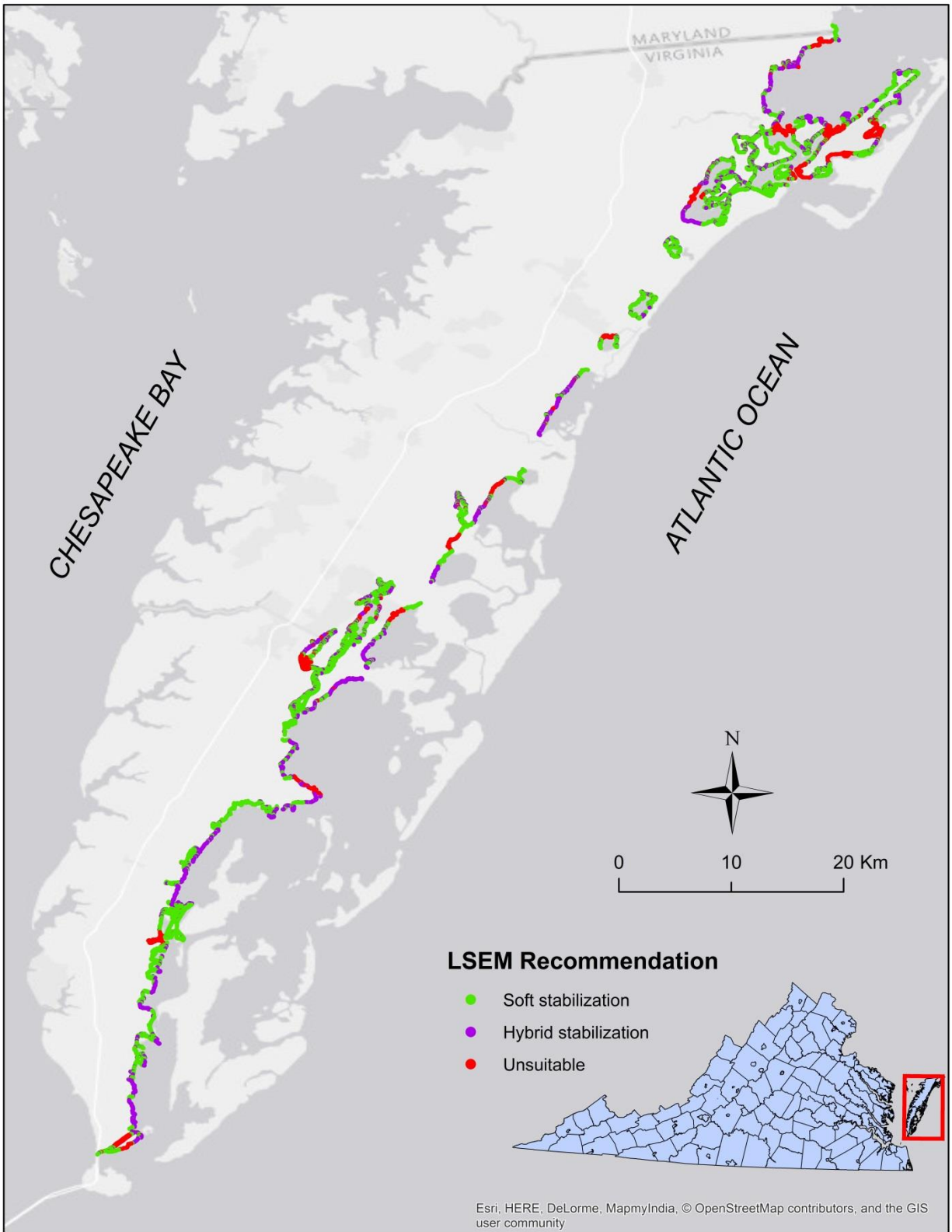


Figure 4.7. Living Shoreline Explorer Model recommendations in the VCR.

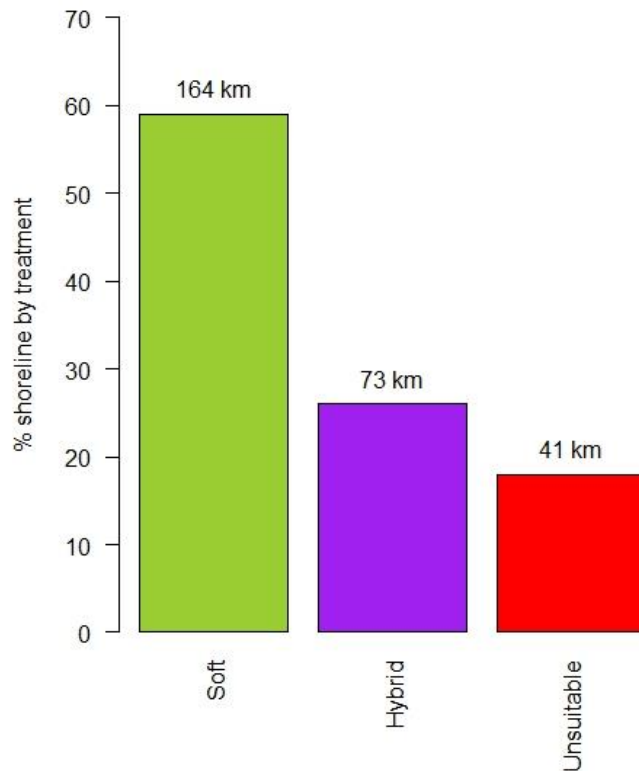


Figure 4.8. The percentage and length of shoreline for each design output. The total length of shoreline considered was 278 kilometers.

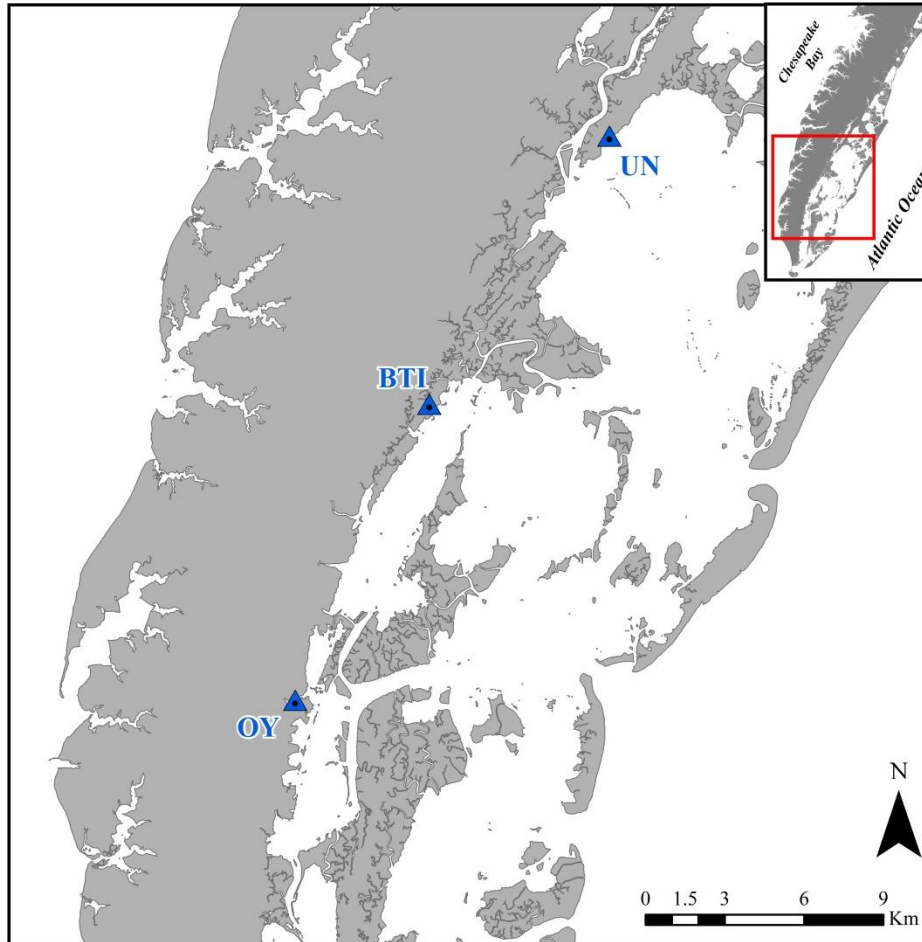


Figure 4.9. Shoreline stabilization recommendations from the LSEM and LSSM were compared for Upshur Neck (UN), Box Tree Idaho (BTI), and Oyster (OY).

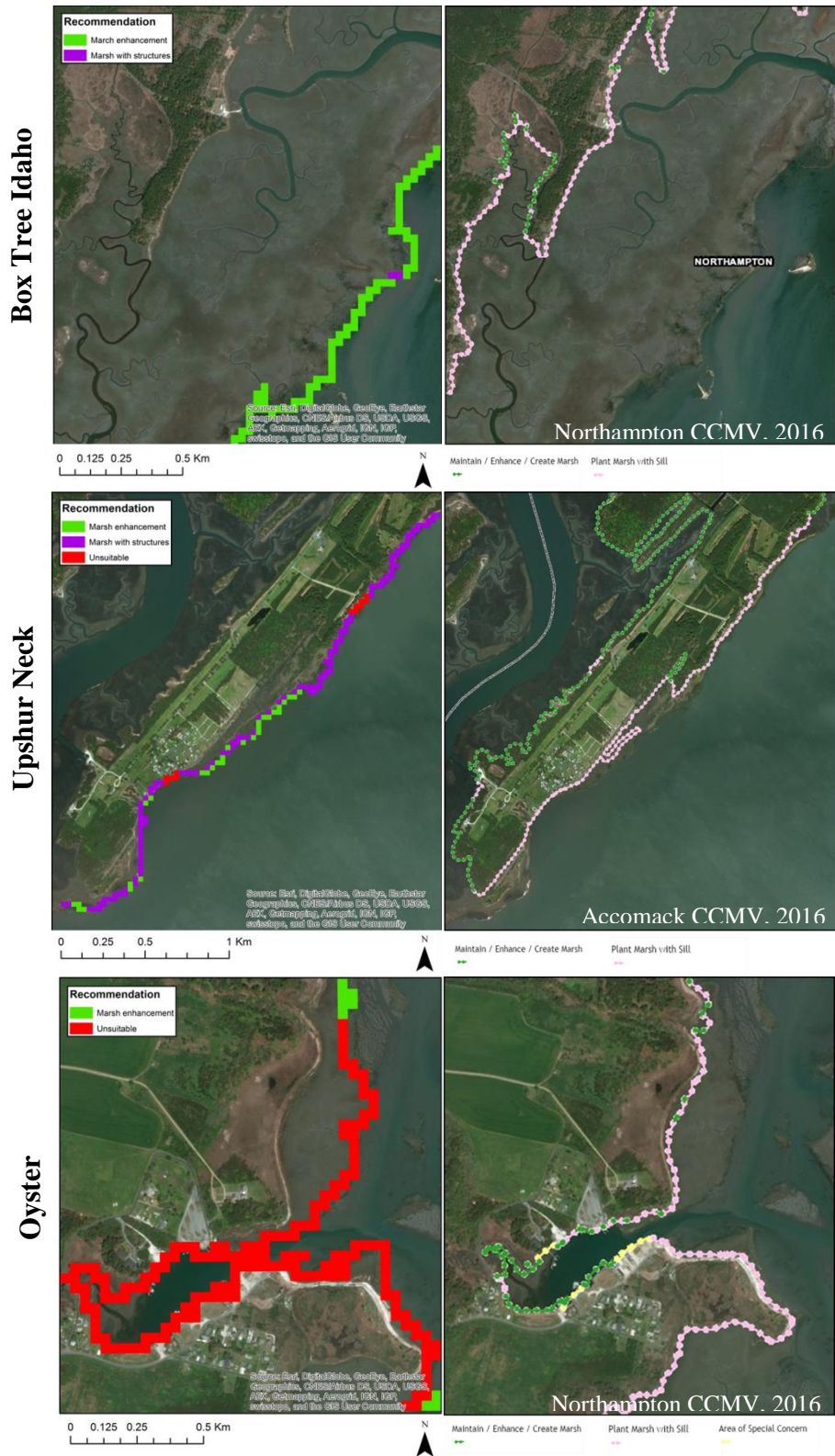


Figure 4.10. LSEM output (*left*) and LSSM (*right*) calculated for BTI, UN, and OY. Of note, only the bay-facing shoreline at UN was used to calculate LSSM metrics.

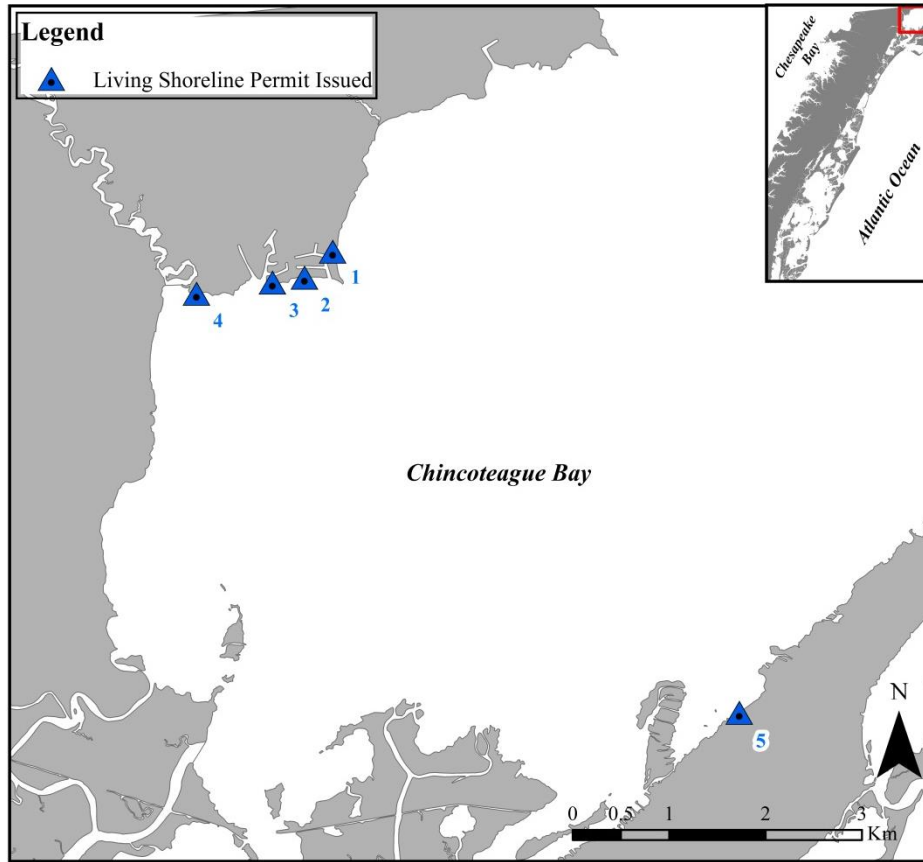


Figure 4.11. Five living shoreline projects permitted by VMRC since 2010. Project details were compared to LSEM recommendations.

Site 1



Site 5

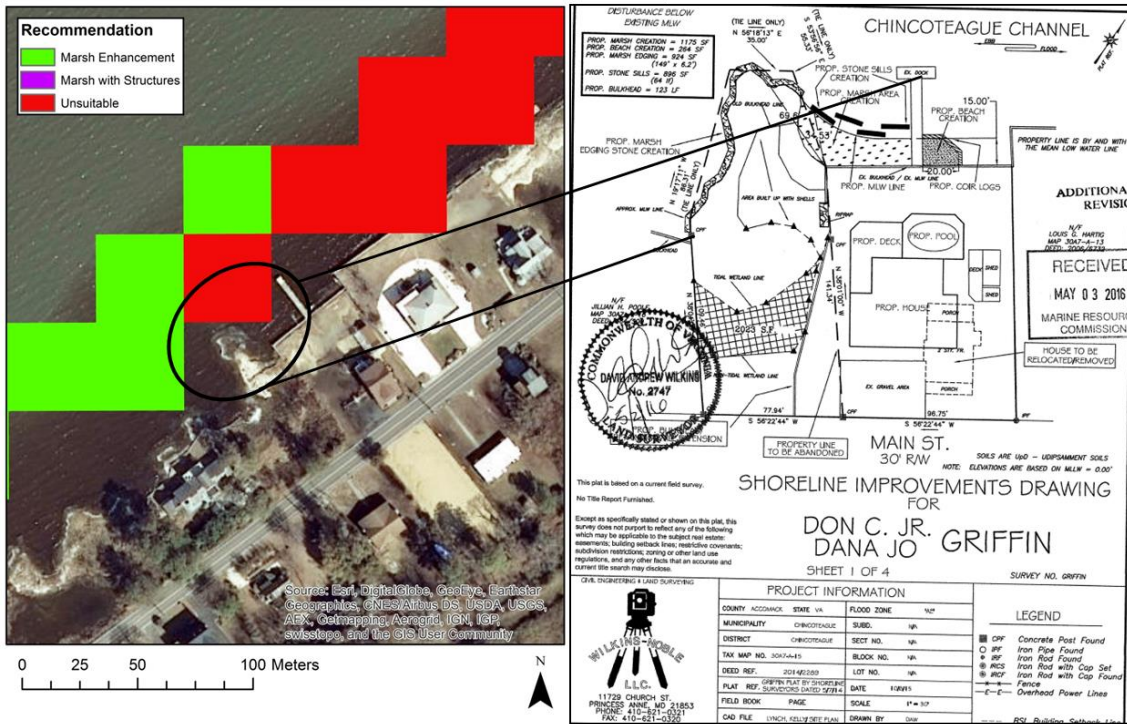


Figure 4.12. Comparison between LSEM recommendations (left) and living shoreline project plans (right) for Site 1 and Site 5.

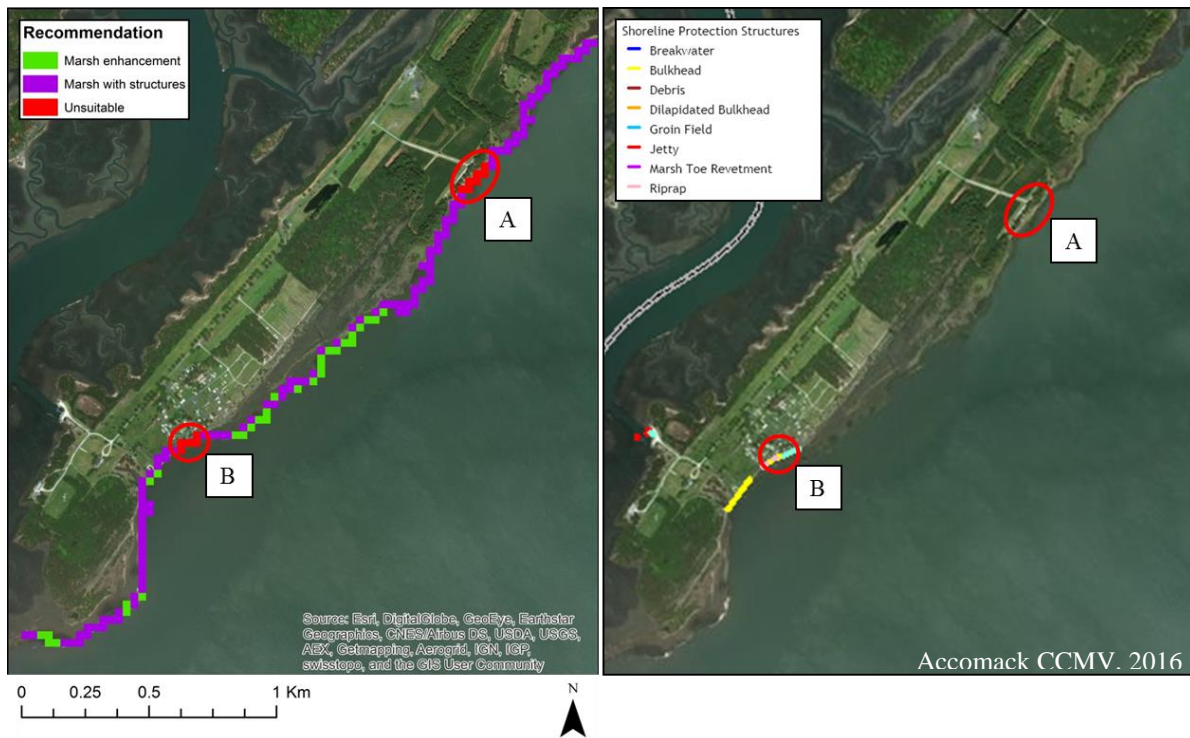


Figure 4.13. Shorelines A and B designated as unsuitable at UN (*left*). Shoreline B is fronted by hardened structures (*right*).

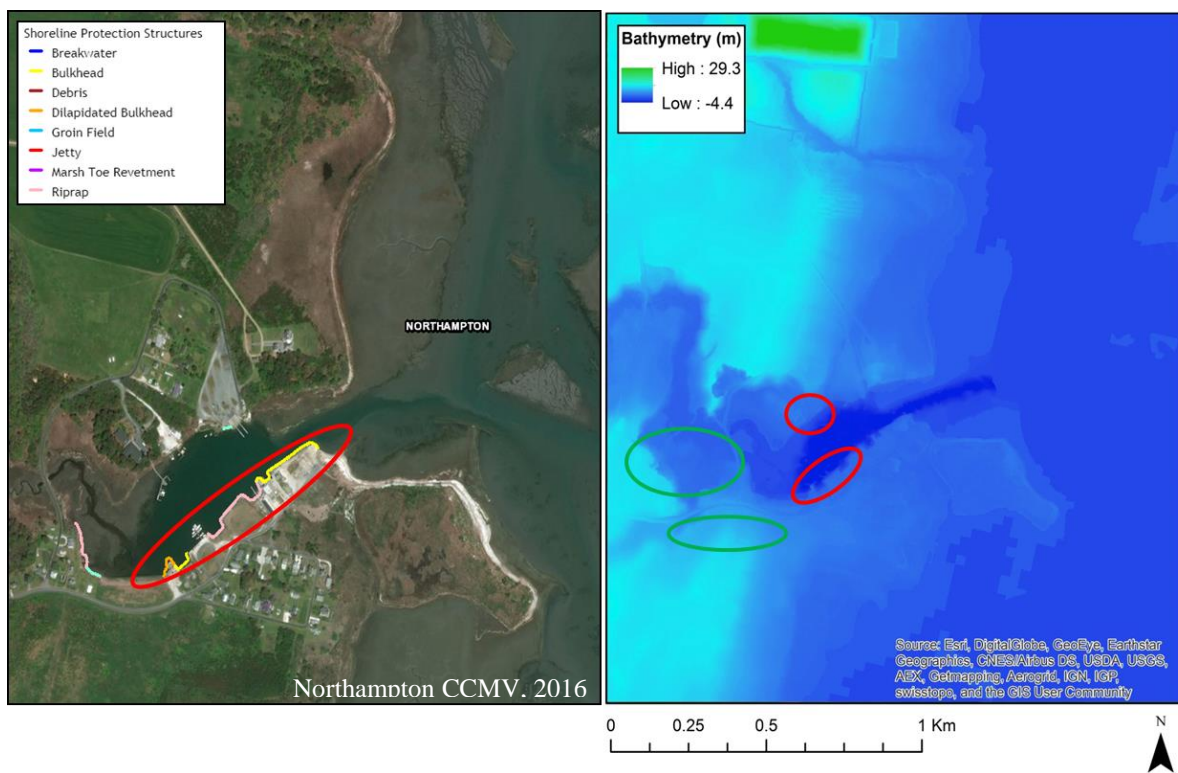


Figure 4.14. Hardened structures highlighted in red along OY shorelines (*left*). Bathymetry in OY (*right*). Red circles indicate shorelines where nearshore depth is not suitable for living shorelines. Green circles indicate shorelines that are likely not impacted by boat activity.

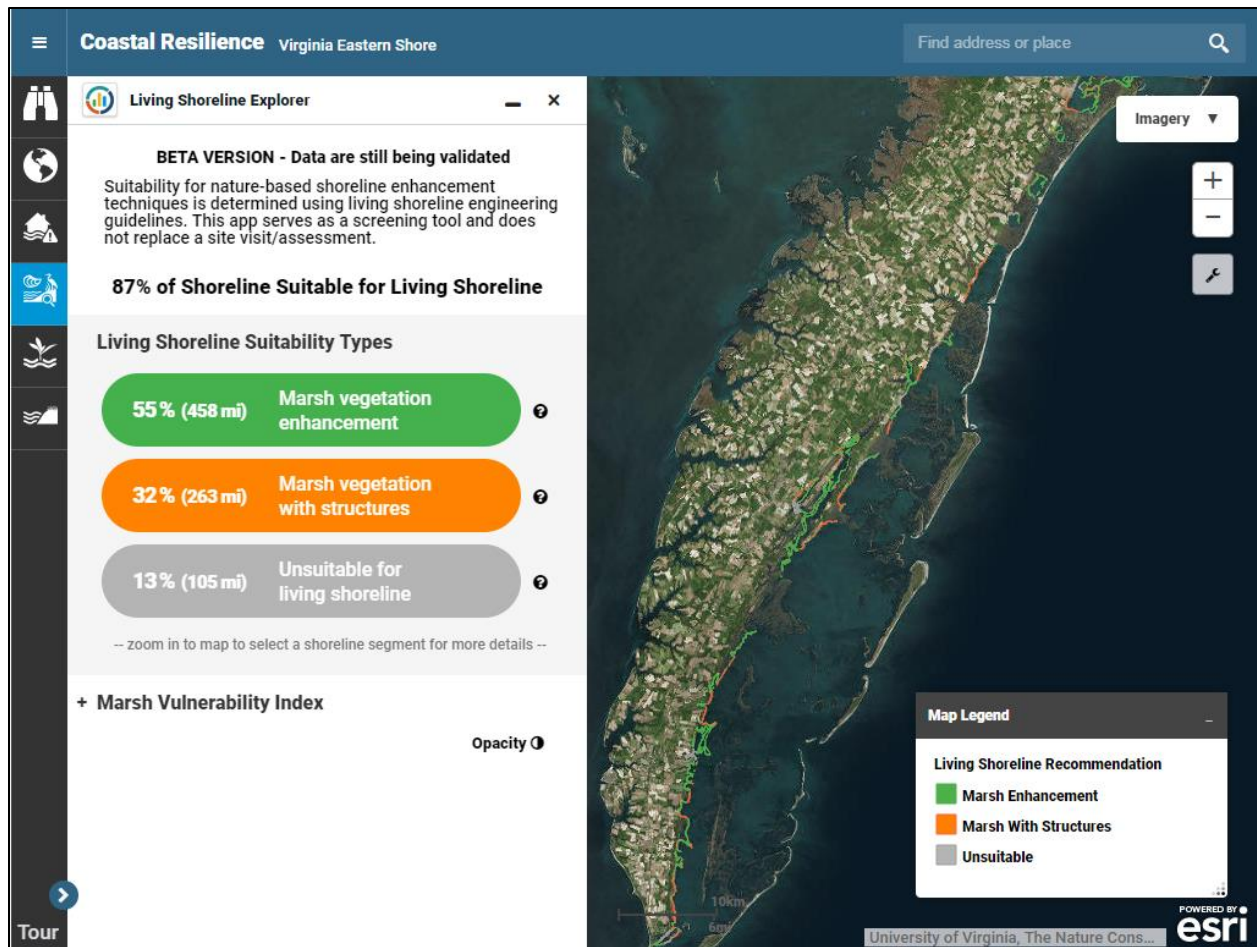


Figure 4.15. Screen capture of the Living Shoreline Explorer app on the TNC *Coastal Resilience* mapping platform. Living Shoreline Explorer Model data are displayed according to stabilization method.

Tables

Variable	Description	Suitability analysis studies
Wave exposure	Wave energy experienced at the shoreline; related to shoreline orientation, water depth, fetch length, and wind characteristics	This study
Distance to boat activity	Boat wake subjects shorelines to short term wave attack	Carey (2013)
Elevation	Influences susceptibility to erosion	Raposa et al. 2016; Carey, 2013; Berman and Rudnicky (2008)
Slope	Reflects the ability of salt marshes to transgress; influences susceptibility to erosion	Boyd et al. 2014
Vegetation buffer width	Presence of wide fringing salt marshes dissipates waves	This study

Table 4.1. Summary of variables and associated definitions used to generate the LSEM.

Data layer	Description	Format	Source(s)	Resolution	Method of development	Date published
Wave exposure	Relative Wave Exposure (RWE) mode quantifies wave height and wave energy at a location	Raster	Ferguson (2017) using NOAA WEMo 4.0	30 m	Quantified wind-wave exposure by taking into account wind statistics, local bathymetry, and shoreline	Aug 2017
*Combined topography/bathymetry	Integrated elevation and bathymetry dataset from multiple sources into a single mostly-seamless digital elevation model (DEM)	Raster	Richardson et al. 2014	3.048 m	LiDAR elevation data and multiple bathymetric datasets were converted to a common vertical datum and merged	Aug 2014
*Wind statistics	Meteorological observations from a network of buoy stations that provide hourly observations of wind speed and direction	Tabular	NOAA NDBC	N/A	Meteorological observations made from NOAA Station WAHV2 - 8631044	Jan 2010 - Dec -2015
Boat wake	Each pixel reflects the distance to public water access point	Raster	Ferguson (2016) using VCR-LTER data	30 m	Derived using ArcGIS geoprocessing tool and VCR-LTER boatramp features	Dec 2016
Elevation	Derived from 2015 LiDAR; vertical accuracy 0.438 ft. at 95% confidence level. Airborne mission flown during low tide conditions (+ - 2 hours of Mean Lower Low Tide)	Raster	Dewberry; USGS	0.762 m	Derived using ArcGIS geoprocessing from LiDAR point cloud	Apr 2015
Slope	Reflects for each pixel the maximum rate of change in value from one pixel to its neighboring pixels; measured in degrees; higher (lower) values are steeper (flatter) terrain	Raster	Ferguson (2016) using Dewberry, USGS data	0.762 m	Derived using ArcGIS geoprocessing tool and 2015 LiDAR DEM	Dec 2016
Vegetation buffer width	Each pixel reflects the marsh vegetation buffer width at that location	Raster	Ferguson (2017); VA Geographic Information Network (VGIN) land cover dataset	1 m	Derived using ArcGIS geoprocessing tools and VGIN land cover dataset	Aug 2017

Table 4.2. LSEM data inventory table. *Combined topography/bathymetry and wind statistics were used to generate wave exposure.

Variable	Category	Reclassification Value
Wave exposure	Low (<200 J/m)	Low = 2
	Moderate (200 - 500 J/m)	Moderate = 1
	High (>500 J/m)	High = 0
Boat wake proximity	Absent (>800 m from boat landing)	Absent = 2
	Present (<800 m from boat landing)	Present = 0
Elevation	Low (<0.09 m)	Low = 2
	Moderate (0.09 - 0.39 m)	Moderate = 1
	High (>0.39 m)	High = 0
Slope	Gentle (<12 degrees)	Gentle = 2
	Moderate (12 - 24 degrees)	Moderate = 1
	Steep (>24 degrees)	High = 0
Vegetation buffer width	Wide (>20 m)	Wide = 2
	Moderate (20 - 10 m)	Moderate = 1
	Narrow (<10 m)	Narrow = 0

Table 4.3. LSEM reclassification scheme.

Attribute	Soft stabilization	Hybrid stabilization	Unsuitable
Wave exposure	Low	Low – Moderate	High
Boat wake proximity	Absent	Present/Absent	Present
Elevation	Low – Moderate	Low – High	Low – High
Slope	Gentle – Moderate	Gentle – Steep	Gentle – Steep
Marsh Buffer Width	Wide – Moderate	Wide – Moderate	Narrow

Table 4.4. Living shoreline design output table.

Design output	Possible combinations
Marsh enhancement	8
Marsh with structures	108
Unsuitable	54

Table 4.5. Number of possible variable combinations for living shoreline design outputs.

Variable	Units	BTI	UN	OY
Wave exposure	J·m ⁻¹	102.99 ± 3.13 ^a	236.14 ± 6.84 ^b	34.47 ± 1.98 ^c
Distance to boat activity	km	6.85 ± 0.04 ^a	3.48 ± 0.02 ^b	0.33 ± 0.015 ^c
Elevation	m	-0.52 ± 0.05 ^a	0.37 ± 0.05 ^b	-0.07 ± 0.07 ^c
Slope	deg	2.22 ± 0.38 ^a	3.33 ± 0.30 ^b	3.27 ± 0.38 ^b
Veg. buffer width	m	50.5 ± 0.11 ^a	41.28 ± 1.12 ^b	34.44 ± 1.46 ^c

Table 4.6. Mean with ± 1 SE suitability variables for BTI, UN, and OY. BTI (n = 79), UN (n = 158), and OY (n = 132). Letters indicate significant differences between sites (p < 0.05). Kruskal-Wallis rank sum and Dunn's test results can be found in Appendix A (22-25).

Site	Model	Shoreline length (m)	Marsh enhancement (m)	Marsh with structures (m)	Unsuitable (m)
BTI	LSEM	1.90	1.84 (97%)	0.06 (3%)	0 (0%)
	LSSM	4.40	0.81 (18%)	3.59 (82%)	0 (0%)
UN	LSEM	3.80	0.72 (19%)	2.81 (74%)	0.27 (7%)
	LSSM	4.44	0.39 (9%)	4.05 (91%)	0 (0%)
OY	LSEM	4.20	0.21 (5%)	0 (0%)	3.99 (95%)
	LSSM	3.34	1.23 (37%)	1.81(54%)	0.30 (9%)

Table 4.7. Comparison between LSEM and LSSM showing the length of shoreline and percentage for each design output at BTI, UN, and OY.

Site	LSEM recommendation	VIMS recommendation	Permit issued
1	Hybrid	Hybrid	Sill: 199 LF Sill fill: 177 y ³ Living shoreline: 199 LF
2	Hybrid	Not available; issued warning against raising bulkhead	Beach nourishment: 8 y ³ Sill fill: 16 y ³ Living shoreline: 119 LF Marsh toe sill: 119 LF
3	Soft	Not available	Beach nourishment: 35 y ³ Breakwater: 25 LF Bulkhead: 95 LF Pier: 25 LF Living shoreline: 50 LF
4	Soft	Not available	Living shoreline: 66 LF Marsh toe sill: 66 LF
5	Soft; unsuitable	Soft; hybrid; remove bulkhead	Beach nourishment: 264 y ³ Bulkhead: 123 LF Sill: 64 LF Core log: 30 LF Living shoreline: 220 LF Marsh toe sill: 149 LF Fill/plantings: 1175 ft ²

Table 4.8. Comparison between LSEM recommendation, VIMS Decision Tree Coastal Management Decision Tool determination, and VMRC permit details for five living shoreline projects.

CONCLUSIONS

The Marsh Vulnerability Index quantified erosion and inundation vulnerability for salt marshes fringing Virginia's coastal bays by considering eight factors that influence wave climate and marsh stability – wave exposure, elevation, slope, vegetation height, vegetation buffer width, storm surge, relative sea level rise, and distance to boat activity. The model assessed the majority of the Virginia Coast Reserve shoreline as having very low to low vulnerability; 51% (594 km) of shorelines were determined to have very low vulnerability and 35% (413 km) were resolved as low vulnerability. Just 0.5% (5 km) of the shoreline was designated with very high vulnerability with the preponderance of these higher values falling along mainland marshes. Principal components analysis indicated that storm surge and vegetation characteristics contributed the greatest amount of variance throughout the system.

Shorelines that experience erosion should correspond to areas characterized as vulnerable by the Marsh Vulnerability Index; but, a comparison between the Marsh Vulnerability Index and shoreline change rates indicated that this was not always the case. Upshur Neck was assessed as moderately vulnerable despite experiencing the lowest shoreline change rates of three comparison sites. Shoreline change rates at Upshur Neck were likely mitigated by the presence of hardened structures. Therefore, a moderate vulnerability designation was appropriate given the site characteristics of high elevation and slope, narrow marsh vegetation buffer, short vegetation height, moderate wave exposure, and very high storm surge.

Field measurements made at four sites in the Virginia Coast Reserve indicate constructed oyster reefs and marsh vegetation may provide effective and sustainable long-term shoreline stabilization. Wave and water-level measurements collected across five constructed oyster reefs in the VCR suggested a strong dependence of wave-dampening capacity on water depth. The

effectiveness of constructed oyster reefs at reducing wave energy is largely limited to shallow water depth conditions. The average reduction in wave heights across all reef sites for shallow water depths (< mean water depth) was 46%, whereas wave height reduction was only 8% when water depths were greater than mean water depth. Waves were rapidly attenuated as they passed over the marsh platform at all four marsh sites. At three of four sites, the greatest attenuation occurred as waves passed over the outer and inner edge stations (i.e., the marsh buffer). Over a 20-meter marsh transect, waves were reduced by an average of 78%, suggesting that a narrow marsh buffer can have a significant impact on wave attenuation. The combination of constructed oyster reefs with marsh vegetation – a hybrid living shoreline stabilization technique – is attractive because it offers a hardened defense of the marsh edge during low to moderate water conditions while encouraging the expansion of salt marsh vegetation with the capacity to buffer waves in deeper water conditions.

The Living Shoreline Explorer Model recommended nature-based shoreline stabilization methods for the Virginia Coast Reserve based on site-specific information related to wave climate and marsh stability: wave exposure, distance to boat activity, elevation, slope, and vegetation buffer width. The model determined that 85% (237 km) of mainland shoreline along Virginia's coastal bays was suitable for nature-based shoreline stabilization projects. 59% (164 km) of the shoreline was recommended for soft stabilization, 26% (73 km) for hybrid stabilization, and 18% (41 km) were unsuitable for living shorelines. Comparison between the Living Shoreline Explorer Model and the Virginia Institute of Marine Science Living Shoreline Suitability Model showed general agreement in their recommendations for mainland shorelines in the VCR. Discrepancies were likely caused by differences in the way shorelines were defined, data sources (type and resolution), and processing methods. A comparison between LSEM

recommendations and Virginia Marine Resources Commission living shoreline permits and project plans revealed that final shoreline stabilization design does not always follow the recommended approach; spatial models cannot resolve information like what a landowner is willing to pay or the designs a consultant is willing to implement.

The intent of the Marsh Vulnerability Index and the Living Shoreline Explorer Model is to offer coastal stakeholders context for understanding their shoreline relative to others and guidance for selecting an appropriate shoreline stabilization consultant. Living shoreline design and placement is complex and requires a site visit for a final determination. As such, the Living Shoreline Explorer Model should be used as a screening tool for coastal stakeholders in examining living shoreline stabilization options. The recommendations provided by these tools is further supported by empirical field evidence from this study and serves as encouragement for landowners to seriously consider living shorelines as an alternative approach for shoreline stabilization.

Spatial and tabular data from this study is available through the Virginia Coast Reserve Data Catalog (<http://www.vcrlter.virginia.edu/home1/?q=dataCatalog>) and the Long-Term Ecological Research (LTER) data portal (portal.lternet.edu). Future iterations of the Marsh Vulnerability Index and Living Shoreline Explorer Model and other related studies will benefit from access to this comprehensive salt marsh database.

REFERENCES

- Abuodha, PAO, and CD Woodroffe. 2010. Assessing vulnerability to sea-level rise using a coastal sensitivity index: a case study from southeast Australia. *Journal of Coastal Conservation* 14: 189-205.
- Anderson, CM, and M Treshow. 1980. A review of environmental and genetic factors that affect height in *Spartina alterniflora* Loisel. *Coastal and Estuarine Research Federation* 3: 168-176.
- Anderson, ME, Smith, JM, and SK McKay. 2011. Wave dissipation by vegetation. US Army Corps of Engineers, ERDC/CHL CHETN-I- 82.
- Arcadis, U.S., Inc. 2016. Estimate of Storm Surge Sensitivity to Sea Level Rise on Virginia's Eastern Shore. 39 p.
- ASMFC (Atlantic States Marine Fisheries Commission). 2010. Living Shorelines: Impacts of Erosion Control Strategies on Coastal Habitats. *Habitat Management Series* 10.
- Augustin, LN, Irish, JL, and P Lynett. 2009. Laboratory and numerical studies of wave dampening by emergent and near-emergent wetland vegetation. *Coastal Engineering* 56: 332-340.
- Barbier EB, EW Koch, BR Silliman, SD Hacker, E Wolanski, J Primavera, EF Granek, S Polasky, S Aswani, LA Cramer, DM Stoms, CJ Kennedy, D Bael, CV Kappel, GME Perillo, DJ Reed. 2008. Coastal ecosystem-based management with nonlinear ecological functions and values. *Science* 321: 319-323.
- Benoit, LK, and RA Askins. 2002. Relationship between habitat area and the distribution of tidal marsh birds. *Wilson Ornithological Society* 114: 314-323.
- Berman, M, and T Rudnicky. 2008. The living shoreline suitability model, Worcester County, Maryland. *Final report to the Coastal Zone Management Program, Maryland Department of Natural Resources*. 51 p.
- Bilkovic, DM and MM Mitchell. 2013. Ecological tradeoffs of stabilized salt marshes as a shoreline protection strategy: Effects of constructed structures on microbenthic assemblages. *Ecological Engineering* 61: 469-481.
- Blum, LK. 1993. *Spartina alterniflora* root dynamics in a Virginia marsh. *Marine Ecology Progress Series* 102: 169-178.
- Borsje, BW, BK van Wesenbeeck, F Dekker, P Paalvast, TJ Bouma, MM van Katwijk, and MB de Vries. 2011. How ecological engineering can serve in coastal protection. *Ecological Engineering* 37: 113-122.

- Boruff, BJ, C Emrich, and SL Cutter. 2005. Erosion hazard vulnerability of US coastal counties. *Journal of Coastal Research* 21: 932-942.
- Boyd, CA, S Dutta and S Jones. 2014. Living shoreline site suitability modeling for Mobile Bay: a GIS & remote sensing-based approach. Grand Bay National Estuarine Research Reserve. Retrieved October 24, 2014 from http://grandbaynerr.org/wp-content/uploads/2014/06/Status-of-research_Boyd.pdf.
- Bozek, CM, and DM Burdick. 2005. Impacts of seawalls on saltmarsh plant communities in the Great Bay Estuary, New Hampshire USA. *Wetlands Ecology and Management* doi: 10.1007/s11273-004-5542-z.
- Brinson, MM, RR Christian, and LK Blum. 1995. Multiple states in the sea-level induced transition from terrestrial forest to estuary. *Estuaries* 18: 648-659.
- Broome, SW, ED Seneca, WW Woodhouse. 1988. Tidal salt marsh restoration. *Aquatic Botany*. 1-22.
- Burke, DG, EW Koch, JC Stevenson. 2005. Assessment of hybrid type shore erosion control projects in Maryland's Chesapeake Bay Phases I and II. Final report in press for Chesapeake Bay Trust, Annapolis, Maryland.
- Carey, M. 2013. Modeling site suitability of living shorelines in the Albemarle-Pamlico estuarine system. Masters of Art Thesis, East Carolina University.
- Center for Coastal Resources Management (CCRM). 2015. <http://ccrm.vims.edu/index.html>. (accessed November 2015).
- CCRM (Center for Coastal Resources Management). 2018. Shoreline Management Model – SMM. <http://www.vims.edu/ccrm/ccrmp/bmp/smm/index.php> (accessed February 2018).
- CCRM. 2015. <http://ccrm.vims.edu/index.html> (accessed November 2015).
- Chandresekhar, N, VJ Viviek, and S Saravanan. 2013. Coastal vulnerability and shoreline changes from Southern tip of India- remote sensing and GIS approach. *Earth Science and Climatic Change* 4: <http://dx.doi.org/10.4172/2157-7617.1000144>.
- CMAP (Comprehensive Map Viewers) for Accomack and Northampton Counties. http://cmap2.vims.edu/CCRMP/Accomack2016/Accomack_CCRMP_Viewer.html; http://cmap2.vims.edu/CCRMP/Northampton2013/Northampton_CCRMP_Viewer.html
- Coastal Water – Virginia and vicinity. The Nature Conservancy, North Carolina Division of Coastal Management; Virginia Institute of Marine Science, Comprehensive Coastal Inventory; USGS, National Hydrography Dataset; Commonwealth of Virginia (Virginia Base Mapping Program), National Agricultural Imagery Program. Accessed September 2017.

- Cooper, JAG, and S McLaughlin. 1998. Contemporary multidisciplinary approaches to coastal classification and environmental risk analysis. *Journal of Coastal Research* 14: 512-524.
- Costa, MJ, JL Costa, PR de Almeida, and CA Assis. 1994. Do eel grass beds and salt marsh borders act as preferential nurseries and spawning grounds for fish? *Ecological Engineering* 3: 187-195.
- Costanza, R, R de Groot, R Sutton, P van der Ploeg, S Anderson, S Kubiszewski, I Farber and RK Turner. 2014. Changes in the global value of ecosystem services. *Global Environmental Change* 26: 152-158.
- Crichton, G. 2013. A novel approach to combating shoreline erosion is taking shape on the Eastern Shore. *The Nature Conservancy*: <http://www.nature.org/ourinitiatives/regions/northamerica/unitedstates/virginia/explore/living-shoreline-1.xml> (accessed November 2015).
- Cui, B, Q Yang, Z Yang, and K Zhang. 2009. Evaluating the ecological performance of wetland restoration in the Yellow River Delta, China. *Ecological Engineering* 35: 1090-1103.
- Culp, MR. 2007. A living shoreline initiative for the Florida Panhandle: taking a softer approach. *National Wetlands Newsletter* 29: 9-19.
- Currin, CA, WS Chappel, and A Deaton. 2010. Developing alternative shoreline armoring strategies: The living shoreline approach in North Carolina, in Shipman, H, MN Gelfenbaum, KL Fresh, and RS Dinicola, eds., *Puget Sound Shorelines and the Impacts of Armoring- Proceedings of a State of the Science Workshop, May 2009*: U.S. Geologic Survey Scientific Investigations Report 2010-5254, p. 91-102.
- Dobbs, BN, MI Volk, NO Nawari. 2017. Living shoreline treatment suitability analysis: a study on coastal protection opportunities for Sarasota County. *Journal of Sustainable Development*: doi: 10.5539/jsd.v10n1p55.
- Douglass, SL, and BH Pickel. 1999. The tide doesn't go out anymore – the effect of bulkheads on urban bay shorelines. *Shore and Beach* 67: 19-25.
- Duhring, KA, TA Barnard Jr, S Hardaway Jr. 2006. A survey of the effectiveness of existing marsh toe protection structures in Virginia. *A final report to the Keith Campbell Foundation for the Environment, Inc.* 25 p.
- Duhring, KA. 2006. Overview of living shoreline design options for erosion protection on tidal shorelines. *Proceedings of the 2006 Living Shoreline Summit*.
- Ellison, AM. 1987. Density-dependent dynamics of *Salicornia europaea* monocultures. *Ecological Society of America* 68: 737-741.
- Emery, Kyle. 2015. Man and Boy Marsh Shoreline Change. Report for The Nature Conservancy.

- Fagherazzi, S, and PL Wiberg. 2009. Importance of wind conditions, fetch, and water levels on wave-generated shear stresses in shallow intertidal basins. *Journal of Geophysical Research* 114: doi: 10.1029/2008JF001139.
- Fonseca, M, and A Malhotra. 2010. WEMo (Wave Exposure Model) for use in Ecological Forecasting. Applied Ecology and Restoration Research Branch, NOAA, National Ocean Service. Version 4.0.
- Garbisch, EW, and JL Garbisch. 1994. Control of upland bank erosion through tidal marsh construction on restored shores: application in the Maryland portion of the Chesapeake Bay. *Environmental Management* 18: 677-691.
- Gedan, KB, ML Kirwan, E Wolanski, EB Barbier, and BR Silliman. 2011. The present and future role of coastal wetland vegetation in protecting shorelines: answering recent challenges to the paradigm. *Climatic Change* 106: 7-29.
- Gedan, KB, BR Silliman, and MD Bertness. 2009. Centuries of human-driven change in salt marsh ecosystems. *Annual Review of Marine Science* 1: 117-141.
- Gittman, RK, AM Popowich, JF Bruno, and CH Peterson. 2014. Marshes with and without sills protect estuarine shorelines from erosion better than bulkheads during a Category 1 hurricane. *Ocean & Coastal Management* 102: 94-102.
- Gjerdrum, C, CS Elphick, and M Rubega. 2005. Nest site selection and nesting success in saltmarsh breeding sparrows: the importance of nest habitat, timing, and study site differences. *American Ornithological Society* 107: 849-862.
- Glennon, Rhonda. 2011. Locating a park through suitability analysis. ArcGIS Blog – Esri Blogs. <https://blogs.esri.com/esri/arcgis/2011/07/01/locating-a-park-through-suitability-analysis/>
- Gornitz, V, TW White, RM Cushman. 1991. Vulnerability of the U.S. to future sea level rise. U.S. Department of Energy, CONF-910780-1.
- Gornitz, VM, RC Daniels, TW White, and KR Birdwell. 1994. The development of a coastal risk assessment database: vulnerability to sea-level rise in the U.S. Southeast. *Journal of Coastal Research* 12: 327-338.
- Hardaway, CS, and K Duhring. 2010. Living shoreline design guidelines for shore protection in Virginia's estuarine environments. NOAA Virginia Coastal Zone Program. Version 1. 112 p.
- Hardaway, CS, and RJ Byrne. 1999. Shoreline management in the Chesapeake Bay. Special Report in Applied Marine Science and Engineering Number 356, Virginia Sea Grant Publication VSG-99-11.

- Hayden, BP, and NR Hayden. 2003. Decadal and century-long changes in storminess at Long-Term Ecological Research sites. *Climate variability and ecosystem response at Long-Term Ecological Research sites*, eds. D. Greenland, D. G. Goodin, and R. C. Smith, 262-285. Oxford, UK: Oxford University Press.
- Hayden, BY, MCFV Santos, G Shao, and RC Kochel. 1995. Geomorphological controls on coastal vegetation at the Virginia Coast Reserve. *Geomorphology* 13: 283-300.
- Hayden, BP, RD Dueser, JT Callahan, and HH Shugart. 1991. Long-term research at the Virginia Coast Reserve. *BioScience* 41: 310-318.
- Hegde, AV, and VR Reju. 2007. Development of Coastal Vulnerability Index for Mangalore Coast, India. *Journal of Coastal Research* 23: 1106-1111.
- Houser, C. 2010. Relative importance of vessel-generated and wind waves to salt marsh erosion in a restricted fetch environment. *Journal of Coastal Research*. 26: 230-240.
- IPCC. 2013. Projections of sea level rise. Working Group 1 contribution to the IPCC Fifth Assessment Report. https://www.ipcc.ch/pdf/unfccc/cop19/3_gregory13sbsta.pdf (accessed September 2016).
- Jackson, CW, Alexander, CR, and DM Bush. 2012. Application of the AMBUR R package for spatio-temporal analysis of shoreline change: Jekyll Island, Georgia, USA. *Computers & Geosciences* 42: 199-207.
- Kirwan, ML, S Temmerman, EE Skeehan, GR Guntenspergen, and S Fagherazzi. 2016. Overestimation of marsh vulnerability to sea level rise. *Nature Climate Change*: doi: 10.1038/nclimate2909.
- Kirwan, ML, and JP Megonigal. 2013. Tidal wetland stability in the face of human impacts and sea-level rise. *Nature* 504: 53-60.
- Kirwan, ML, GR Guntenspergen, A D'Alpaos, JT Morris, SM Mudd, and S Temmerman. 2010. Limits on the adaptability of coastal marshes to rising sea level. *Geophysical Research Letters* 37: doi: 10.1029/2010GL045489.
- Kremer, M. 2016. Wave dissipation over constructed oyster reefs in the Virginia Coast Reserve. *Undergraduate Distinguished Majors Program Thesis*. University of Virginia.
- Kumar, TS, RS Mahendra, S Nayak, K Radhakrishnan, and KC Sahu. 2010. Coastal vulnerability assessment for Orissa State, East Coast of India. *Journal of Coastal Research* 26: 523-534.

- Lee, HJ, YS Chu, YA Park. 1999. Sedimentary processes of fine-grained material and the effect of seawall construction in the Daeho macrotidal flat—nearshore area, northern west coast of Korea. *Marine Geology* 157: 171-184.
- Leonardi, N, NK Ganju, and S Fagherazzi. 2016. A linear relationship between wave power and erosion determines salt-marsh resilience to violent storms and hurricanes. *PNAS* 113: 64-68.
- Leonardi, N, and S Fagherazzi. 2014. How waves shape salt marshes. *Geology*: doi: 10.1130/G35751.1
- Lusk, Bowdoin. 2015. Man and Boy Marsh Photos.
- Malhoutra, A, and MS Fonseca. 2007. WEMo (Wave Exposure Model): Formulation, Procedures, and Validation. NOAA Technical Memorandum NOS NCCOS #65. 28p.
- Mariotti, G, and S Fagherazzi. 2010. A numerical model for the coupled long-term evolution of salt marshes and tidal flats. *Journal of Geophysical Research*: doi:10.1029/2009JF001326.
- Mariotti, G, S Fagherazzi, PL Wiberg, KJ McGlathery, L Carniello, and A Defina. 2010. Influence of storm surges and sea level on shallow tidal basin erosive processes. *Journal of Geophysical Research* 115: doi: 10.1029/2009JC005892.
- McLeod, E, GL Chmura, S Bouillon, R Salm, M Bjork, CM Duarte, CE Lovelock, WH Schlesinger, BR Silliman. 2011. A blueprint for blue carbon: toward an improved understanding of the role of vegetated coastal habitats in sequestering CO₂. *Frontiers in Ecology* 9: 552-560.
- McLoughlin, SM, PL Wiberg, I Safak, and KJ McGlathery. 2015. Rates and forcing of marsh edge erosion in a shallow coastal bay. *Estuaries and Coasts* 38: 620-638.
- McLoughlin, SM, K McGlathery, and P Wiberg. 2011. Quantifying changes along mainland marshes in the Virginia Coast Reserve. *Final report for The Nature Conservancy*. 60 p.
- McLoughlin, SM. 2010. Erosional processes along salt marsh edges on the eastern shore of Virginia. Master's thesis, University of Virginia. 157 p.
- Meyer, DL, EC Townsend, GW Thayer. 1997. Stabilization and erosion control value of oyster cultch for intertidal marsh. *Restoration Ecology* 5: 93-99.
- Miller, JK, A Rella, A Williams, and E Sproule. 2016. Living Shoreline Engineering Guidelines. Stevens Institute of Technology: Davidson Laboratory, Center for Maritime Systems.

- Minollo, TJ, KW Able, MP Weinstein, and CG Hays. 2003. Salt marshes as nurseries for nekton: testing hypotheses on density, growth, and survival through meta-analysis. *Marine Ecology Progress Series* 246: 39-59.
- Möller, I, M Kudella, F Rupprecht, T Spencer, M Paul, BK van Wesenbeeck, G Wolters, K Jensen, TJ Bouma, M Miranda-Lange, and S Schimmels. 2014. Wave attenuation over coastal salt marshes under storm surge conditions. *Nature Geoscience* doi: 10.1038/NGEO2251.
- Möller, I. 2006. Quantifying saltmarsh vegetation and its effect on wave height dissipation: results from a UK East coast saltmarsh. *Estuarine, Coastal, and Shelf Science* 69: 337-351.
- Möller, I, and T Spencer. 2002. Wave dissipation over macro-tidal saltmarshes: Effects of marsh edge typology and vegetation change. *Journal of Coastal Research* 36: 506-521.
- Möller, I., Spencer, T., Rawson, J., 2002. Spatial and temporal variability of wave attenuation over a UK East-coast saltmarsh. Proceedings of the 38th International Conference on Coastal Engineering, Cardiff, July 2002.
- Möller, I, T Spencer, JR French, DJ Leggett, and M Dixon. 1999. Wave transformation over salt marshes: A field and numerical modelling study from North Norfolk, England. *Estuarine, Coastal and Shelf Science* 49: 411-426.
- Moon, S. 2012. Virginia Coastal Zone Management Program. <http://www.deq.virginia.gov/Programs/CoastalZoneManagement/CZMIssuesInitiatives/LivingShore.aspx> (accessed August 2016).
- Murray JMH, A Meadows, and PS Meadows. 2002. Biogeomorphological implications of microscale interactions between sediment geotechnics and marine benthos: a review. *Geomorphology* 47: 15-30.
- Nageswara Rao, K, P Subraelu, T Venkateswara Rao, B Hema Malini, R Ratheesh, S Bhattacharya, and AS Rajawat. 2008. Sea-level rise and coastal vulnerability: an assessment of Andhra Pradesh coast, India through remote sensing and GIS. *Journal of Coastal Conservation* 12: 195-207.
- NOAA Tides and Currents. 2015. 8631044 Wachapreague, VA: <http://tidesandcurrents.noaa.gov/met.html?id=8631044> (accessed November 2015).
- NOAA Coastal Change Analysis Program Land Cover Data for 2010. <https://coast.noaa.gov/ccapftp/#/>

- Oertel, GF. 2001. Hypsographic, hydro-hypsographic, and hydrological analysis of coastal bay environments, Great Machipongo Bay, Virginia. *Journal of Coastal Research* 17: 775-783.
- Oertel, GF, JC Kraft, MS Kearney, and HJ Woo. 1992. A rational theory for barrier-lagoon development, p. 77-87. *Quaternary Coasts of the United States: Marine and Lacustrine Systems*, SEPM Special Publication No. 48, Society for Sedimentary Geology. Tulsa, Oklahoma.
- Ozyurt, G, and A Ergin. 2010. Improving coastal vulnerability assessments to sea-level rise: a new indicator-based methodology for decision makers. *Journal of Coastal Research* 26: 265-273.
- Pendleton, EA, JA Barras, SJ Williams, and DC Twichell. 2010. Coastal vulnerability assessment of the Northern Gulf of Mexico to sea-level rise and coastal change. USGS Report Series 2010-1146.
- Pendleton, EA, S Jeffress, and RW Thieler. 2004. Coastal vulnerability assessment of Assateague Island National Seashore (ASIS) to sea-level rise. U.S. Geological Survey Open-File Report 2004-1020.
- Peterson, MS, BH Comyns, JR Hendon, PJ Bond, and GA Duff. 2000. Habitat use by early life-history states of fishes and crustaceans along a changing estuarine landscape: differences between natural and altered shoreline sites. *Wetlands Ecology and Management* 8: 209-219.
- Phillips, JD. 1986. Spatial analysis of shoreline erosion, Delaware Bay, New Jersey. *Association of American Geographers* 76: 50-62.
- Piazza, BP, PD Banks, and MK La Peyre. 2005. The potential for created oyster shell reefs as a sustainable shoreline protection strategy in Louisiana. *Restoration Ecology* 13: 499-506.
- Plant, NG and GB Griggs. 1992. Interactions between nearshore processes and beach morphology near a seawall. *Journal of Coastal Research* 8: 183-200.
- Richardson, D, J Porter, G Oertel, R Zimmerman, C Carlson, K Overman and C Carlson. 2014. Integrated Topography and Bathymetry for the Eastern Shore of Virginia. Virginia Coast Reserve Long-Term Ecological Research Project Data Publication knb-lter-vcr.210.8 (<http://www.vcrlter.virginia.edu/knb/metacat/knb-lter-vcr.210.8/lter>).
- Rohweder, J, JT Rogala, BL Johnson, D Anderson, S Clark, F Chamberlin, and K Runyon. 2008. Application of wind fetch and wave models for habitat rehabilitation and enhancement projects. United States Geological Survey Open File Report 2008-1200.
- Safak, I, Wiberg PL, Richardson, DL, and MO Kurum. 2015. Controls on residence time and exchange in a system of shallow coastal bays. *Continental Shelf Research* 96: 7-20.

- Schwimmer, RA. 2001. Rates and processes of marsh shoreline erosion in Rehoboth Bay, Delaware, U.S.A. *Journal of Coastal Research* 17: 672-683.
- Scyphers, SB, SP Powers, KL Heck Jr., D Bydron. 2011. Oyster reefs as natural breakwaters mitigate shoreline loss and facilitate fisheries. *PLoS ONE* 6: doi:10.1371/journal.pone.0022396.
- Shaw, J., Taylor, R.B., Forbes, D.L., Ruz, M.-H., and Solomon, S., 1998. Sensitivity of the Canadian Coast to Sea-Level Rise, Geological Survey of Canada Bulletin 505, 114 p.
- Stanhope, JW, Anderson IC, and WG Reay. 2009. Base flow nutrient discharges from Lower Delmarva Peninsula Watersheds of Virginia, USA. *Journal of Environmental Quality* 38: 2070-2083.
- Stricklin, AG, MS Peterson, JD Lopez, CA May, CF Mohrman, MS Woodrey. 2010. Do small, patchy, constructed intertidal oyster reefs reduce salt marsh erosion as well as natural reefs? *Gulf and Caribbean Research* 22: 21-27.
- Taube, SR. 2013. Impacts of fringing oyster reefs on wave attenuation and marsh erosion rates. Master's thesis, University of Virginia. 166 p.
- Theuerkauf, SJ, DB Eggleston, BJ Puckett, KW Theuerkauf. 2016. Wave exposure structures oyster distribution on natural oyster reefs, but not on hardened shorelines. *Estuaries and Coasts*, doi: 10.1007/s12237-016-0153-6.
- Thieler, ER, EA Himmelstoss, JL Zichichi, and A Ergul. 2012. Digital Shoreline Analysis System (DSAS) version 4.0—An ArcGIS extension for calculating shoreline change (ver. 4.3, April 2012): U.S. Geological Survey Open-File Report 2008-1278.
- Thieler, ER, and ES Hammar-Klose. 1999. National Assessment of Coastal Vulnerability to Sea-Level Rise: Preliminary Results for the U.S. Atlantic Coast. U.S. Geological Survey Open-File Report 99-593.
- Tibbetts, JR and D van Proosdij. 2013. Development of a relative coastal vulnerability index in a macro-tidal environment for climate change adaptation. *Journal for Coastal Conservation* 17: 775-797.
- TNC (The Nature Conservancy). 2017. Living Shoreline Explorer App Fact Sheet. http://media.coastalresilience.org/VA/LivingShorelineExplorerApp_FactSheet.pdf
- Toft, JD, AS Ogston, SM Heerhartz, JR Cordell, and EE Flemer. 2013. Ecological response and physical stability of habitat enhancements along an urban armored shoreline. *Ecological Engineering* 57: 97-108.

Wiberg, P, S Taube, M Kremer, M Reidenbach. *In Revision*. Wave attenuation by oyster reefs in shallow coastal bays. *Estuaries and Coasts*.

Zylberman, JM. 2016. Modeling site suitability of living shoreline design options in Connecticut. Master's Thesis. University of Connecticut.

Valiela, I, JM Teal, and WG Deuser. 1978. The nature of growth forms in the salt marsh grass *Spartina alterniflora*. *The American Naturalist* 112: 461-470.

APPENDIX A

1. Kruskal-Wallis rank sum and Dunn's test results for comparison of MVI hot spots across marsh types (Figure 2.23).

Kruskal-Wallis rank sum test			
MVI by marsh type	K-W chi-squared	df	p-value
	327.86	2	<0.001

Dunn's test for multiple comparison		
	FP (mainland marsh)	HI (backbarrier marsh)
HI (backbarrier marsh)	<0.001	-
MB (marsh island)	<0.001	<0.001

2. Linear model (regression) results predicting shoreline change from MVI values (Figure 2.26).

Regression for Man and Boy				
Erosion ~ MVI	R²	df	F-statistic	p-value
	0.13	290	44.04	<0.001

Regression for Box Tree Idaho				
Erosion ~ MVI	R²	df	F-statistic	p-value
	0.25	112	46.00	<0.001

Regression for Upshur Neck				
Erosion ~ MVI	R²	df	F-statistic	p-value
	0.003	176	0.50	0.48

3. Kruskal-Wallis rank sum and Dunn's test results for shoreline change and MVI risk categories at Man and Boy (Figure 2.26).

Man and Boy: Kruskal-Wallis rank sum test			
Erosion by MVI risk category	K-W chi-squared	df	p-value
	36.60	3	<0.001

Dunn's test for multiple comparison			
	High	Low	Moderate
Low	0.206	-	-
Moderate	0.447	< 0.001	-
Very Low	0.041	0.055	<0.001

4. Kruskal-Wallis rank sum and Dunn's test results for shoreline change and MVI risk categories at Box Tree Idaho (Figure 2.26).

Box Tree Idaho: Kruskal-Wallis rank sum test			
Erosion by MVI risk category	K-W chi-squared	df	p-value
	35.86	2	<0.001

Dunn's test for multiple comparison		
	Low	Moderate
Moderate	0.350	-
Very Low	<0.001	<0.001

5. Kruskal-Wallis and Dunn's post hoc results for shoreline change and MVI risk categories by Upshur Neck (Figure 2.26).

Upshur Neck: Kruskal-Wallis rank sum test			
Erosion by MVI risk category	K-W chi-squared	df	p-value
	1.678	4	0.795

Dunn's test for multiple comparison				
	High	Low	Moderate	Very High
Low	0.92	-	-	-
Moderate	0.64	0.70	-	-
Very High	0.81	0.77	0.66	-
Very Low	0.45	0.39	0.22	0.86

6. Welch Two Sample T-test for vegetation height measured by LiDAR and field samples (Table 2.3).

Welch Two Sample T-test			
Height by collection method	t	df	p-value
	1.49	67	0.141

7. Kruskal-Wallis rank sum and Dunn's test results for MVI values by site (Table 2.7).

Kruskal-Wallis rank sum test			
MVI by site	K-W chi-squared	df	p-value
	168.11	2	<0.001

Dunn's test for multiple comparison		
	BTI	MB
MB	0.03	-
UN	<0.001	<0.001

8. Kruskal-Wallis rank sum and Dunn's test results for erosion by site (Table 2.7).

Kruskal-Wallis rank sum test			
Erosion by site	K-W chi-squared	df	p-value
	276.37	2	<0.001

Dunn's test for multiple comparison		
	BTI	MB
MB	<0.001	-
UN	<0.001	<0.001

9. Kruskal-Wallis rank sum and Dunn's test results for wave exposure by site (Table 2.7).

Kruskal-Wallis rank sum test			
Wave exposure by site	K-W chi-squared	df	p-value
	126.40	2	<0.001

Dunn's test for multiple comparison		
	BTI	MB
MB	<0.001	-
UN	<0.001	<0.001

10. Kruskal-Wallis rank sum and Dunn's test results for elevation by site (Table 2.7).

Kruskal-Wallis rank sum test			
Elevation by site	K-W chi-squared	df	p-value
	159.46	2	<0.001

Dunn's test for multiple comparison		
	BTI	MB
MB	0.750	-
UN	<0.001	<0.001

11. Kruskal-Wallis rank sum and Dunn's test results for slope by site (Table 2.7).

Kruskal-Wallis rank sum test			
Slope by site	K-W chi-squared	df	p-value
	96.27	2	<0.001

Dunn's test for multiple comparison		
	BTI	MB
MB	<0.001	-
UN	<0.001	<0.001

12. Kruskal-Wallis rank sum and Dunn's test results for vegetation marsh buffer by site (Table 2.7).

Kruskal-Wallis rank sum test			
Vegetation marsh buffer by site	K-W chi-squared	df	p-value
	29.60	2	<0.001

Dunn's test for multiple comparison		
	BTI	MB
MB	0.33	-
UN	<0.001	<0.001

13. Kruskal-Wallis rank sum and Dunn's test results for vegetation height by site (Table 2.7).

Kruskal-Wallis rank sum test			
Vegetation height by site	K-W chi-squared	df	p-value
	14.90	2	<0.001

Dunn's test for multiple comparison		
	BTI	MB
MB	0.04	-
UN	<0.001	0.02

14. Kruskal-Wallis rank sum and Dunn's test results for distance to boat activity by site (Table 2.7).

Kruskal-Wallis rank sum test			
Distance to boat activity by site	K-W chi-squared	df	p-value
	14.90	2	<0.001

Dunn's test for multiple comparison		
	BTI	MB
MB	0.04	-
UN	<0.001	0.02

15. Kruskal-Wallis rank sum and Dunn's test results for storm surge by site (Table 2.7).

Kruskal-Wallis rank sum test			
Storm surge by site	K-W chi-squared	df	p-value
	274.07	2	<0.001

Dunn's test for multiple comparison		
	BTI	MB
MB	<0.001	-
UN	<0.001	0.54

16. Mann-Whitney U test for vegetation height by species (Figure 3.21).

Mann-Whitney U test	
Height by species	p-value
	<0.001

17. Mann-Whitney U for vegetation width by species (Figure 3.21).

Mann-Whitney U test	
Width by species	p-value
	<0.001

18. 1-way ANOVA and Tukey multiple comparisons for vegetation stem height by site (Figure 3.22; Table 3.6).

1-way ANOVA				
Stem height by site	SS	df	F-statistic	p-value
	240.0	2	433.8	<0.001

Tukey multiple comparisons	
	Site
FP-16/BTI-16	<0.001
MBE-17/BTI-16	<0.001
MBE-17/FP-16	<0.001

19. Kruskal-Wallis rank sum and Dunn's test for vegetation stem width by site (Figure 3.22; Table 3.6).

Kruskal-Wallis rank sum test			
Stem width by site	K-W chi-squared	df	p-value
	455.78	2	<0.001

Dunn's test for multiple comparison		
	BTI-16	FP-16
FP-16	<0.001	-
MBE-17	<0.001	<0.001

20. 1-way ANOVA and Tukey multiple comparisons for vegetation density by site (Figure 3.22; Table 3.6).

1-way ANOVA				
Stem density by site	SS	df	F-statistic	p-value
	9.55	2	6.69	0.005

Tukey multiple comparisons	
	Site
FP-16/BTI-16	<0.001
MBE-17/BTI-16	<0.001
MBE-17/FP-16	<0.001

21. Kruskal-Wallis rank sum and Dunn's test for change in wave height by site (Figure 3.35).

Kruskal-Wallis rank sum test			
Wave height by site	K-W chi-squared	df	p-value
	725.95	2	<0.001

Dunn's test for multiple comparison		
	BTI-16	FP-16
FP-16	<0.001	-
MBE-17	<0.001	0.2

22. Kruskal-Wallis rank sum and Dunn's test for wave exposure by site (Table 4.6).

Kruskal-Wallis rank sum test			
Wave exposure by site	K-W chi-squared	df	p-value
	291.81	2	<0.001

Dunn's test for multiple comparison		
	BTI	OY
OY	<0.001	-
UN	<0.001	<0.001

23. Kruskal-Wallis rank sum and Dunn's test for distance to boat activity by site (Table 4.6).

Kruskal-Wallis rank sum test			
Distance to boat activity by site	K-W chi-squared	df	p-value
	318.66	2	<0.001

Dunn's test for multiple comparison		
	BTI	OY
OY	<0.001	-
UN	<0.001	<0.001

24. Kruskal-Wallis rank sum and Dunn's test for elevation by site (Table 4.6).

Kruskal-Wallis rank sum test			
Elevation by site	K-W chi-squared	df	p-value
	82.36	2	<0.001

Dunn's test for multiple comparison		
	BTI	OY
OY	<0.001	-
UN	<0.001	<0.001

25. Kruskal-Wallis rank sum and Dunn's test for slope by site (Table 4.6).

Kruskal-Wallis rank sum test			
Slope by site	K-W chi-squared	df	p-value
	14.89	2	<0.001

Dunn's test for multiple comparison		
	BTI	OY
OY	0.025	-
UN	<0.001	0.074